A 'Hydro-kinematic' Method for Quantifying Glide Efficiency of Swimmers

By

Roozbeh Naemi

Doctor of Philosophy

The University of Edinburgh

November 2006

Statement of Authorship

I, Roozbeh Naemi, hereby declare that except where explicit reference is made in the text of the thesis, this thesis contains no material published elsewhere or extracted in whole or in part from a thesis by which I have qualified for or been awarded another degree or diploma. No other person's work has been relied upon or used without due acknowledgment in the main text and bibliography of the thesis.

This research was conducted under the supervision of Professor Ross Sanders, as the principal supervisor and Professor Bill Easson as the second supervisor.

This thesis has been prepared to conform to the guidelines provided by The University of Edinburgh and is based upon the style recommended in the Publications Manual of Postgraduate Assessment Regulations for Research Degrees (Sep. 2006).

Roozbeh Naemi
CANDIDATE

Abstract

The purpose of this thesis was to introduce and test methods of quantifying the glide efficiency and the hydrodynamic parameters related to an underwater glide of a human body in a streamlined position and to investigate their relationship with the size and shape characteristics of a body with consideration of actual anthropometry, morphology and posture of body in a streamlined glide position.

The thesis comprises three studies. The aim of the first study was to develop and test a method of quantifying glide efficiency in a way that accounts for both the inertial and resistive characteristics of the gliding body as well as the differences in the instantaneous velocities. To achieve this, a displacement function was derived from the equation of motion of the body during a horizontal rectilinear glide. By fitting this function to the position-time data of a body during a rectilinear horizontal glide, a glide factor that indicates the glide efficiency was quantified. This factor represented a combined kinematic and hydrodynamic measure of a glide. As the glide efficiency of a body is influenced by the body shape as well as by the body size, the size-related and shape-related glide efficiencies were determined as separate entities. The validity and applicability of the method was established. Also the glide factor enabled the exact prediction of deceleration during a glide which was not possible knowing the resistive factor alone. It was found that the glide factor increased with decreasing velocity. The method was shown to be able to detect differences in the glide efficiency between subjects and across trials within subjects.

The aim of the second study was to develop and test a method of quantifying the hydrodynamic properties of a human body in a streamlined position during an underwater glide so that the values of the resistive factor and the virtual mass can be determined separately. To achieve this aim a displacement function was derived from the equation of motion of the body during an inclined rectilinear glide. By fitting this function to the position-time data of a body during a rectilinear inclined glide, and taking

advantage of the component of net buoyancy as a constant parameter in the equation of motion, the resistive and inertial parameters were quantified. As the resistive and inertial parameters of a body are influenced by the body shape as well as by the body size, the drag and added mass coefficients were determined to investigate resistive and added inertial properties of a body independent of its size. The validity and applicability of the method was established. The method was able to quantify the hydrodynamic resistance and added inertia parameters considering the glide under realistic conditions. Also added mass of a body during deceleration was quantified with this method. It was found that the added mass decreased with increasing velocity while the resistive force increased.

The aim of the third study was to determine the true relationship between the size and the shape characteristics of the body and its hydrodynamic and glide efficiency parameters. In the third study the actual anthropometric measures, morphological indices and postural angles of the body in a streamlined position were determined, in order to quantify the size and shape characteristics of a body in a streamlined position. The correlations between these parameters and the glide efficiency and the resistive and added inertia parameters were obtained. It was found that the gliding ability is more dependent on having a good shape than on having a large body mass with a low cross-sectional area. Also the difference of hydrodynamic parameters including the resistive factor and the added mass between two bodies is the result of the differences in the shape characteristics including morphological indices and postural angles rather than due to the differences in size. The results indicated that some of the morphological indices and joint angles investigated in this study were correlated to the glide efficiency and hydrodynamic parameters. The belief that more streamlined objects possess a lower added mass coefficient seems not to be applicable to the human body.

The method developed has practical applications in testing swimming suits designed to improve performance. Using the 'Hydro-kinematic' method the suit effect on the ability of a body to entrain added masses of water together with its ability to reduce drag as well as the combined effect on the glide efficiency may be quantified. The results of this

study indicate that in talent identification the evaluation should be based on the shape of the body rather than its size. The existence of relationship between some of the morphological indices and the hydrodynamic and glide efficiency parameters would also allow identifying the streamlining degree of a body without the requirement for the direct drag force measurements.

Table of Contents

List of Tables

List of Figures

List of Abbreviations

Re: Reynolds number

FR: Fineness ratio

CR: Cross-sectional ratio

TI: Taper index

Fr Froude number

SSE: Sum of Squares due to Error

R^2: R-square

RMSE : Root Mean Squared of Errors

SEM : Standard Error of Measurement

RSEM: Relative Standard Error of Measurement

Sdev: Standard Deviation

SEC: Standard Error of Calculation

RSEC: Relative Standard Error of Calculation

Hz: Hertz

m: Metres

kg: Kilogram

s: Second

Coef. : Coefficient

Dis.: Distance

WK: Week

X-section: Cross-section

Acknowledgments

To start and complete a task of this nature would be impossible without the guidance and support of many people. The following words represent an attempt to show my enormous appreciation and reward the extent of the contributions to my work by such persons.

The guidance, support and friendship of experienced and motivated supervisors are crucial to the successful completion of any Doctoral thesis. Sincere thanks are extended to Professor Ross Sanders for his un-obligated assistance, sharing his extraordinary knowledge and for demonstrating to me the qualities required to become an exemplary researcher and scientist. Considerable appreciation is felt for his help during the write up.

Thanks are bestowed to Professor Bill Easson for his assistance and time spent discussing and 'learning' me the Hydrodynamic principles.

Thanks also to those PESLS staff who supported me throughout this time. My sincere appreciation goes to Dr Simon Coleman who provided help with the use of software. To my friends Ian Hamilton and Jon Kelly, your efforts as technicians have been significant and are equally acknowledged. Sincere thanks also go to the CSE life guards for their assistance during data collections.

Particular thanks are bestowed to Stelios Psycharakis and Carla McCabe for putting exhaustive hours acting as subjects throughout the pilot studies as well as providing assistance. Special thanks go to Dr. Shuping Li and Chris Connaboy for their priceless helps throughout the process of data collection.

I thank Dr. Frederik Dekoninck for his insightful and extremely valuable advice in statistics, and writing up, and for helping me through difficult times.

The warmest of appreciation is extended to Dr. Morteza Shahbazi and Dr. Ahmadreza Arshi for supporting my PhD application to continue my study here at the University of Edinburgh.

Throughout the completion of this thesis there have been many people, in addition to those already mentioned, who have lent assistance in some form and of varying degrees. Without preference and in no specific order the following people are deserving of acknowledgement in recognition of their help and support, which I am grateful; Kia Katoozi, Dr Jone Deffeys, Katie Mattews and Kelly Meyers.

Thanks goes to the many swimmers and squad coaches who volunteered both time and efforts to make each study within this thesis possible. In particular, I would like to specially thank Warender, city of Edinburgh, Mid-Lothian and the University of Edinburgh Swimming team. Their efforts are immensely appreciated.

The warmest appreciation goes to my uncle Ebrahim Naemi whose helps, supports and encouragements have been all away with me throughout the PhD years.

To my parents Makhsooseh Bigdeli Moghaddam and Siroos Naemi whom I owe much more than simply thank you, for their unwavering support. Without their belief, untiring assistance and love this journey could never have begun yet be completed. Thanks to my sister Mahsa for your unconditional love and support.

To my wife Sara Kazemi Yazdi for believing in me, and for encouraging and loving me the way you do. Your presence in my life has made the stages of this thesis less arduous and I am truly grateful for your patience, support and selfless love.

To all those people who offered encouragement, believed in me, and were there for and with me until the end, I thank you with the utmost gratitude and respect.

A 'Hydro-kinematic' Method for Quantifying Glide Efficiency of Swimmers

Chapter 1

Introduction

The glide phase represents an important part of each swimming race. The glide corresponds to the phases of starts, turns and strokes where the swimmer adopts a passive 'streamlined position' characterised by an elongated posture with arms extended forward with hands pronated and overlapping, and the feet together and plantar flexed. The swimmer tries to minimize the resistive force by minimizing the cross-sectional area perpendicular to the direction of fluid flow. Maintaining a passive streamlined posture after starts and turns while at velocities higher than that which can be sustained by kicking has been established to be more beneficial than kicking (Lyttle, *et al.* 2000).

The relationship between the time taken in the glide phase and the total time spent during starts and turns is strong, especially in short course events where more turns are required in any given race distance than in long course events (Hay and Guimares, 1983, Thayer and Hay, 1984 and Chow. *et al.*, 1984).

Average velocity during a glide is a measure of glide performance which can be improved by covering a given distance in a shorter time during a glide. Thus improvement in glide performance improves the overall race performance of the swimmers by increasing the average velocity during starts and turns.

Optimizing glide performance is also important during transitional phases of all strokes (Vorontsov and Rumyantsev, 2000), and is particularly important in breaststroke in which the gliding phase corresponds to more than 40% of the swimming time at all race distances and is a determining factor for distinguishing superior swimmers (D'Acquisto. *et al.*, 1988).

Average glide velocity is an indicator of glide performance (Figure 1). It is determined by initial velocity and the rate of change of velocity over time (deceleration). Initial velocity of the glide is related to the preceding actions, and is affected by characteristics of the pre-glide phase including entry after start, push-off force and body position during wall contact in turns and stroke characteristics in power phase of breaststroke. According to Newton's second law of motion, the rate of change in velocity (deceleration) depends on the net forces applied to a body and its inertial properties during the streamlined glide. In the absence of any propulsive force, as is the case in passive glides, the net force is equal to the resistive force.

The resistive forces are the hydrodynamic forces acting on a gliding body opposite the direction of travel. These forces are highly related to velocity. The rate at which the forces slow the gliding body depends on the magnitude of the resistive forces and the inertia of the body (Figure 1). Inertia of a gliding body is the sum of the body mass plus the mass of water entrained with the body. This mass of entrained water adds to the inertia and therefore reduces the rate of slowing of a gliding body and is referred to as 'added mass'. The inertia of a gliding body, being the sum of body mass and the added mass, is termed its 'virtual mass' in an unsteady motion.

Because the magnitude of resistive forces acting on a gliding body is related to velocity, it can be concluded that deceleration is also dependent on the velocity. Thus the value of deceleration alone can not be a good measure of gliding ability unless it is considered in accordance with the instantaneous velocity at which the body glides.

Glide efficiency can be defined as the ability of a gliding body to maintain its momentum through time at each corresponding velocity during a passive retarding motion. Considering two gliding bodies starting a glide interval with the same initial velocity, the body with higher glide efficiency can travel a greater distance during the same period of time.

Although increasing initial velocity of a glide is one of the ways to optimize the glide performance, improving glide efficiency by minimizing resistance and/or maximizing inertia at each corresponding velocity can be beneficial because an advantage is gained without increasing the metabolic cost. Also, with increasing the glide efficiency the glide speed can be sustained above the speed attainable in mid-pool swimming for a longer period thereby saving energy. Thus, knowledge of factors that affect efficiency of the passive glide including inertia and resistance assists in improving glide performance in a way that restrains physiological cost.

Previous research on glide performance has involved measuring time to glide a known distance and determining the maximum glide distance after push-offs from the wall (Cureton, 1940). As the glide performance depends on the initial velocity, efficiency of a glide cannot be quantified independently in this way.

More recently, using kinematic data of a glide, Sharp and Costill (1989) compared the changes in gliding velocity over a period of time. Starling *et al.* (1995) also measured the distance covered by gliding bodies over a glide time interval. Both the methods considered the glide intervals starting at the same initial velocity as the rate of changes in velocity and the distance covered in each interval are highly correlated to the initial glide velocity.

The methods used in the early studies of glide do not allow comparison of the glide efficiency at different velocities. More importantly these methods do not relate the kinematic characteristics of a glide to the hydrodynamic characteristics of a body in a streamlined position. To date a comprehensive method of quantifying glide efficiency specifically that relate the glide's kinematic and hydrodynamic characteristics has not been developed for human underwater gliding.

Thus, the first purpose of this thesis is to develop a new method to quantify glide efficiency that accounts for the inertial and resistive characteristics of the gliding body. The method proposed is to fit an appropriate mathematical function, based on the equation of motion of the gliding body, to the kinematic position-time data of a swimmer performing a rectilinear glide with horizontal alignment and direction of motion. From the fitted function a glide factor that represents the ratio of inertia to the resistive factor will be deduced that defines the glide efficiency. This factor represents a combined kinematic and hydrodynamic measure of a glide as it is an indicator of a normalized rate of change in velocity, and demonstrates a ratio of assistive to resistive hydrodynamic parameters. The glide factor is a measure of glide efficiency and enables comparison between glide intervals both within and between individuals.

While working with glide factors has the advantage of considering a combined inertial-resistive efficiency, separating them as two distinct parameters would be beneficial for quantifying the body's hydrodynamic parameters in the streamlined position. Most if not all the swimming research studies on the human body in streamlined position have focused on the resistive parameters only. Inertial properties have been ignored. Thus, there is a need for a method that enables the inertial and resistive effects to be considered separately.

The majority of studies to quantify hydrodynamic resistance on a human body in streamlined posture have relied on the so called "quasi-static" approach. These include the studies with fixed apparatus towing (Karpovich, 1933; Alley, 1952; Counsilman, 1955; Hairabedian, 1964; Chatard, *et al.* , 1990; Sheehan and Laughrin, 1992; Klauck, 1998; Lyttle *et al.* , 1998; Benjanuvatra *et. al.* 2001); moving apparatus towing (Van Manen and Rijken, 1974; Jiskoot and Clarys, 1975; Clarys and Jiskoot, 1975; Clarys *et al.* ,1974; Clarys, 1979; Williams and Kooyman, 1985; Mollendorf *et al.*, 2004) flume (Miyashita and Tsunoda, 1978; Maiello. *et al.*, 1998; Roberts *et al.*, 2003; Chatard and Wilson, 2003; Vennell *et al.* , 2005) and wind tunnel (Waring, 1999). The assumption implies that resistive forces measured at constant velocity also reflect the drag forces

acting at corresponding velocities during a passive glide. The quasi-static approach is not suited for measuring the inertia associated with the deceleration of the swimmer and the added mass of water during a glide since it measures forces at constant velocity with no acceleration. Also natural posture and flow characteristics around a swimmer's body would be affected in these methods which do not represent the glide under real conditions. These methods are highly dependent on the equipment setup and design that affect the reliability of the data gathered from these methods.

On the other hand, methods based on the kinematics of the glide for quantifying hydrodynamic resistive parameters overcome the deficiencies of the conventional direct force measurements by allowing the swimmer's drag to be measured in a non-invasive way during a more realistic gliding condition. In addition, the variability which arises as a result of the dependency on equipment and setups in the direct force measurements is eliminated. However quantifying resistive forces based on the kinematics of glide can be affected by inaccuracies in measuring the kinematic data and inappropriate hydrodynamic assumptions about added mass.

Previous studies using glide kinematics for quantifying hydrodynamic resistance (Klauck and Daniel, 1976 and Oppenheim, 1997) did not consider the effect of the added mass as an important contributor to the inertia. Ignoring the added mass in using the kinematics of a glide for quantifying the hydrodynamic resistance would lead to underestimation of the resistive force (Vogel, 1994).

Using the glide kinematics and approximating the value of added mass on the basis of the data bases available for the streamlined shapes, can provide reasonable results for quantifying the hydrodynamic resistance of aquatic mammals (Lang and Daybell, 1963; Feldkamp, 1987; and Stelle, *et al.*, 2000). The value of added mass of a human body could not be approximated by the known added mass values of the streamlined shapes. Without solving the added mass problem, the values of resistive forces calculated on the basis of the glide kinematics would not resemble the actual values.

To overcome this limitation another method is proposed in this thesis based on the kinematic behaviour of the body in a rectilinear glide in which the direction of motion and alignment are inclined rather than horizontal. A mathematical function based on the equation of motion will be fitted to the position time data of a rectilinear inclined glide. Taking advantage of the component of buoyancy opposite the direction of travel the inertial and resistive factors can be determined and separated as independent parameters.

Unlike the controllable parameters influencing the hydrodynamic characteristics of a body such as, depth, and angle of attack, the size and the shape characteristics of bodies are not controllable and account for the main source of variability of the glide efficiency and hydrodynamic parameters between individuals.

In line with the effect of size of the body on the hydrodynamic parameters, some of the anthropometric parameters like the head and thorax circumferences, thorax depth and breadth have been found to be significantly correlated to the drag values (Clarys, et al. 1974). Following this finding, Chatard, *et al.* (1990); Lyttle, *et al.* (1998); Benjanuvatra, *et al.* (2001) have found the chest girth and maximum cross-sectional area, the body surface area, mass and height to correlate with the drag force. However the majority of studies to date have measured the anthropometric parameters of the body while the subject stands in an upright position with hands on the side. As the resistive forces are measured on a body in a streamlined position it is important to measure the anthropometric parameters while the body adopts a similar position.

To quantify the shape characteristics of body, the morphological indices important in the hydrodynamic studies of the aquatic animals were adapted for the human body. The relation between morphological indices of a human body and the resistive forces applied to it during glides has been investigated, from which some were found to be strongly correlated with the passive drag (Clarys, *et al.* 1974; Clarys, 1978a and Lyttle, *et al.* 1998). Similar to the anthropometric measures, the morphological indices in previous

studies have not been defined for the human body in a streamlined position that may affect the validity of those findings.

Posture is another important factor affecting the shape characteristics of body, hence its hydrodynamic parameters. The lower drag forces found for the more flexible swimmers were related to their ability to maintain a more streamlined posture during a glide (Chatard, *et al.* 1990). However no study until now has directly quantified the postural angles during glide, despite the fact that the shape of body is influenced by variations in the postural angles including the joint angles and the segmental angles of attack.

Thus in order to determine the true relationship between the size and shape characteristics of the body and its hydrodynamic and glide efficiency parameters there is a need to quantify the anthropometric measures, morphological indices and postural angles in the streamlined position.

In this thesis the relationship between the size and shape characteristics and the glide efficiency and hydrodynamic parameters are investigated with the new methods developed and with consideration of the actual anthropometry, morphology and posture of body in the streamlined gliding position.

1.1. Statement of the Problem

The purpose of these studies is to develop methods of quantifying the glide efficiency and the hydrodynamic parameters related to the performance in the glide phase of swimming. The important aspect of validity of the methods including their ability to distinguish between subjects in their glide efficiency and hydrodynamic parameters will be investigated. As the glide and the hydrodynamic characteristics are influenced by the size and the shape characteristics of the body during a glide, the relationships between the anthropometric measures, morphological indices and postural angles of the body in a

streamlined position with the glide efficiency and hydrodynamic parameters are investigated. .

To achieve this purpose the research comprises a series of studies:
Study 1: A displacement function is derived from the equation of motion of the body during a horizontal rectilinear glide. By fitting this function to the position time data of a body during a rectilinear horizontal glide, the glide efficiency is quantified. As the glide efficiency of a body is influenced by the body shape as well as by the body size, the size-related and the shape-related glide efficiencies are determined as separate entities. The validity and applicability of the method is established.

Study 2: A displacement function is derived from the equation of motion of the body during an inclined rectilinear glide. By fitting this function to the position time data of a body during a rectilinear inclined glide, and taking advantage of the component of net buoyancy as a constant parameter in the equation of motion the resistive and inertial parameters are quantified. As the resistive and inertial parameters of a body are influenced by the body shape as well as by the body size, the drag and added mass coefficients are determined to investigate resistive and added inertial properties of a body independent of its size. The validity and applicability of the method is established.

Study 3: The actual anthropometric measures, morphological indices and postural angles of the body in a streamlined position are determined, in order to quantify the size and shape characteristics of the body in the streamlined position. The correlations between these parameters and the glide efficiency and hydrodynamic parameters are investigated to determine the true relationships.

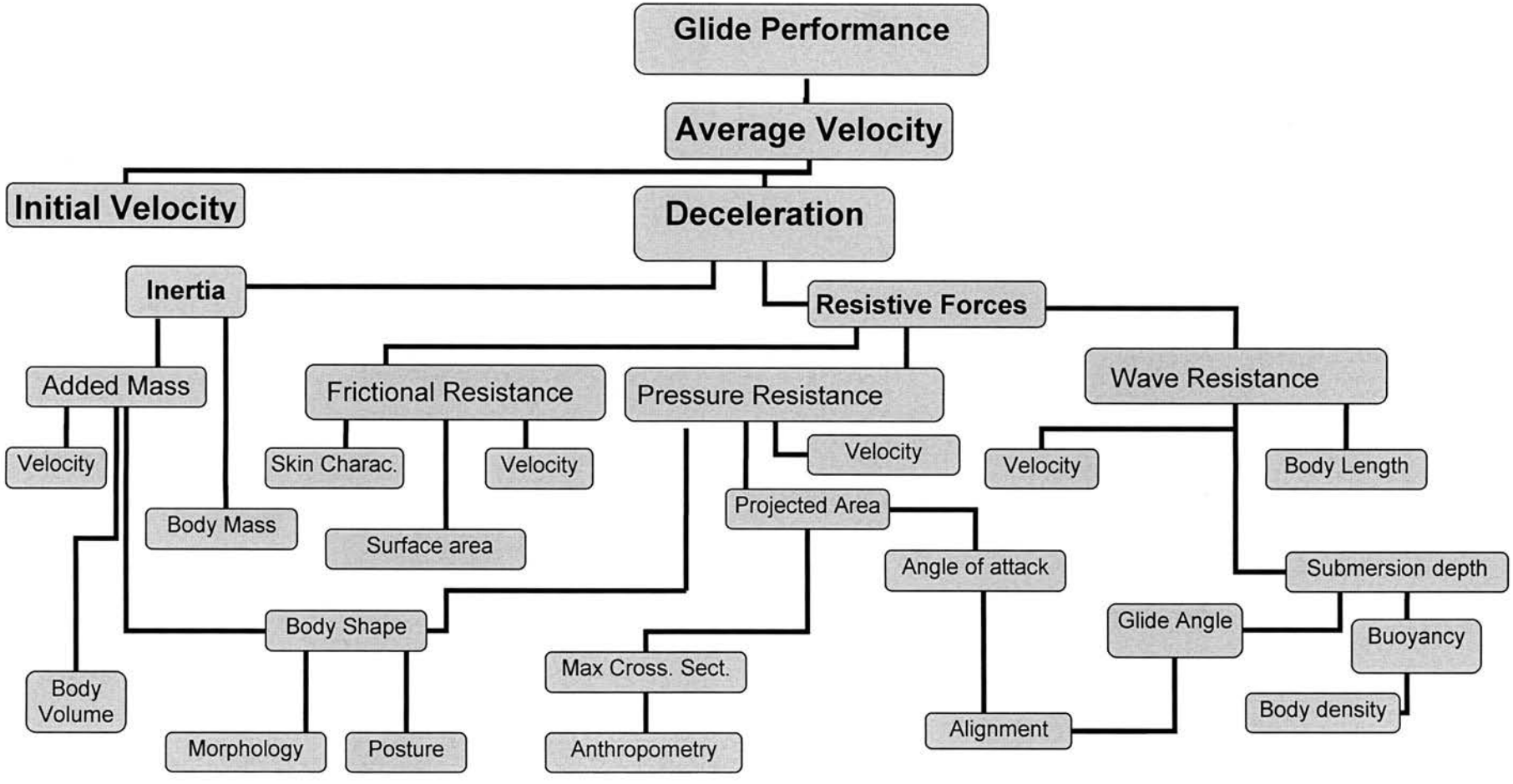

Fig .1. Deterministic model of glide performance and the influential kinematic and hydrodynamic parameters

Chapter 2

Literature Review

Glide efficiency has been introduced as an important aspect of glide performance in Chapter 1. Improving the glide efficiency can optimize glide performance while restraining physiological costs. Despite the fact that improvement in the glide efficiency can lead to substantial improvements in start, turn and stroke times; little is known about the efficiency of the glide and the hydrodynamic parameters contributing to it at realistic glide conditions.

This chapter starts by representing the glide model with specific focus on glide performance and its contributing factors. Studies that have examined the glide performance then are summarised to demonstrate the importance of introducing a new method to quantify the glide efficiency. Owing to the importance of hydrodynamics in glide efficiency a general background of fluid mechanic definitions and formulas applicable to the glide will be reviewed. This part of the review will focus on different types of the flow, sources of the hydrodynamic resistance, total drag and inertial properties including the added mass. This is followed by a review of hydrodynamic studies of the human body with great emphasis on methods of quantifying hydrodynamic parameters. Because the methods of quantifying hydrodynamic resistance based on the kinematics of a glide have been more frequently used for the hydrodynamic studies of aquatic animals than for the humans, studies in this area are reviewed along with the studies on the humans using similar methods. In reviewing the previous work attention is focused on scrutinizing the method, as the main purpose of the current study is to establish methods that would be useful for quantifying the glide efficiency and hydrodynamic parameters related to glide performance. Where possible the interdependency of the hydrodynamic parameters with anthropometric and

morphological characteristics is discussed.

2.1. Glide Model

Although a particular model that contains the specific glide contributing factors has not been developed before, the models for starts and turns have included the glide as one of their components.

Hay (1992) presented a model of the factors affecting the glide time, considering distance and speed as the basic factors, and related the changes in speed to the resistive impulse. Lyttle (1999) extended Hay's model to incorporate the resistive force components including the wave, friction and pressure drags. The new model considered the wetted surface area, cross-sectional area and glide depth. Sanders (2002) also extended Hay's model by including the depth, body posture and body alignment as the factors contributing to the resistive impulse.

Of the models in the extant literature to date, none includes the inertial properties as another important contributing factor to the glide efficiency. Thus, for the purposes of this study a new model is proposed with a specific focus on the glide performance and the factors affecting it. The factors like orientation, angle of attack, body mass and added mass have been added to the factors already known from the previous models.

The model in Figure 1 shows the influential factors and the relationship between the kinematic and hydrodynamic variables which determine the glide performance. The average velocity, as a measure of glide performance, depends on the initial velocity and the deceleration. Taking into account the Newton's second law of motion, and in the absence of any propulsive force, the deceleration is proportional to the resistive force and inversely proportional to the inertia. The inertia is the sum of the body mass and the added mass of water entrained with the body. The resistive force is a combination of different types of resistance including the skin, form, and wave drags.

All types of resistive force are correlated with the velocity of the moving body in a fluid. The frictional resistance (skin drag) is affected by the skin characteristics and the total surface area. The pressure resistance (form drag) depends on the projected area and the body shape. The projected area depends on the maximum cross-sectional area and the angle of attack while the body shape depends on the body morphological and postural characteristics. The maximum cross-sectional area is influenced by the anthropometric characteristics of the body, while the angle of attack is affected by the body alignment.

Wave drag is influenced by the body length and the submersion depth of the body. The buoyancy force and the glide angle influence the depth. The buoyancy is influenced by the body density, while the glide angle is influenced by the body alignment.

Elaborations of how these influential factors affect each parameter are presented in the 'Fluid Dynamics Background' section.

2.2. Glide Specific Studies

Methods of investigating glide characteristics include the timing and the measurement of average velocity and deceleration. An early method of studying the passive glide efficiency was introduced by Cureton (1940). He measured the time for gliding a known distance following push-off from the wall. He also measured the ability to glide for gaining the maximum distance before ceasing the forward motion. Although these can quantify the average velocity during a glide as a measure of the glide performance, the initial velocity and the deceleration may not be separated in this way.

To overcome this deficiency, the velocity of the body needed to be quantified for each instant. Craig and Pendergast (1979), proposed a method of measuring the instantaneous velocities of a swimmer using a swim-meter. The swim-meter consisted of a fine stainless steel wire which was attached to the swimmer from one end and going through

a system of pulleys and tension control sensors to a fishing reel from the other end. When the swimmer moves through the water the wire turned a DC generator and the voltage transmitted to the computer was proportional to the velocity.

Sharp and Costill (1989) directly measured the decay rate of velocity (deceleration) to detect differences between the shaved and unshaved bodies. A non-elastic line connected a waist belt of a swimmer to a wheel, rotated the shaft of a direct current generator. An exponential regression analysis was utilized to determine an exponential decay rate constant between 1 and 2 m/s for each trial.

Instead of using a swim-meter, Starling *et al.* (1995) determined the velocity profiles by digitising the hip as a marker representing the swimmer's body from the video collected at 50Hz. To detect the effect of the suit design on the swimming performance, Starling *et al.* (1995) compared the distances covered during 1.5 sec glide intervals at identical velocities. The distance covered during a 1.5 second interval was calculated by approximate integration of the area under the velocity curve over a 1.5 s interval. Although the significantly greater distance (0.05m) that was covered while wearing a torso swimming suit compared to the standard suit was attributed to the possibility of a decrease in the resistance, the increases in the inertia may also be considered as a source of advantage. Even if assuming that a wet torso suit and a standard swimming suit weigh the same, the increased inertia may be the result of a larger amount of water that would be entrained with the body when wearing a torso suit. This amount of entrained water, known as the 'added mass', is discussed further in the 'Inertia' section.

A limitation of these methods is that they are unsuitable for comparing inter-individual glides over different velocity ranges. Also, problems arise when comparing between individuals with different inertial properties.

In order to have a better understanding of the hydrodynamic factors contributing to the glide efficiency, a general knowledge of fluid dynamics is essential.

2.3. Fluid Dynamics Background

Glide efficiency is affected by the resistive force and the inertia. An overall knowledge of these two contributing factors helps to understand how the glide efficiency is related to these parameters. In order to recognize these concepts, the knowledge of different types of flow and their characteristics is essential.

2.3.1. Laminar and Turbulent Flow

Two distinct conditions of flow around a body are defined. These are the 'laminar' and the 'turbulent' flows. The laminar flow is characterized by smooth motion in layers of the fluid. The turbulent flow is characterized by the random three-dimensional motion of the fluid particles superimposed on the mean motion.

Whether the flow acting on a body is considered laminar or turbulent can be determined by calculating the Reynolds number which defines the ratio of the inertial to the viscous forces on the flow particles acting on a body. This can be calculated by

$$\mathrm{Re} = \frac{\rho.V.L}{\mu} \qquad \text{(Equation 2.1)}$$

Where, ρ is the fluid density, V is the body's velocity; L is the characteristic length of the object in the direction of the flow and μ represents a constant known as 'viscosity'.

For calculation purposes, when flow is parallel to the surface of a flat plate under typical flow conditions, the transition from a laminar to a turbulent flow is usually considered to happen at Reynolds numbers of 5×10^5. Surface roughness and free-stream turbulences are among the factors that affect the laminar to turbulent transition.

If assuming that the transition from laminar to turbulent flow of a gliding body such as the human in a streamlined position occurs at the same Reynolds number as for a flat plate, at a velocity of about 1m/s, only the flow over the arms and part of the head would remain laminar. At higher velocities (the initial stages of the glide) the length of body in laminar flow decreases. For example at a velocity of 2.5 m/s, only about 20cm of the body length which includes only the hands will remain in a laminar flow.

The transition from laminar to turbulent flow occurs earlier in a decelerating flow compared to a steady flow (Schlichting, 2000). Thus the transition happens at even lower Reynolds numbers in gliding bodies with decreasing velocity than in the bodies moving with a constant velocity. Skin roughness that embodies the height and shape of irregularities on the surface and the free stream turbulences, that is, the amount of random motions of the fluid particles, can cause the transition to occur even earlier for the glides under real conditions. Thus it may be concluded that for the ranges of Reynolds number corresponding to glides of the human body in the competitive swimming, the turbulent flow is dominant.

2.3.2. Resistive Force

A resistive force acts opposite the direction of travel as a body moves in water. This resistance, known as 'drag', is highly related to the flow conditions and the body characteristics. The term 'passive drag' refers to the hydrodynamic resistive force acting on a body that is not changing the orientation of the body segments, that is, on a body during a glide. The term 'active drag' refers to the hydrodynamic resistive force acting on a body that is changing the orientation of the body segments in an attempt to propel the body, for example, when kicking and stroking in swimming. The focus of this thesis is the resistive force due to passive drag.

2.3.2.1. Types of resistance

For a body travelling through water close to the surface three sources of resistance act on the body. Karpovich (1933) introduced three contributions to drag known as 'friction'; 'pressure' and 'wave making' resistances to swimming. Alternative terms are 'skin drag', 'form drag', and 'wave drag' respectively. In the model (Figure 1) used in this study the terms used are 'frictional resistance', pressure resistance' and 'wave resistance' respectively.

Frictional resistance (skin drag)

Frictional resistance or 'skin drag' is the contribution to the drag that exists due to the presence of a 'boundary layer'. According to the boundary layer theory the flow around a body is divided into two regions, one close to the body surface and the other covering the rest of the flow domain. Boundary layer is defined as that part of the flow adjacent to the solid boundary in which the effect of viscosity is important. In this area the flow velocity at the surface of the body is considered to be zero due to no-slip conditions. At increasing distances from the body surface the flow velocity increases until it reaches the free stream velocity at the boundary layer border. Beyond this border, which is outside the boundary layer, the flow is regarded as without friction since the velocities of different layers of the flow are the same.

In the boundary layer, the shear stress presents as a result of velocity variation is determined by the following formulae:

$$\tau = \mu . \frac{dv}{dy} \qquad \text{(Equation 2.2)}$$

Where τ is the shear stress, μ represents a constant known as viscosity and dv/dy represents the rate of change in tangential velocity to vertical displacement perpendicular to the surface. As a result of the no-slip condition, the velocities of the fluid particles at the surface of the body are assumed to be zero. On the other hand on

the boundary layer edge the velocity of the fluid particles is approximately (99%) of the 'free stream' velocity. Knowing the thickness of the boundary layer at different parts of the body, the average shear stress caused by the tangential flow can be quantified.

Because the velocity profile merges smoothly and asymptotically in the free stream the boundary layer thickness is difficult to be quantified analytically (Fox and McDonald, 1992). Although there are theoretical approaches to evaluate the boundary layer thickness, it is appreciably easier to evaluate it from experimental data.

The friction drag which is the total shear force applied to the body by the flow can be determined by the following experimental formulae:

$$D_f = \frac{1}{2} C_f . \rho . S . v^2 \qquad \text{(Equation 2.3)}$$

Where S is the total surface area or the wetted area, C_f is the empirical friction drag coefficient and v represents the velocity of the moving body.

For the reasons stated earlier it can be assumed that for a gliding human body at the gliding velocities during competition (1 to 3 m/s), flow is turbulent for most parts of the body. Turbulent flow has a thicker boundary layer and also much higher wall shear stress than the laminar flow. This causes the friction drag for the turbulent flow to be higher than for the laminar flow.

Surface roughness and characteristics affect the friction drag coefficient. Decreasing roughness to create a smoother surface decreases the amount of the frictional resistance for a gliding body. Latex swimming caps and body shaving are believed to reduce the friction drag by decreasing the surface roughness (Rushall *et al.*, 1994).

Although the friction drag may not be quantified for a human body with the experimental methods, Rumyantsev (1982), as cited by Vorontsov and Rumyantsev (2000), estimated friction drag to be only 2% of the magnitude of pressure drag for a swimmer travelling at 2 m/s, and therefore its contribution to total drag was assumed to be negligible.

Pressure resistance (form drag)

Pressure drag is the result of the differences between pressure at the leading and trailing edges of the body. Loss of momentum of fluid particles can cause a deficiency in the dynamic pressure within the wake of a body and results in the pressure drag.

Aquatic animals have a well streamlined shape and the skin friction is the dominant type of drag on them. On the other hand a human body lacks the ability to perfectly react with the flow and the pressure drag increases substantially as a result of this imperfection. In order to understand the reason for the increase in pressure drag, an understanding of how the water flows around a body is essential.

Flow impinges on the body somewhere at the frontal edge at a point called a 'stagnation point'. Then it divides into several parts each going to the sides, top and underneath the body. From this stagnation point, up to the point of maximum thickness, flow particles inside the boundary layer experience a net pressure in the direction of flow, that enable them to overcome the friction on the surface of the body (Fox and McDonald, 1992).

After passing the point of maximum thickness the pressure increases in the direction of flow. Thus the fluid elements experience a net pressure force opposite their direction of motion that slows them down. As the fluid particles in the boundary layer are also slowed down by the wall shear stress as a result of the skin friction, finally the momentum of the fluid in the boundary layer is insufficient to carry the element further in the region of increasing pressure. The flow layer adjacent to the body surface will be brought to rest and flow will separate from the surface at the point of separation.

Boundary layer separation results in formation of a relatively low-pressure region behind the body (Fox and McDonald, 1992). This region, which is deficient in momentum, is called 'wake', although wake is not necessarily the product of separation (Hoerner, 1965). Separation of the flow from the body leads to the formation of large and small eddies at the downstream part of the body and results in great changes in pressure distribution causing the pressure drag (Schlichting, 2000).

Pressure resistance can be quantified by the following formulae:

$$D_p = \frac{1}{2} C_p . \rho . A . v^2 \qquad \text{(Equation 2.4)}$$

Where D_p represents the pressure drag, C_p is the pressure drag coefficient, ρ is the fluid density, A is the projected area to the flow, and v represents the velocity of the moving body. Any inclination in the body alignment to the upcoming flow increases the projected area.

The term $\frac{1}{2} . \rho . v^2$ is called the 'dynamic' or 'stagnation' pressure, and is defined as the pressure required to bring a fluid particle to rest at the body. C_p depends on the body shape, angle of attack and the Reynolds number. The shape and the contour of body are important factors affecting the pressure resistance because they determine where the flow would separate from the body. Streamlined bodies are tapered in a particular way that enables the flow particles to be attached to their contour and result in moving the separation point to the trailing edge of the body (Fish and Hui, 1991).

The 'streamlined position' used in swimming is achieved by decreasing the exposed area to the flow and maintaining a tapered shape. These can be achieved by maintaining an elongated and stretched posture while maintaining a body alignment to the upcoming flow such that the 'angle of attack' is zero. Miyashita and Tsunoda (1978) found that having the head above the water while being towed on the surface increases the drag compared to having the head remains underwater. They explained that the increase in

the frontal surface area when the head is elevated causes a substantial increase in the magnitude of the pressure drag.

The exposed area or the projected area on a plane perpendicular to the upcoming flow has its minimum value when the angle of attack is zero. In this case the projected area can be replaced by the maximum cross-sectional area in the drag formulae and hence minimises the pressure drag value.

By streamlining, the swimmer reduces the adverse pressure gradient that occurs behind the point of maximum thickness on the body. This delays boundary layer separation and thus reduces the resistive force. For example, having the arms apart would create 7% more resistance than the streamlined posture with one hand above the other. The position with the arms alongside the body such as after the long pull breaststroke creates about 21% more drag than the streamlined posture (Bulgakova and Makarenko, 1996) [as cited in Vorontsov and Rumyantsev, 2000]. The reduced drag force in a streamlined position is the result of a decrease in the projected area when the arms are extended forward compared to when they are positioned around the chest area. Also in a streamlined position the bluff areas of the body like the shoulder and the head are partially covered by the arms so that less change in the momentum of the flow occurs when passing around these parts of the body.

Another factor that affects the pressure drag is the 'fineness ratio'. The fineness ratio is regarded as an indicator of the degree of streamlining and can be quantified by the following formulae.

$$FR = \frac{h}{d} \qquad \text{(Equation 2.5)}$$

Where h is the length and d is the thickness of a body. It has been found that the fast-swimming animals possess an optimum range of fineness ratio to reduce the pressure

drag (Fish and Rohr, 1999). A fineness ratio of 4.5 would give a streamlined body the lowest pressure drag coefficient for a maximum volume (Hertel, 1966). The greater length and lower thickness of a human body in a streamlined position than the position with arms alongside the body would result in a higher fineness ratio. This may be regarded as another advantage a swimmer gains by adopting a streamlined position.

Another indicator of the degree of streamlining is the position of maximum cross-sectional area that determines where the flow separation is likely to occur (Mordvinov, 1972). The relative position of maximum cross-sectional area can be defined by the following formula.

$$P_s = \frac{h_c}{h} \qquad \text{(Equation 2.6)}$$

where h_c is the distance between the leading edge and the maximum cross-sectional area and h is the body length. The larger values of the relative position of maximum cross-sectional area indicate that the flow would be separated further downstream on the body. For more streamlined bodies the transition to turbulent is expected to happen at this point. For example, the relative position of maximum cross-sectional area of 0.34-0.45 for dolphins is believed to be responsible for maintaining a laminar flow up to 45% of the body length (Fish and Hui, 1991).

Further delay in separation is also possible by promoting the turbulent flow in advance. Having a higher momentum, a turbulent boundary layer is more resistant to separation. Thus, attempts have been made to increase the surface roughness by adding dimples on a golf ball which have been designed to "trip" the boundary layer and to guarantee the turbulence. Adding a roughness element to a sphere also can suppress local oscillation in location between laminar and turbulent flow in the boundary layer and reduce the variations in drag (Fox and McDonald, 1992).

Another way of delaying separation is to mix the high speed free-stream flow with the low-speed flow in the boundary layer. This increases the momentum at the near wall region and decreases the pressure drag. 'Vortex generators' are low aspect ratio profiles installed upstream of the vulnerable areas to prevent separation. For swimming, vortex generators have been used on the areas vulnerable to separation on the back of a swimming suit and decreased resistance in experiments in a wind tunnel (Waring, 1999).

Although the pressure drag may not be quantified for a human body with the experimental methods, Rumyantsev (1982), as cited by Vorontsov and Rumyantsev (2000), estimated the pressure drag to account for 95% of total drag for a swimmer travelling at 2 m/s, and therefore make a significant contribution to the total drag.

Wave making resistance (wave drag)

Wave making resistance or wave drag is another kind of drag acting on a body moving close to the surface. Part of the energy from the moving body is used to lift the water against gravity resulting in the formation of waves on the surface (Vorontsov and Rumyantsev, 2000).

Wave drag can be calculated according to the following formulae:

$$D_w = \frac{A^3}{\lambda^2}.\rho.\sin^3\alpha.\cos\alpha.\Delta t.v^3 \qquad \text{(Equation 2.7)}$$

where A is the amplitude of the wave, and λ is the wavelength, v is the velocity of the body and α is the angle between the direction of general centre of mass movement and front of the prime wave (Vorontsov and Rumyantsev, 2000).

The wave drag is highly related to Froude number that determines the ratio of inertial to gravitational forces applied to fluid particles. This dimensionless ratio can be quantified as:

$$Fr = \frac{v}{\sqrt{L.g}}$$ (Equation 2.8)

v is the velocity of the moving body, L is the length of body in direction of flow and g is the gravitational acceleration constant.

Wave drag is believed to increase with the Froude number, above a Froude number of 0.25 drag increases rapidly. The drag increase would be again more moderate when the Froude number reaches the value of 0.45, mainly due to the excess lift generated by the body moving on the surface. Assuming the human body in a streamlined position with an extended length of 2.5 m, it can be anticipated that for the velocities between 1 to 2.5 m/s on the surface the wave drag contributes to at least 50 % of the total resistance (Vennell *et al.*, 2005).

Depending on the depth at which the body travels it experiences different amounts of the wave drag. Hertel (1966) performed experiments on a spindle in laminar flow at different submersion depths. He found that at a depth of three times the body thickness the wave drag becomes negligible, and wave drag has its maximum value when it is submerged just underneath the surface.

Lyttle *et al.* (1998) and Vennell *et al.* (2005) established that a swimmer encounters relatively higher resistance at the surface and this excess resistance would be negligible at a depth of about 0.6 m underwater. This can be the main reason that after starts and turns swimmers try to glide at adequate depth whenever possible to avoid the excess effect of the wave drag.

Surface is not the only limiting factor for an underwater glide, as the fixed surface effect on the bottom limits the maximum velocity a body could travel (Larsen *et al.*, 1981). The maximum velocity a body can travel through a fluid with known depth could be determined by the following formulae.

$$V_{max} = \sqrt{g.H}$$ (Equation 2.9)

where g is the gravity acceleration and H is the water depth from the surface to the bottom. This gives a maximum velocity of 4.5 m/s for the standard swimming pools with a depth of 2 m.

Although the wave drag may not be quantified for a human body with experimental methods, Rumyantsev (1982), as sited by Vorontsov and Rumyantsev (2000), estimated the wave drag to account for only 6% of the total drag for a swimmer travelling at 2 m/s, and therefore did not consider it to make a significant contribution to the total drag.

2.3.2.2. Overall resistance (total drag)

The sum of different types of resistance a body experiences in a fluid is known as 'total drag'. Total drag can be estimated by the following formulae,

$$D_d = \frac{1}{2} C_d.\rho.A.v^2$$ (Equation 2.10)

D_d represents the total hydrodynamic resistance, ρ is the water density, v is the velocity of body and A is the reference area. Depending on which source of drag is the dominant type of resistance for different types of bodies 'A' can be referred to as either projected area or the total surface area. In the case of humans, because of the dominance of pressure drag compared to other types of drag for a submerged body at an adequate depth, the projected area replaces the reference area in the total drag formulae. When the body is well aligned to the flow with minimum projected area, and zero angle of attack the projected area has its minimum value equal to the maximum cross-sectional area.

In cases where selection of reference area is difficult; a parameter would be defined as drag-area that is the product of reference area and the drag coefficient (Hoerner, 1965). Drag-area is the ratio of total drag force to the dynamic pressure and can be interpreted

as a virtual area on which a normal force equal to the drag force would be applied if the area would be exposed to a pressure equal to the dynamic pressure.

Drag coefficient (C_d) is an empirical constant, which is dependent on the body shape, angle of attack, surface roughness and the flow characteristics and is an indicator of the streamlining level. Because of the complexity of human morphology compared to other objects or aquatic animals, there is not an exact behaviour for the drag coefficients along wide ranges of Reynolds numbers. Since the values of C_d are not completely known for different ranges of Reynolds numbers and shapes, the total drag forces are usually determined by experiment and measuring the drag force directly.

It is highly popular in the swimming literature to report a resistive factor as the ratio of total drag force (D_d) to the velocity squared. A resistive factor (C_R) incorporates the maximum cross-sectional area (A), the fluid density (ρ) and the drag coefficient (C_d) according to the following formula.

$$C_R = \frac{1}{2} C_d . \rho . A \qquad \text{(Equation 2.11)}$$

Although it has been established that the streamlined position creates the minimum hydrodynamic resistance compared to other postures (Counsilman, 1955; Hairabedian, 1964 ; Kent and Atha, 1970 and Maiello *et al.*, 1998), the human body is far from being completely streamlined and does not possess the basic hydrodynamic features for efficient progression in the water (Clarys, 1978b). While it has the same fineness ratio (defined based on height not the extended length), as a dolphin, the human body experiences much greater hydrodynamic resistance at the same speed. The reason for that is the existence numbers of areas of sudden changes in the flow like the head, shoulders, buttocks, knees, and heels, which prevent the water from flowing smoothly around the body and increases the overall resistance (Vorontsov and Rumyantsev, 2000).

2.3.3. Inertial Properties

Newton's first law of motion states that "every body persists in its state of rest or uniform motion in a straight line unless it is compelled to change that state by a force impressed on it". The characteristic of a body that retains its uniform motion and resists any change in its status is its 'inertia'.

Thus, a gliding body tends to keep moving without any changes in the velocity while the resistance is acting to slow it down. In a vacuum the only source of inertia is the mass of the body, while in the presence of a fluid a particular amount of the fluid around body 'added mass' acts as inertia in addition to the body mass.

The added mass acts as a resistance when the body is accelerating as it resists the increase in velocity. When decelerating, added mass helps to retain the body's velocity and acts as a virtual propulsive force.

Analytical studies of the added mass have been based on the potential flow theory that assumes no viscosity for the entire flow. Using this assumption the added mass coefficient has been found for the spheroids and for the bodies of revolution (Landweber, 1961).

2.3.3.1. Source of added mass

The added mass represents the particles of fluid adjacent to the body that move with the body to varying degrees, depending on their position relative to the body. In principle every fluid particle would accelerate to some extent as the body moves, and the added mass is the weighted integration of this entire mass (Newman, 1977).

It can be argued that the added mass is affected by the same phenomena that contribute to the resistive forces namely the boundary layer, the flow separation and the presence of waves at the surface.

Skin-related added mass

When the fluid is stationary and the body is moving due to no slip conditions at the body surface (as was explained under skin friction), the fluid particles at the surface of the body would move with the same velocity as the body, while outside the boundary layer the fluid particles stay still. In the boundary layer, shear stress causes the different layers of fluid to move with the speeds that decrease with increasing distance from the body surface. A simplifying assumption is that a fraction of the boundary layer thickness moves with the same speed as the body and the remaining part stays still. The moving water represents a source of added mass in the areas of attached flow. The amount of the added mass then depends on the thickness of the boundary layer and the relative velocity distribution of the flow in the boundary layer.

The fact that "due to viscosity, bodies in real fluids experience other effects in unsteady motion, and measured values of the added mass differ somewhat from theory-based predictions that assume an ideal fluid" (Massey, 1998) further supports the above argument.

Wake-related added mass

In the areas of flow separation a wake forms in which the relative velocity of the fluid particles to the body is zero. During deceleration this bulk of fluid needs to be decelerated at the same rate as the body and acts as an added inertia. The fact that the direction of motion and the flow pattern affect the added mass (Massey, 1998) can further support this statement.

Wave-related added mass

The waves created by a swimmer move at the same velocity as the body. During an unsteady motion the waves entrain with the body and act as a source of added mass. During acceleration the wave formed at the leading edge of the swimmer known as the bow wave, would be pushed forward to gain the same velocity as the body. This acts as

a source of excess resistance in acceleration and hence contributes to the added mass. During deceleration the waves formed at the trailing edge known as a 'stern wave' push the body forward and acts as a virtual propulsive force and hence contribute to the added mass. The same argument can be applicable to the transverse waves that propagate on lateral sides of the body if the components of velocity of these waves parallel to the velocity of travelling body are considered. This can be a justification for the changes in the amount of added mass by the presence of other boundaries like the free surface (Massey, 1998).

Note

As the phenomena mentioned above are not exclusive features of the unsteady conditions, even in the steady conditions some fluid is entrained with the body (moving with the same velocity as the velocity of the travelling body). However, in the steady conditions in which acceleration is zero the inertia does not contribute to the balance of forces (i.e. the resultant force applied to a body is equal to the virtual mass times zero acceleration), the virtual mass only would be taken in to account when the inertia becomes important, that is, during the periods of acceleration or deceleration.

2.3.3.2. Total added mass

Thus, the total added mass is the sum of the added masses according to the contributions of the added mass due to each of the boundary layer, separation, and wave effects. The total added mass can be determined by the following formula:

$$m_a = C_a.\rho.V \qquad \text{(Equation 2.12)}$$

Where m_a is the added mass, ρ is the density of water, and V is the body volume. C_a is the dimensionless added mass coefficient and can be defined as the ratio of the accelerated mass to displaced mass of the fluid by the body (Newman, 1977).

The added mass coefficient for a prolate spheroid, a shape like a rugby ball, of a length twice the diameter is 0.20. Increasing the length to diameter ratio to six will decrease the added mass coefficient to 0.05 (McNeill, 1968). Added mass decreases with increasing the streamlining. For a porpoise the added mass coefficient is about 0.045 (Lang and Daybell, 1963). There is no information available on the amount of added mass for deceleration during a glide of a human body.

2.3.3.3. Virtual mass

During a glide, the inertia is the sum of mass of swimmer and the added mass of water. This sum is called 'virtual mass'.

$$M = m + m_a \qquad \text{(Equation 2.13)}$$

Where M represents the virtual mass, m represents the body mass and m_a is the added mass. A virtual mass coefficient (c_m) can be defined as the ratio of virtual mass (M) to the mass of body (m).

$$M = c_m.m \qquad \text{(Equation 2.14)}$$

The relationship between the virtual mass and the added mass coefficients

Replacing the added mass from Equation (2.12) and the virtual mass from Equation (2.14), in Equation (2.13) yields the following Equation (2.15):

$$c_m = 1 + \frac{C_a.\rho.V}{m} \qquad \text{(Equation 2.15)}$$

As the ratio of the body mass to the body volume represents the body density, Equation (2.15) can be rewritten as,

$$c_m = 1 + \frac{C_a \cdot \rho}{\rho_b}$$ (Equation 2.16)

ρ_b represent the body density, ρ is the density of water, C_a is the added mass coefficient and C_m is the virtual mass coefficient.

2.4. Hydrodynamic Studies from Swimming Literature

Due to difficulties of quantifying hydrodynamic parameters of a human body theoretically, the majority of the studies have relied on experimental methods. In experimental methods the total drag can be quantified either by directly measuring the force or by calculating drag based on the kinematics of a gliding body.

The direct method requires measuring the resistive forces while the body is towed or exposed to a flow. The methods of calculating hydrodynamic drag based on kinematics of a glide do not require force measurement devices and drag can be calculated based on the kinematics of a gliding body knowing its added mass. But the added mass of a human body during deceleration may not be approximated by the added mass of bodies of revolution (Landweber, 1961) due to the fundamental shape differences and there has not been any known method to measure it directly.

In this part the literature would start by reviewing the method of direct force measurement that has been more popular in the swimming literature. The limitations and advantages of each method would be discussed. This then would be followed by reviewing the methods of calculating the resistive forces based on the kinematics of glide. For each study the outcomes were discussed with reference to the underlying fluid dynamics principles.

2.4.1. Force Measurement Methods

The force can be measured while a body is being towed in the still water or exposed to a flow respectively. The forces acting on a body in this condition are the drag force opposite the relative direction of motion of the body to the flow and the holding or towing force in the relative direction of motion of the body to the fluid. In accordance with Newton's second law of motion, the resultant force applied to the body equals the virtual mass multiplied by the acceleration. At a constant velocity the total drag force is equal to the towing or holding force. In this equilibrium condition the inertia does not affect the measurements.

2.4.1.1. Force measurement during towing

This includes measuring the towing force required to move a body within the still water. For this purpose the stationary and the moving apparatuses can be used.

Stationary apparatuses

These apparatuses have been used widely in the study of the hydrodynamic resistive forces in swimming. In these kinds of devices a cable on a rotating winch on the waterside pulls the body through the still water. The drag force is equivalent to the towing force measured for different constant velocities.

According to Karpovich (1933), attempts to measure passive drag by towing were pioneered at the beginning of the twentieth century by DuBois-Reymond (1905) who towed subjects behind a rowboat and measured force by a dynamometer. Difficulty in maintaining a steady speed resulted in a low reliability of the results.

Amar (1920) stated that water resistance for a towing body could be calculated by multiplying a constant and area of the greatest cross section times the velocity squared. He reported the constant to be equal to 73 or 55, which correspond to the drag

coefficients of 0.11 to 0.15. Due to lack of information on the method of the measurement the values presented had been under question.

To find the hydrodynamic resistance of a body on the surface in a more accurate way, Karpovich (1933) developed a more advanced apparatus known as a 'Resistogragh' to measure the towing forces. He used an electric motor with various rotating speeds to tow the subject on the surface. Using a system of pulleys and a spring he developed a smart way of recording both the forces and the towing velocity graphically. By towing 11 male and three female swimmers at different constant velocities he found the resistive factor to be more while towing subjects on their back (supine) than in the prone position. Also in his study, men had greater resistance than women in the both gliding positions. Although Karpovich reported the body mass and the height to make comparisons possible, there was a lack of information on the body cross-sectional area and so a drag coefficient could not be quantified.

Karpovich also found that turning the head to breathe increased the level of resistance. And suggested that during breathing some changes in the body posture might occur that increase the projected area exposed to the flow. It was observed that resistance increased when the swimmer was towed with acceleration compared to a steady speed at each corresponding velocity. Although he did not address the possible cause of this difference it is now known that the discrepancy is due to the effect of added mass that acts as an excess resistance during acceleration.

Alley (1952) used a suspended type apparatus for measuring the drag forces of the subjects while towing them at the surface. A system of motor, shaft and pulleys was mounted on the wooden framework while in a balanced position. The force exerted by towing the swimmer via a cord caused the suspended system to deviate from its vertical alignment. The force upon the suspended apparatus was transferred by a flexible chain and measured by a spring. In order to eliminate the effect of between individual differences on the resistive force values, Alley (1952) measured the drag forces of a

single subject in a prone streamlined position over velocities between 0.34 m/s and 1.94 m/s on the surface. He found that there was a shift between the drag forces when towing velocity increased from 1.6 to 2 m/s mainly due to an abrupt increase in the values of the wave drag due to the observed bow wave. Alley (1952) also observed that the drag was relatively lower when a floating device supported the legs, than in an unsupported condition, especially at the lower towing velocities. This can be attributed to the increase in the projected area when the legs 'drop', and the consequent substantial increase in the pressure drag (Figure 1). Too much swinging motion of the apparatus was one of the disadvantages of his method. Also, due to a higher position of the whole towing system, the towing rope could not be connected to the subject in a horizontally aligned orientation and the rope exerted some upward force as well. This caused variations in the swimmers' positions and inaccuracies in the measurements.

To prevent swinging motions and eliminate the effect of a system's own weight on the force measurements, Counsilman (1955) introduced a rigid apparatus by replacing the spring by two rigid metal beams with a strain gauge attached. This increased the accuracy of the force measurement. Counsilman towed the subjects at 10 different speeds at prone, side, and rolling positions on the surface. Minimum drag occurred in the prone position and the maximum drag when the subjects were rolling. He concluded that the increased drag during the rolling was due to the fact that the body was less streamlined because the legs were used as rudders to create rotation. He also related it to the fact that the excess velocity of the body segments due to having both the rotational and transitional motion-compared to a non–rotating glide in which the velocity of body is only due to transitional motion-may increase the drag. Counsilman concluded that this may have caused an abrupt change in the direction of the flow that increased the possibility of flow separation and a substantial increase in the size of the wake and the pressure drag. It can also be argued that the body rotation may have increased the wave drag by creating more disturbances to the surface.

Instead of measuring the towing force, Hairabedian (1964) decided to measure the power requirement for towing a body in still water. The towing system was an electric motor with a gear reduction apparatus and a clutch system, which allowed attainment of the desired speed in a short time. The power requirement for towing the swimmer at a constant speed on the surface over a 20 m length was measured by a power meter over velocities of 1.7 m/s, 2.1 m/s and 2.5 m/s. Different power requirements were found for towing the subjects on the surface with different hand and head positions. A significantly higher power requirement was found for towing bodies in a streamlined position in which the hands were apart compared to when they were together. This was due to the fact that having the hands apart expose the head directly to the flow. Also, raising the head increased the amount of power required to tow the body, due to difficulties in maintaining a streamlined posture and substantial increase in the projected area. Despite the ability of this method to distinguish the differences between the powers required for the two different positions, a drag value could not be quantified separately due to the difficulties in quantifying the power lost in other ways like the heat in bearings at various speeds.

Kent and Atha (1971) used a motor driven drum to tow the swimmers at different passive positions on the surface resembling those in breaststroke. A three-pulley dynamometer recorded forces while towing three male subjects at velocities up to 1.5 m/s while adopting five different body positions each time. They concluded that the post-trust position (similar to a streamline position with the legs abducted) produces twice as much resistance as a streamlined position with the legs adducted. When the legs are apart part of the legs would fall outside the maximum cross-sectional area of the body in a streamlined position (the chest area). This causes an increase in the projected area to the flow that leads to an increase in the pressure drag and overall resistance.

Chatard *et al.* (1990) used a mechanical winch for towing the swimmers at 1.4 m/s on the surface over a 13 m distance. A strain gauge with a load cell connected to a strain bridge was used to measure the forces of the towed swimmer dragged via a flexible steel

cable. For improved accuracy the linearity of the strain gauge had been tested across different forces. There was a negative correlation between the passive drag and the swimming performance that was attributed to the ability of the elite swimmers to maintain a more streamlined position during the towing as a result of the practice during training. Height, body surface area and weight were found to be significantly correlated to the passive drag. Although height was expected to have negative correlations with the wave drag, the existence of a positive correlation with the total drag may be due to the interdependency of height with the maximum cross-sectional area between the subjects. It is possible that tall subjects possessed higher maximum cross-sectional areas than short subjects thereby causing greater drag among tall subjects. Also, since the total surface area was calculated based on a regression formula that incorporates both the height and the weight (Du Bois and Du Bois, 1916) a positive correlation between the drag and the total surface area could have been expected.

Chatard and colleagues also found a significant increase for the drag force when swimmers exhaled maximally compared to when the swimmers were maximally inhaled. As the cross-sectional area of the chest decreases in a maximal expiration, a lower drag would have been expected. However, due to a higher buoyancy force when maximally inhaled, the body would be positioned higher relative to the surface resulting in a decrease in the wave drag (Hertel, 1966).

Instead of towing a body with a winch and measuring forces with a strain gauge, Sheehan and Laughrin (1992) developed a versatile towing device using a dropping mass and a series of pulleys and sprockets. By choosing a definite set up, the gravitational force on the dropping mass was transformed and reduced to a factor of 9 to be applied as the towing force to the body. On the other hand a maximum falling distance of 1.5 m could tow a subject over a 13.5 m distance at predetermined depths. The dropping velocity of the weight was measured by monitoring the rotational velocity of the sprocket with a potentiometer. Knowing the velocity of the dropping mass the velocity of the towed body could be quantified simply. Each towing contained a period

of acceleration, a period of dynamic equilibrium with a constant speed. The towing force equal to the weight of the dropping mass was correspondent to the drag force for a particular velocity during the constant velocity period. By testing a single subject it was found that the resistive force a body encounters during towing at a velocity of 0.86 m/s is half the resistance at 1.3 m/s. Sheehan and Laughrin (1992) predicted that for creating higher velocities a heavier weight is required and this may restrict the use of these devices.

Klauck (1998) developed the dropping mass device to be used under both the accelerated and the constant velocity towing. A special pulley and wheel system, consisting of two concentrically attached wheels with the diameter ratio of 1/10, was developed to move a body at the surface from rest to a constant speed. A mass of 100 kg dropping over a 5 m distance was used to rotate the smaller wheel, while the larger wheel was connected to a rope for towing a body over a 50 m distance. Measuring the rotational velocity of the pulley and wheel and knowing the radius and the moment of inertia of the wheel the towing force was calculated. Assuming the drag to be proportional to the velocity squared, a resistive factor was calculated for the subjects ranging from 25 to 35 kg/m for the velocity range of 1.0 - 1.6 m/s.

Klauck also considered the period of acceleration to measure the added mass. By calculating the towing force created by a dropping mass in acceleration, and assuming that the resistive forces are the same for each corresponding velocity in the accelerated and the constant velocity towing, the added mass was calculated. The values of the added mass were found to range between 30-70 kg but no explanation regarding the causes of the variations was proffered. It is possible that due to an insufficient lift that is required to maintain legs aligned with the body the subjects were not able to maintain their horizontal alignment at lower velocities resulting in the excess drag forces (Alley, 1952). It should also be borne in mind that the value of added mass during acceleration is different from the added mass values during deceleration. Therefore, the accelerated towing method cannot be used to determine the added mass of body during a glide.

In order to determine the depth effect on the amount of the resistance experienced by the body underwater Lyttle *et al.* (1999) developed an adaptive towing device. A servo controlled mechanical winch was used to tow the swimmer along a 12 m measuring distance. A pulley system was designed to enable the towing at the different depths with a horizontal force. In their towing apparatus the load cell and the amplifier moving upstream of the body transmitted the signals via a FM transmitter to the data collection computer. This could have the advantage of recording the forces closer to the body and eliminating the effect of the cable length and weight on the measured forces. On the other hand the increase in free stream turbulence caused by the capsule container upstream of the swimmer affects the values of the friction drag and the total drag measurements.

Using this device Lyttle *et al.* (1998) found different drag forces for different constant towing depth and velocities, resembling those experienced by glides following starts and turns. Four constant depths were set from the surface to 0.6 m underwater with 0.2m increments. Each subject was towed at six different velocities, ranging from 1.6 to 3.1 m/s in 0.3 m/s increments in each depth. Significantly higher drag forces at 0.2 m depth were found compared to 0.4 or 0.6 m which did not show any significant drag difference in-between. This was attributed to the effect of the wave drag and it supports the findings of Hertel (1966). Based on the results Lyttle and colleagues suggested that for gaining the maximum drag reduction the swimmers should do their glides at a depth of more than 0.4 m underwater especially for the velocities more than 1.9 m/s.

Lyttle *et al.* (1998) also found that the chest girth and slenderness index were significant covariates of the drag forces. This highlights the need to include them in passive drag studies. As the chest represents the maximum cross-sectional area of the body in a streamlined position, the dependency of the chest girth to the chest cross-sectional area may be assumed to be the reason for the correlation between the drag force and the chest girth. The slenderness index as the ratio of body height to the cubed body weight was

declared to be significantly correlated to the total drag. Despite the belief in the dependency of the wave drag and the slenderness index, no specific explanation on how this would affect the wave drag was provided.

Benjanuvatra *et al.* (2001) used the device developed by Lyttle *et al.* (1999) to measure the passive drag of the young swimmers on the surface at five different velocities. While no significant correlation was found between any of the anthropometric measures with the drag forces at towing velocities of 1.3 and 1.6 m/s, as the velocity increased, significant positive correlations were found between the drag forces and the height, mass, chest girth, cross-sectional and the body surface areas. The positive correlation between the chest girth, cross-sectional area, and the body surface area indicated a contribution of both the pressure and friction drag to the total drag. The existence of correlations between the height and the mass may also be a result of the interdependency of these parameters to the values of maximum cross-sectional area and the body surface area. A significant negative correlation was found between the ratio of the height squared to the maximum cross-sectional area and the passive drag values. Despite assuming this to be related to a decrease in pressure drag, no explanation on how it may affect this particular type of resistance was presented.

The fixed apparatus towing devices have been the most widely used device in the studies of the hydrodynamic resistive forces in swimming. Although the majority of these devices have been designed for towing bodies on the surface more recent designs by Sheehan and Laughrin (1992) and Lyttle *et al.* (1999) facilitated the underwater force measurements at different depths. This enabled the hydrodynamic resistance to be measured under the depths at which a body normally glides in a streamlined position. While measuring the body resistance and the added mass is possible with accelerated towing (Klauck, 1998), the measurement during deceleration to resemble glides is not feasible with a fixed apparatus towing method.

Moving apparatuses

These kinds of devices are moving carriages that have the ability to move with an adjustable speed above the water, while towing the body along. In comparison to fixed towing apparatus these devices have been used more recently in the swimming research. According to Van Manen and Rijken (1975), the use of the water channels with original application for the ship model drag measurements, was introduced to swimming in 1968. A towing carriage driven on the rail by a precisely controlled speed electric motor towed the subject via a telescopic rod. The telescopic rod allowed the towing at the different depths. The forces were measured with a strain gauge force transducer while towing the subjects along a 200 m water tank.

A number of studies on the human body hydrodynamics used the same device for measuring the hydrodynamic resistance in prone streamlined positions including the studies of Van Manen and Rijken (1975), Jiskoot and Clarys (1975), Clarys and Jiskoot, (1975), Clarys *et al.* (1974), Clarys (1978a), Clarys (1978b) and Clarys (1979).

Van Manen and Rijken (1975) detected differences in the passive drag of the subjects with variable levels of the swimming skill. Three swimmers with the similar weight and height but each at a different level of the swimming performance at world, national and average club levels were towed at the surface. It was found that the drag force decreased with an increase in the swimming level. It was concluded that the skilled swimmers were more able to control their body and adopt a more streamlined position than the swimmers at the lower levels. This is related to the ability of elite swimmers to adopt the most appropriate body alignment and subsequent decrease in the pressure drag.

Jiskoot and Clarys (1975) towed the male physical education students at the surface at the velocities between 0.7 to 2 m/s and underwater for the velocities ranged from 1.5 to 2 m/s with 0.1 m/s increments. They found that the resistive force to be greater when subjects were towed in prone streamlined position at a depth of 0.6m underwater than at the surface. The results were contrary to the findings of Hertel (1966) who found a

decrease in the body's total resistance due to the reduction in wave drag with increasing depth. Given the lack of any visual control on the posture of the towed swimmer, it is quite possible that the posture under the surface was not controlled properly and the misalignments increased the angle of attack and the projected area. Also the higher drag forces underwater may have resulted from adopting a less streamlined posture and consequently increased the pressure drag.

Clarys and Jiskoot (1975) showed the differences between passive drag of towing bodies in the prone and the side (45 degree twisted) streamlined positions on the surface when towed at the velocities ranging from 1.5 to 1.9 m/s. The side position creates significantly less resistance than the prone position for the towing velocities up to 1.8 m/s. At 1.9 m/s resistance was less for the prone position. Their results contradicted the finding of Counsilman (1955). This can be attributed to the differences between definitions of the side position between the two studies. The measured resistive forces for the prone streamlined position agreed well with the results of Karpovich (1933) and Alley (1952).

Clarys *et al.* (1974), Clarys (1978 a), Clarys (1978 b) and Clarys (1979) studied the effects of the anthropometry on the passive drag forces measured by towing subjects across the towing velocities of 1.5 to 2 m/s on the surface. They measured the body volume, cross-sectional area and the wetted surface area of the whole body and the breadths, thicknesses, circumferences and the lengths of different limbs for each subjects. Some of the anthropometric parameters including the head and thorax circumferences trochanterion and the stylion breadth and thorax depth were significantly correlated with the resistive forces. These studies highlighted the influence of the anthropometric parameters on the hydrodynamic resistance and indicate the need to report them in any hydrodynamic study of the human body.

Clarys *et al.* (1974), Clarys (1978 a), Clarys (1978 b) and Clarys (1979) also developed a rationale based on the shape parameters that are important for the ship resistance, and

measured series of the dimensionless indices such as the ratios of height to maximum breadth, height to thickness, height squared to maximum cross-sectional area, height squared to wetted surface area and the breadth to thickness for each subject. A 'slenderness index' was defined as the ratio of height to the third root of the body volume as an indicator of a body's wave making aptitude. It was concluded that the dimensionless ratios like the height to cross-sectional area and the height squared to the surface area that were significantly correlated to the passive drag values were indicators of the pressure and friction drag respectively. However, no specific explanation on how these indices may contribute to different types of drag was presented.

In order to collect force data over a longer period of time, the moving apparatus can be used continuously over a circular path. For measuring drag on the seals, Williams and Kooyman (1985) utilized a special electrically driven towing carriage that travelled the perimeter of a 'ring' tank. The towing force was measured using a load cell, which was attached to a nylon towing towrope. Using this device the drag of a submerged human at a depth of 1m and velocity of 2m/s was found to be five times the drag for a submerged seal with similar weight at the identical depth and velocity. This study highlights further the fact that the human body does not possess a streamlined shape compared to the aquatic animals. As a result of the presence of the areas of sudden change to the flow on a human body like buttocks as well as the head and the hollow area between the forearms, the water is not able to flow as smoothly as it flows over the streamlined body shape of a seal which is a single fuselage with round contours.

Mollendorf *et al.* (2004) used a rotating platform with adjustable speed to tow the swimmers in the streamlined positions in an annular pool with 58.6 m circumference. The swimmer held onto a handle which was connected to a mounted dynamometer fixed on the platform. The method was used to detect differences between different types of swimming suits that covered different parts of the body. By making the assumption that the friction drag is a function of the velocity, the pressure drag is proportional to the squared velocity and the wave drag to the fourth power of velocity the different types of

drag for each suit were separated. Their claim about wave drag seems to be different from the previous authors that believed the wave drag increases with the cubed velocity (Vorontsov and Rumyantsev, 2000). The validity of using a flat plate friction drag coefficient for the human body and the possibility that the different coefficients 'play against each other' should further be examined when using this method.

Generally, moving apparatuses enable towing forces to be measured over a longer distance of the water tanks or the annular pools, compared to the stationary apparatus that enable the towing over a shorter length of a swimming pool. The moving apparatus also provides the opportunity for the forces to be measured in deceleration, as a rigid rod attached to the body enables the force to be measured in both the forward and backward directions. Although the decelerated towing of a body in a way that resembles the glide kinematics seems to be arduous, measurement of the hydrodynamic resistance and the added mass under a closer condition to the glide may be possible.

2.4.1.2. Force measurements by exposing the body to the flow

Drag measurement in a fixed position requires exposing the body to the moving fluid and measuring the force required to hold it in the flow. Flumes and wind tunnels can produce a uniform flow appropriate for testing.

Flumes

For measuring the drag with this device the body can be exposed to the oncoming flow while fixed with the force measuring devices.

Miyashita and Tsunoda (1978) used a flume with a speed control impeller, which has the capability of producing a flow current of up to 2.5 m/s. A cord held by the swimmer was attached to a load cell that allowed measuring the tension in the rope. By measuring forces at different velocities for the male and the female subjects, they found that a

female body creates less resistance on the surface than a male body. This can be a result of a lower cross-sectional area of the female subjects compared to the male subjects, as well as a higher buoyancy force of the female swimmers due to a higher fat content. This enables the female swimmers to have a higher position relative to the water surface than their male counterparts. Also as McLean and Hinrichs (1998) found, the distance between the centre of buoyancy and the centre of mass is higher in the male compared to the female group. Therefore, the female swimmers have smaller rotating moments that tend to 'sink' the legs. This advantage enables the female subjects to have a more horizontally aligned body compared to their male swimmers.

In order to find the effect of submersion on the resistive forces on the human body, Maiello *et al.* (1998) used the flume system to compare the drag forces on 11 subjects in a streamlined position. They compared drag forces with the different hand positions on the surface and underwater at the depth of half meter in two different preset velocities. The position called 'closed hands' had the least resistance compared to the other arm positions. However, no further explanation of the different arm positions was provided. The underwater resistance was found to be lower than the resistance on the surface similar to the findings by Hertel (1966). Also a 23% increase in the surface drag and 17% increase in the underwater drag were found when the towing velocity was increased from 1.5 to 1.9 m/s. The relatively higher increase in the total drag at the surface can be considered as a result of contribution of the wave drag at the surface and the fact that this kind of drag changes more rapidly with increasing velocity compared to the other types (Rushall, *et al.* 1994).

To detect any drag reducing benefit from wearing a body suit, Roberts *et al.* (2003) measured the drag forces in an underwater streamlined position using a flume. Water was circulated via two pumps capable of producing flow velocity ranging from 1.2 to 3 m/s. The fact that no significant differences between different swimming suites were detected could be the result of filtering the signal at 1 Hz. Because of the fluctuations of the drag forces due to the surface pressure fluctuations generated by the transitional,

separated and the turbulent boundary layers, and the free stream turbulence (Wang *et al.* 2002 and Howe *et al.* 2001) the instabilities in the resistive force are anticipated to happen at the wide frequency ranges. Filtering the force data at a low frequency eliminates the chance for any differences to show and part of the real signal at higher frequency could be filtered out.

In order to increase the accurately of the drag forces measurements in a flume the free-stream turbulence and the own wave of a flume that affect the values of pressure and wave drag should be controlled. To achieve this goal Chatard and Wilson (2003) used a 1.5 m depth, 2.5 m width and 10 m length flume that allowed the effect of the wave and free stream turbulence to be minimised. The force was transferred by a system of ropes and pulleys to a load cell that was mounted 10 cm above the water and directly ahead of the swimmer. A 20% drag reduction was found in a drafting position of 50 cm behind the leading body compared to the non-drafting situation. This was attributed to less momentum of fluid particles when passing the lead body resulting in a lower dynamic pressure upstream of the drafting body.

While using a flume with a consistent flow can help measurements to be made more accurately, adopting a consistent streamlined posture for a live subject may not be an easy task. To overcome this problem, Vennell *et al.* (2005) investigated the drag on a human body replica while fixing it with rods lying back at the different depths and towing velocities. The mannequin was attached to a horizontal rod. The rod was connected to a support strut via a load cell, which was sampling the drag force at 100 Hz. They towed the mannequin at the velocities from 0.4 to 2.4 m/s with 0.2 m/s increment and five different depths of 0, 0.1, 0.3, 0.6 and 1 m. They found significantly higher drag for shallow depths close to the surface than deep depths and concluded that for escaping the wave drag after starts and turns swimmers must maintain a streamlined position at a depth between 0.45 and 0.7 m below the surface.

While a flume can be used to measure the drag forces, the amount of the free stream turbulence may vary the condition compared to the real glide conditions. For testing numbers of swimmers the process of making an exact replica of a swimmer's body may be time-consuming. Also the rigid body surface of a mannequin would respond to the flow in a way that differs from that of a live body with a compliant skin, and this may cause differences between the drag forces measured on a live subject and on a mannequin.

Wind tunnels

Based on the similarity law, two bodies with similar Reynolds numbers would have the same drag coefficients in two different fluid media. For quantifying drag of a submerged body underwater, it is possible to measure the drag force of a body replica in a wind tunnel at comparatively higher air velocities compared to the water speed. Waring (1999) used a closed-circuit wind tunnel to study the effect of using drag reducing mechanisms on swimming suits. By measuring the drag forces on a half scale body replica in a streamlined position he found that the presence of the fabric on the replica's body would increase the drag coefficient. This can be the result of an increase in the surface roughness as a result of wearing a fabric and a subsequent increase in the friction drag.

Waring (1999) also found that a special arrangement of 'vortex generators' decreases the total drag on the replicated model of a swimmer in the wind tunnel. Vortex generators are used to mix the flow outside the boundary layer with the flow from inside and give excess momentum to the fluid particles near the body surface to prevent separation. This then decreases the size of the wake and decreases the pressure drag.

The inability to simulate the effect of wave drag and the mannequin's vibrations at the higher Reynolds numbers are the hindrances in the further use of the wind tunnels in swimming research.

The reviewed experimental methods for quantifying the hydrodynamic parameters of body during a glide are unable to examine the behaviour of the body under the real glide conditions. Even if they would be able to reproduce the acceleration encountered in a glide, matching the acceleration with velocity in a way that resembles the kinematics of a glide requires knowing the unique velocity-time function of each gliding body under the real condition.

2.4.2. Quantifying Hydrodynamic Drag based on Glide Kinematics

To overcome the limitations and the deficiencies of the other methods, such as the inability to measure the hydrodynamic forces in the real gliding condition, another method was introduced to quantify the resistive force based on the glide kinematics. The method is based on the Newton's second law of motion that calculated the total drag force applied on a body during a glide as the deceleration of the body multiplied by the virtual mass. The virtual mass can be calculated as the sum of the body mass and the added mass of the body from theoretical data bases (Landweber, 1961). Thus by measuring the acceleration, the total drag can be calculated under natural conditions of a glide.

According to Bilo and Nachtigall (1980) the method originally was known as 'deceleration measurement' for quantifying the drag, and had been used for finding the drag coefficient of cars prior to World War II. The modifications of the measurement systems and the further developments for using it underwater occurred since then.

The deceleration method has been introduced to aquatics by Lang and Daybell (1963) for measuring the drag coefficient of the gliding dolphins in a water tank. Filming the gliding dolphins in a water tank the time taken for the gliding dolphin to reach from one hoop to another one in known the distance was measured to calculate the initial and final velocities of a glide. The added mass coefficient was assumed to be 4.5 % of the body

mass as for an ellipsoid with similar shape and has been added to the dolphin's mass to calculate the virtual mass.

Since the derived acceleration data contains large fluctuations as a result of amplified noise it is always preferred to work with the velocity as a lower derivative with lower fluctuations. Assuming that drag is proportional to the velocity squared, the drag-area (the drag coefficient multiplied by the maximum cross-sectional area) was found based on the virtual mass, and the initial and final velocities and the time elapsed to reach from the initial point to the final one.

Instead of using the initial and final velocities, Klauck and Daniel (1976), used the instantaneous velocities during a glide to estimate the coefficient of hydrodynamic drag of a human body. In their method based on the solution of differential equations for a gliding body, and knowing the drag as a quadratic function of the velocity, the velocity was found as a hyperbolic function of time. Then a resistive factor was determined by fitting a hyperbolic velocity function to the measured instantaneous velocity-time data. The glide's velocity was measured with a method called 'chronocyclograph' that was based on detecting a lamp attached to the swimmer's head on a sequence captured by pin rotating cameras while the time difference between each consequent sampling was 0.05 s. The advantage of fitting a curve to an instantaneous velocity sequence compared to using two instantaneous velocities is that fitting a function to numbers of points compensate for the errors as a result of fluctuations in the instantaneous velocity data and decreased the chance of being incorrect about the calculated resistive force. Despite this advantage the added mass has not been considered for the body and the body mass has been assumed to be equal to the virtual mass. For this reason Klauck and Daniel (1976) found lower drag forces based on the kinematics of a glide than the drag forces for the same subjects during the towing experiments at the constant velocities.

Instead of fitting velocity changes with a hyperbolic function, Bilo and Nachtigall (1980) fitted the reciprocal velocity data with a linear function using a least squares

method for quantifying the drag coefficient of a passively gliding penguin. The slope of this fit was used to calculate the drag coefficient values. While using a least square fit was more accurate than previous methods based on the kinematics of a glide, similar to the study of Klauck and Daniel (1976), the added mass was ignored.

Oppenheim (1997) introduced a kinematic model that represented the velocity changes of a body during a glide by assuming the total resistive forces underwater to be the sum of a linear and a quadratic functions of velocity to account for the friction and pressure drags. By fitting the function to the instantaneous velocity sequence measured with a swim-meter the friction and the pressure drag constants were quantified. Although Oppenheim concluded that the function that the combined linear and quadratic drags improved the fit to the instantaneous velocities of the glides, determining each of the constants with a high level of confidence was not achieved.

Surprisingly, neither of the methods developed after Lang and Daybell (1963) accounted for the effect of the added mass, as they assumed the total virtual mass to be the same as the mass of the body (Klauck and Daniel, 1976; Bilo and Nachtigall, 1980; and Oppenheim, 1997). The added mass has been either assumed to be negligible (Bilo and Nachtigall, 1980), ignored (Klauck and Daniel, 1976) or declared to be a manifestation of the friction drag (Oppenheim, 1997).

It has been found that the drag coefficients calculated from the other methods were greater than the measurements based on the kinematics of the glide in the studies of the hydrodynamic drag on the humans (Klauck and Daniel, 1976) and the seals (Williams and Kooyman, 1985). This emphasises the need for considering the added mass as an important part of the inertia. When the added mass is not considered the drag force is underestimated (Vogel, 1994).

To calculate a realistic drag coefficient for the aquatic animals using the kinematics of glides, the added masses have been estimated based on the values for the three-

dimensional bodies of revolution with the same fineness ratios (Landweber, 1961). This provided realistic drag coefficients in studies of seals by (Feldkamp, 1987), and sea lions (Stelle, *et al.*, 2000). Due to the minor differences between the aquatic mammals and the three-dimensional bodies of revolution the method provided close estimations of the drag for the aquatic animals. However, in studies of the human gliding, replacing the added mass coefficients with the coefficients from the bodies of revolution is not a reasonable estimation due to the major morphological differences between the human bodies and the streamlined objects.

Because of the methodological difficulties and limitations of measuring the added mass with the towing methods (Klauck, 1998), the differences between the added mass values during acceleration and deceleration, and the impossibility of using values from the other databases due to the differences between human bodies and other objects, added mass of human has been assumed to be zero. This assumption has affected the resistive force estimations based on the kinematic of a glide (Klauck and Daniel, 1976 and Oppenheim, 1997).

In the previous methods of quantifying the resistive force based on the kinematics of glides, the instantaneous velocity data show considerable fluctuations (Bilo and Nachtigall, 1980; Klauck and Daniel, 1976 and Oppenheim, 1997). These oscillations are a result of the noise and the fluctuations in the real signal. The noise could be due to the errors in calculating the instantaneous velocities. The instabilities in the drag as a result of the vortex shedding at different frequencies, surface pressure fluctuations generated by the transitional, separated and the turbulent boundary layer, and the free stream turbulence (Howe *et al.*, 2001 and Wang *et al.*, 2003), causes the instantaneous velocity of a gliding body to fluctuate at different frequencies. By deriving the raw displacement (Bilo and Nachtigall, 1980; Klauck and Daniel, 1976) the noise would be amplified and affect the accuracy of the resistive parameters calculated with these methods.

2.4.3. CFD Studies

'Numerical simulations' involving solving the Navier-Stokes differential equations that govern the equation of motion of the fluid particles is a relatively new approach in the swimming that provides visualization of the entire flow domain and can distinguish between the different sources of resistance including the pressure and friction drag. Using CFD for analysis of flow over the body in streamlined positions can produce reliable results for the resistive forces if the exact geometry and the transient conditions of the velocity can be modelled. Uncertainties about the level of the upstream turbulence and skin surface roughness may cause discrepancies between the resistive force values based on the CFD analyses and the real values (Ramsay, 2004). Possible effects of the surface compliance, which might affect the hydrodynamic characteristics of the body, cannot be modelled with the CFD itself and requires a contribution from other 'solid solution' software that would be able to model the surface displacement as a result of the forces applied to the surface.

There has not been any study in which the added mass in swimming using CFD has been considered despite the ability of CFD to model glide as an unsteady problem. For running a body model under unsteady flow conditions, the time dependent input velocity function needs to be known beforehand from the experiments.

2.5. Review Summary

Glides in swimming correspond to the passive transitional motion of a body while adopting its so-called 'streamlined' position with fixed body posture where the initial momentum is reduced as a result of the resistive impulse. The glide performance is affected by initial velocity and the rate of change in velocity over time. Improving the glide performance can be achieved by either increasing the initial velocity or improving the glide efficiency. Whereas increasing the initial velocity can only be achieved with the price of increasing the metabolic cost during the pre-glide action, increasing the glide efficiency by maintaining the streamlined position restrains the physiological costs.

However, despite the numerous studies (Cureton 1940; Craig and Pendergast, 1979 and Sharp and Costill, 1989), the glide efficiency has not been studied as an independent parameter that contributes to the overall performance.

During glides the body undergoes a retarding motion as a result of the resistive force that applies in the opposite direction of the motion, while the inertia tends to maintain the same speed. Thus, a glide efficiency parameter should be based on the kinematic behavior of a glide while considering both the resistive force and the inertia. Until now, no study had been conducted to consider the combined effects of the resistive and the inertial properties in the glide phase, despite the importance of the combined characteristics in optimising the performance.

Although there have been several studies that quantify the passive drag using the direct force measurement methods, none of these account for the effects of decelerations that occur in the passive glides resembling those under the glide conditions. Also, added mass in deceleration may not be quantified by the conventional methods due to the difficulties of replicating flow characteristics in the experiment similar to those in the actual glides. There is an inconsistency in the drag values obtained in the previous studies due to the differences between the different testing setups for measuring the hydrodynamic forces. Despite the importance of the anthropometric parameters and the morphological characteristics on the drag values these parameters have not been reported in the majority of the studies, and where reported they did not represent the body's posture and shape characteristics in real glide conditions. Based on the review of the above mentioned methods it is apparent that the hydrodynamic parameters of a glide must be studied in a manner that avoids the use of the constraints or devices that could affect a swimmer's performance and natural pace.

Although CFD is emerging as an aid in swimming research, in order to simulate the glides under real conditions, the velocity-time function needs to be known beforehand from the kinematic analyses of a glide. The time required for scanning the different body

shapes, and the processing time of running models with an adequate number of elements in a transient approach are hindrances in using the CFD for the glide phase of swimming.

Calculating the resistive forces based on the kinematics of a glide has overcome these limitations by allowing the body to maintain its natural posture. Even with these advantages, the precision of this method depends on the accurate quantification of the added mass as part of the procedure or on using added mass known from other experiments. Because added mass has not been quantified for a human body previously, the calculation of the resistive forces based on the kinematics of a glide seems not to be able to provide valid results for the human bodies. Thus, a new method that determines the added mass as part of the procedure is required.

Utilising a new method that uses the kinematics of a glide to derive the information about the glide efficiency and the hydrodynamic parameters including the resistance and the added mass enables these parameters to be quantified in a realistic glide condition. This allows meaningful relationships between the hydrodynamic and glides efficiency parameters with the anthropometric, morphological and postural variables to be investigated.

Chapter 3

Study 1: Underwater Glide Efficiency of a Human Body in a Streamlined Position

Nomenclature

X: Horizontal axis

Y: Vertical axis

x: Horizontal displacement of the body (m)

v_x: Horizontal velocity of the body (m/s)

V_{x0}.: Initial horizontal velocity of each rectilinear glide interval (m/s)

D: Drag or the total resistive force opposite the direction of travel (N)

L: Lift, the downward force perpendicular to drag (N)

B: Buoyancy, the hydrostatic force applies to the body in the vertical direction (N)

W: Weight, the gravity force applied to body (N)

C_G: Glide factor (m)

C_R: Resistive factor (kg/m)

C_g: Glide coefficient (dimensionless)

C_d: Drag coefficient (dimensionless)

C_m: Virtual mass coefficient (dimensionless)

M: Virtual mass of the body in direction of travel (kg)

m: Mass of the body (kg)

A: Maximum cross-sectional area, the projected area in transverse plane perpendicular to the direction of travel (m^2)

ρ: Water density (kg/m^3)

K_1: Constant of integral in the velocity equation

K_2: Constant of integral in the displacement equation

Re_{ave}: Average Reynolds number over a glide interval (dimensionless)

υ: Kinematic viscosity (m^2/s)

V_{ave}: Average velocity for the glide interval (m/s)

λ: Glide constant (m)

3.1. Introduction

Knowledge about the factors contributing to glide performance in swimming has advanced in parallel with advances in the methodological approaches. Early studies by Cureton (1940) involved time measurement for gliding a known distance and also measuring the maximum distance a body could glide after a maximal push-off. However the measured values were highly dependent on the release velocity from the wall and therefore the ability to push-off strongly.

More recently, Sharp and Costill (1989) and Starling *et al.* (1995) calculated the changes in the gliding velocity and quantified the distance travelled by the gliding bodies during specific time intervals. The effect of the initial velocity was eliminated from the glide performance by considering the glide intervals starting at the same initial velocity. However, these methods have limitations when one wants to compare the glide efficiency between the two glide intervals starting at different velocities.

In accordance with Newton's second law of motion the rate of change of velocity for a body during a passive glide is proportional to the resistive force applied to the body, and inversely proportional to the body's inertia. In other words, the kinematic behaviour of a gliding body is influenced by both the resistive force and also by the body's virtual mass

that includes the mass of water that is accelerated with the swimmer in addition to the mass of the swimmer. Thus for quantifying the glide efficiency these the two parameters need to be considered in conjunction with each other.

Further, because the magnitude of the resistive force is dependent on the instantaneous velocity, it is clear that to compare the glide efficiencies, a method is required that takes into account the effect of differences in the instantaneous velocities on the magnitude of decelerations.

Glide efficiency was defined in Chapter 1 as the ability of a gliding body to maintain its momentum through time at each corresponding velocity during a passive motion in which no propulsive forces exist and the resistive force acts on the body opposite the direction of travel. The aim of this study was to develop and test a method of quantifying the glide efficiency in a way that accounts for both the inertial and resistive characteristics of the gliding body as well as the differences in the instantaneous velocities. By defining a glide efficiency parameter, a comparison of the glide efficiencies at different velocities would be possible. The logical and construct validities, accuracy and reliability would be investigated to determine the validity of the method in quantifying the glide efficiency.

In this task the logical validity includes the extent to which the underlying principles and assumptions are realistic as well as the logical progression of the mathematical steps in developing the model. These influence how closely the model can approximate the kinematic data of a gliding body. An essential process in establishing the validity is to compare the produced kinematic data based on the model with the real kinematic values of a human body during a glide, that is, the closeness of the fit throughout the glide interval.

Another important issue related to the validity of the method is its accuracy in quantifying the glide efficiency. During the process of developing the method, further

steps would be taken to reduce the effect of the potential sources of error to maximize the accuracy of the calculations. The goodness of fit is an indicator of the accuracy as well as the logical validity. However, other factors should be considered in order to ensure the accuracy of the method. For further assessment of the accuracy of the method the confidence in the calculated glide efficiency parameters, and the errors associated with the underlying assumptions would be determined.

The reliability of the method, that is the variability in the measures of the glide efficiency across repeated trials, depends on the variability that occurs naturally between trials as well as the magnitude of random errors. The random error include the errors associated with the mathematical model and is related to the accuracy issue, errors in the data associated with the data collection methods and the precision limits of the data collection and digitising equipment, and digitising errors when digitising manually. The effect on reliability of the last of these can be eliminated by using the automatic digitizing. Knowing the error associated with the mathematical model from the accuracy issue, the remaining within-subject variability would be due to the errors associated with the data collection method as well as the variability that occurs naturally between the trials.

The errors associated with the methods of data collection are difficult to separate from the within-subject variability that occurs naturally between trials. However, in this study, the procedures have been standardised to minimise the within-subject variability. Therefore, a strong indication of the reliability and the associated ability to distinguish between performances could be gained through the comparisons of glide efficiency measures across trials within the subjects. The inter-day reliability which would be referred to as 'stability' and the same day reliability known as 'internal consistency' would be investigated to establish the reliability of the method with respect to the extent the glide efficiency of a body at the same velocities remains consistent for a subject.

Construct validity is the ability to distinguish between subjects in their glide efficiency. A high level of construct validity is necessary if the method is to be useful in an applied context. The inherent variability in the body shape and size between two individuals affect the resistive force and the virtual mass of the body and consequently their glide efficiencies are expected to be different. Being able to distinguish between the glide efficiencies of individuals is important for the purposes of, for example, talent identification.

Another indicator of the validity of a method is whether the measured variable is similar to those produced by other accepted methods. As the glide efficiency has not been quantified before, it was not possible to directly compare the results of this study with comparative data from the literature. Instead the 'glide efficiency parameters' were calculated based on the kinematic values which were reported in the literature.

At each velocity, the resistive characteristic of a body is dependent on the cross sectional area and the body shape. Also, the inertial characteristic is dependent on the body mass as well as the amount of entrained mass of water which is determined by the body shape characteristics. Thus, factors contributing to the resistive and inertial characteristics of a body during a glide include the factors related to the body size including the body mass and the cross sectional area and to the factors related to the shape characteristics of a body. Consequently the glide efficiency is affected by both the size and the shape characteristics of a body.

It is highly desirable to identify whether differences in the performance between gliding bodies is due to the body's size including the mass and the cross-sectional area, or due to the body's shape characteristics. Separating a glide efficiency parameter into the size-related and shape-related glide efficiency parameters allows a more specific investigation of each of the contributing factors to the glide efficiency. Thus, one of the desirable aspects sought in developing the new method was to be able to distinguish between the shape-related and size-related glide efficiencies. As the virtual mass of a

body depends on the body mass and the amount of water it can entrain with itself affected by its shape, the factors contributing to the virtual mass contribute to the glide efficiency.

3.2. Methods

3.2.1. Subjects

3.2.1.1. Subject characteristics

Sixteen experienced swimmers (eight male and eight female) volunteered for this study. Ethical approval was granted by the University of Edinburgh Ethics Committee. The data were collected in separate sessions for each subject. To determine the stability (inter-day reliability) of the method one male and one female subject were tested on three separate sessions. Height and weight were measured for each subject in accordance with the ISAA (International Standard for Anthropometric Assessment) methods. Subject characteristics are presented in Table 3.1.

Table 3. 1. The average and standard deviation of subject's age, distance swimming per week, height and mass for the male, female and the total group.

Group	Age (yrs)	Dis/wk(km)	Height (cm)	Mass(kg)
Female	22.3±2.19	24.3±7.41	173.5±7.70	66.8±5.22
Male	19.4±3.02	44.5±6.23	186.2±5.90	77.5±4.91
Pooled	20.9±2.92	33.2±7.17	179.0±8.71	71.8±7.14

3.2.1.2. Marking the subjects

Prior to the pool test, each subject was marked with the permanent black markers at eight anatomical landmarks. Six anatomical landmarks including the styloid process of the ulna, olecranon process of the ulna, head of the humerus, greater trochanter of the femur, level of the most lateral side of the patella (the lateral epicondyle of the femur),

and the lateral malleolus of the fibula were marked on the left side of the body to represent the joint centres at the wrist, elbow, shoulder, hip, knee and the ankle. The third distal phalanx of the left hand (dactylion) and of the left foot (akropodion) on the left side of the body were also marked to represent end segmental points for the left hand and the left foot respectively. A marker on the left side of the head at the eye level on the side of the goggle was used to assess consistency in the head angle during the trials. The markings facilitated the process of digitizing during the glides and allowed using the automatic digitizing as a faster and more reliable option than the manual digitizing.

3.2.1.3. Calculation of subjects' cross sectional areas and extended height.

A Photogrammetric method was used to calculate the maximum cross-sectional area and the extended height. This method is based on digitizing photographs from the side and front views of the subject to determine the breadth and thickness of the areas likely to be the maximum cross-sectional area.

Two photographs were taken from the side and front view of the subject on land in an upright streamlined position resembling that adopted for a streamlined glide. For this purpose the subject was requested to stand on an angled support that facilitates standing still with the ankles plantar flexed as in the streamlined position. The camera was placed at 10m from the subject with the camera axis perpendicular to the sagittal and frontal planes of the subject in side and front views respectively. Another photograph was taken from a calibration chart that was replaced at the position where the subject's mid-sagittal and mid frontal planes were located in the front and side photographs. This calibration chart was held perpendicular to the cameras optical axis and allowed the subsequent calibration of each view.

The two images were digitized in the image processing software (Microsoft Photo Editor 3.01, Media Cybernetics, L.P.). The thickness and breadths of the areas likely to be the

maximum cross-sectional areas, including the chest and the buttocks, were calculated from the digitized outline. On the basis of the assumption that the segmental cross sectional area of a human body could be well replaced by an appropriate ellipse with the same thickness and breadth (Jensen, 1978), the cross sectional areas of these parts were calculated with the largest area subsequently regarded as the projected area. In all cases the zone with the largest cross-sectional area was in the chest. Extended height was measured as the distance between dactylion to akropodion while the subject was in an upright streamlined position.

3.2.2. Data Collection

3.2.2.1. Instruction and protocol

Prior to the pool test, the subject was instructed to push-off the wall and to adopt a streamlined position during the glides. A 'glide' was defined as a passive motion without further actions after the feet left the wall. The 'streamlined position' was defined as the position normally used by the swimmers following turns and after entry characterised by the arms extended forward towards the direction of travel with hands pronated and overlapping, and feet together and plantar flexed.

A submersion, preparation and push-off protocol was taught to the subject in order to facilitate a horizontal rectilinear glide at an adequate depth. This protocol included submerging underwater by exhaling the air from the lungs steadily while sculling water upwards to reach an adequate depth of 70 cm. Close to neutral buoyancy was achieved when the subject was completely submerged at a depth of 70cm and had no tendency to sink or float. This was perceived experimentally by the subject when there was no need to scull to maintain the depth. The subject was requested to hold the breath as soon as attaining close to neutral buoyancy and to maintain it during the glides. The feet were placed at push-off marks at a depth of 70cm below the surface, while the arms were sculling the water backwards to enable the body to maintain contact with the wall. Simultaneously the subject resumed a streamlined position with the arms and trunk

horizontally aligned while the hips and knees were in a flexed position ready to push-off the wall.

A moderate rather than a maximum push-off was recommended to facilitate the adoption of a streamlined position immediately after the wall release. The subject was requested to sustain a horizontally aligned position during the period of the glide and to maintain the depth. It was emphasized that the lateral deflection of the body (the lateral sway of legs), arching of the back (hyperextension) or 'twisted trunk' (the misalignment of lines connecting shoulders and hips) should be avoided as much as possible.

3.2.2.2. Filming and feedback procedure

A JVC KY-F32 color camera sampling at 50 fields per second was positioned underwater 10 m from the subject's intended glide path with its axis perpendicular to the intended glide path and zoomed to a field of view of 6 meters in the direction of the glide. The lane prior to the last lane was used to eliminate the effect of the pool wall on the water flow around the subject's body. A second camera with the same specification as the first camera was mounted on a boom at a 5 m height directly above the subject's line of glide with its axis perpendicular to the intended glide path. The videos from these cameras were displayed on a live poolside monitor enabling a check for the deviations of the glide path from the intended path also the poor alignment of the body (Figure. 3.1). Each recording was replayed to each subject on the poolside as feedback regarding their ability to comply with the desired gliding characteristics.

3.2.2.3. Warm-ups and the main trials

The subject participated in warm-ups comprising 8×25 m swims starting from a static push-off from the wall and followed by a rectilinear horizontal glide. After each 25 m the subject was informed about the possible changes required to improve performance of the glides. Based on the prior pilot studies it had been found that the eight warm-up glides were enough for a swimmer at this level to be familiar with the procedure and to

be able to glide in accordance with the requirements.

For the main trials subjects had at least two minutes rest between each trial to prevent fatigue and to allow any possible turbulence or current in the water created by the previous glide to be completely cleared before starting a new trial. It was essential to make sure that there were enough trials from which the adequate numbers of glide intervals complying with the criteria could be extracted for the whole range of the velocities corresponding to the passive glides of each subject. It was found that at least 15 acceptable trials were required for this purpose based on the pilot studies performed prior to the main data collection. Depending on the subject's ability and consistency to perform the acceptable glides according to the instructions the total numbers of glides performed by each subject ranged from 22 to 27 to achieve the 15 acceptable glide trials.

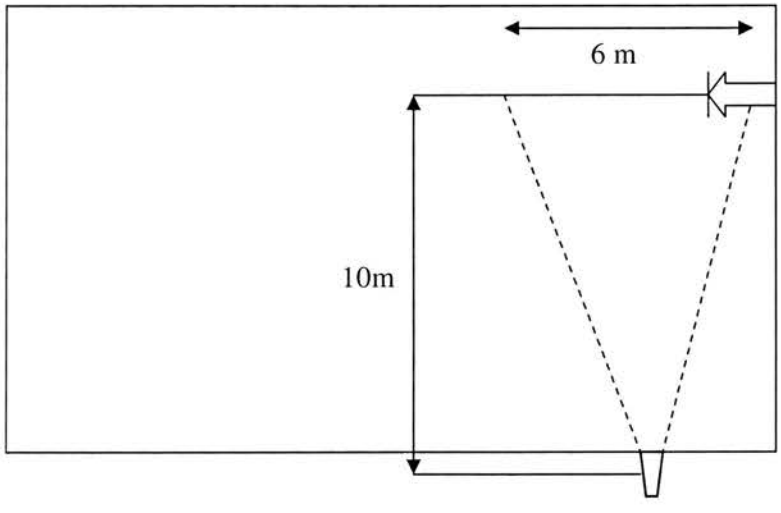

Figure 3. 1. Schematic view of the testing set-up and camera view

3.2.3. Data Processing

3.2.3.1. Trimming process

In order to eliminate the possible effect of the lens distortion at the edges of the field of view, the video files were trimmed using Ariel Performance Analysis System (APAS) software to the period corresponding to the subject passing through the middle 4 m view of the camera's 6 m field of view.

3.2.3.2. Digitizing process

The eight skin markers together with a marker on the left goggle were automatically digitized using Ariel Performance Analysis System (APAS) in order to perform a 2D analysis of the glide in the sagittal plane.

Ten reference points on the 'T' line at the bottom of the pool and on the push-off wall with the known distance were digitized to calibrate the frame using the two-dimensional Direct Linear Transformation (DLT) techniques (Walton, 1981).

3.2.4. Definitions and Underlying Principles to Ensure the Logical Validity of the Method

To develop a method to quantify the glide efficiency the following definitions and underlying principles were necessary.

3.2.4.1. Passive glide: A glide in which the propulsive forces are zero and the body is subjected to the hydrodynamic resistance.

3.2.4.2. Angle of attack: Defined as the angle between the chord line and the direction of travel (upcoming flow). The chord line is defined as the line between the leading and the trailing edges of a body. In the case of the human glides in this study the chord line was defined as the straight line that connects the dactylion to the hip.

3.2.4.3. Virtually zero angle of attack: Because of the instabilities in the flow and the variations in hydrodynamic forces, it is impossible to exactly maintain a zero angle of attack in the real conditions. Thus, the term 'virtual' has been used to describe angles of attack that are close to zero when the flow is considered to be directly opposite the direction of motion and the orientation of the body is represented by the chord line. Because the random errors in extracting the angle of attack exist when the digitized points are not at the centre of the skin marker in the vertical direction, a maximum limit for changes in angle of attack could be calculated based on the size of the skin markers and the distance between the akropodion (the tip of finger) and the hip. When the digitized points are at the lower edge of one skin marker and the upper edge of another, a maximum angle of ±1.2 degree was calculated as a limit and glide intervals with the higher angle of attack were eliminated.

3.2.4.4. Rectilinear glide: A passive glide in which the direction of the instantaneous velocity of the body remains on a straight-line trajectory and the body is aligned with a virtually zero angle of attack.

3.2.4.5. Consistency of posture and shape: It is crucially important for a body to maintain its posture during the glides since changes in the posture would cause the differences in the hydrodynamic parameters and consequently affect the glide efficiency. The joint angles including wrist, shoulder, hip, knee and ankle as well as the neck angle (that is defined as the angle between the line that connects the shoulder to the head marker and the trunk line) were considered to change over a maximum acceptable limit during glides. Like the maximum angle of attack these limits were calculated based on each limb's length and marker size as when the digitized points are at the lower edge of one skin marker and the upper edge of another, these limits included 5 degrees for the wrist, 4 degree for the elbow, 3 degree for the shoulder, 2 degrees for the hip, 3 degree for the knee, and 5 degree for the ankle joint.

3.2.4.6. Consistency of maximum cross sectional area:

As a result of the consistency in the shape and virtually zero angle of attack, the maximum cross sectional area remains constant during the glide.

3.2.4.7. Consistency of projected area: The projected area remains the same as the maximum cross sectional area when the shape remains constant and the angle of attack is virtually zero.

3.2.4.8. Virtually constant glide angle (α) or rectilinearity: The glide angle, that is the angle to horizontal of the best regression line passing through the positions of the anatomical landmarks of the body at different instants in time must remain 'virtually' constant during the whole glide interval. In other words the glide trajectory should be a straight line or a rectilinear path for the glide interval period. Although it is impossible to completely maintain the constancy of this angle in the real conditions because of the instabilities in the flow and hydrodynamic forces, the term "virtual" is used to imply that the variability in the angle is small. The linear regression line passing through glide's trajectory path should have a minimum coefficient of determination value of R^2=0.99 for a glide to be considered as rectilinear.

3.2.4.9. Virtually horizontal path: For a glide to be considered to be appropriate for this model the rectilinear path should match the horizontal line. In other words there should not be any changes in the depth. Although for a subject maintaining the exact depth is not completely possible, a maximum limit was set for a glide interval to pass this criterion. The average vertical position of the skin markers relative to the water surface represented the depth of the body. The average vertical position of the markers was set not to change beyond 2 cm in each glide interval.

3.2.4.10. Adequacy of depth: All rectilinear glides were done at a depth of approximately 0.7 m. This depth was considered to be an adequate depth to prevent excess effect of wave drag on the total drag in accord with the finding by Lyttle *et al.* (1998) that the effect of wave drag is negligible at depths greater than 0.6 m.

3.2.4.11. Hydrostatic balance and hydrodynamic stability: When the locations of the centre of buoyancy and the centre of mass of a statically submerged human body in a streamlined position do not fall on the same vertical line the weight and buoyancy force form a force couple with a moment acting to rotate the body (McLean, and Hinrichs, 1998). This misalignment of the buoyancy and weight forces is common due to the disparate densities of the chest and lower limbs. Exhaling air out of the lungs decreases the moment arm of the buoyancy force, hence decreases the moment around the centre of mass (McLean and Hinrichs, 2000). To maintain a rectilinear glide with a virtually zero angle of attack the moment that results from the differences between the locations of the centre of mass and the centre of hydrostatic pressure needs to be cancelled by the hydrodynamic moment created by the lift and drag forces. The balance between the hydrostatic and the hydrodynamic moments prevents the body from rotating about the transverse axis (pitch), rotating about the longitudinal axis (roll) and rotating around anterior-posterior axis (yaw). The ability of a gliding body to maintain its stability is determined by the locations of its centres of dynamic pressure, inertia, added mass, and the centre of buoyancy (Aleyev, 1977). Although this study does not consider these effects, maintaining a rectilinear glide with a virtually zero angle of attack indicates that the subject was successful in balancing the moments.

3.2.4.12. Consistency of added mass: The proposed method requires the added mass coefficient to remain close to constant over a glide interval.

Thus, it was important to define the glide intervals in a way that the added mass coefficient variations over limited ranges of Reynolds number would be very small.

3.2.4.13. Consistency of drag coefficient for limited ranges of Reynolds number: The proposed method requires the drag coefficient to remain constant during a glide interval. It was important to define the glide intervals with appropriate durations so that the drag coefficient variations over limited ranges of Reynolds number would be very small.

3.2.4.14. Symmetry: As the streamlined position is symmetric in the sagittal plane, in each glide the motion of the digitized coordinates of the left side can be assumed as being representative of the motion of the whole body.

3.2.4.15. Two-dimensionality or planarity: Each rectilinear glide is a transitional motion in the photographic plane perpendicular to the optical axis of the camera. There should not be any non-coincidence between the plane of motion and the photographic plane.

Based on these criteria the appropriate glide sequences were selected from each trial and the sequences not complying with the criteria of passive rectilinear horizontal glide were eliminated.

3.2.5. Mathematical Model

This section describes the mathematical model and its underlying principles for determining the glide efficiency parameters of a swimmer during a horizontal rectilinear glide. Figure (3.2) demonstrates the free body diagram of a gliding subject in a horizontal rectilinear glide. The body is affected by the hydrodynamic, hydrostatic and gravitational forces. Since there is no motion in the vertical direction, the lift force

which might result predominantly from the shape of the body, would be cancelled by the existing net buoyancy (Figure 3.2).

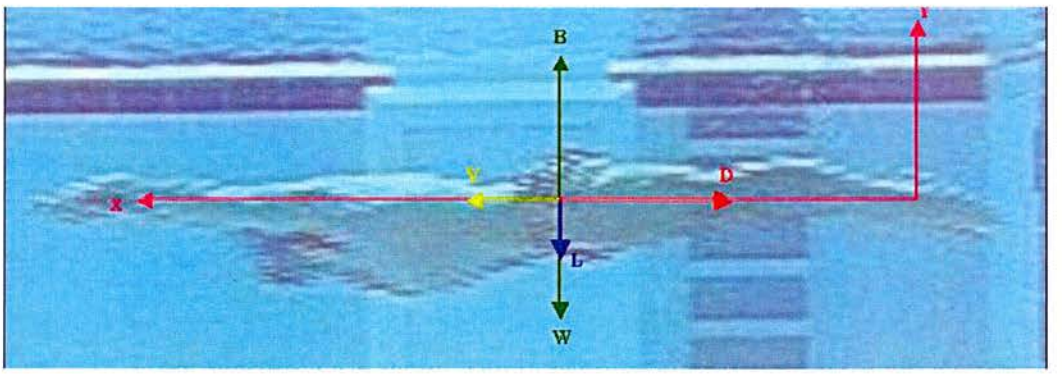

Figure 3. 2. The free body diagram of a swimmer in the streamlined position during a horizontal rectilinear passive glide.

Newton's second law of motion can be applied in the horizontal direction. In the absence of any propulsive force we have:

$$M.\frac{dv_x}{dt} = -D \qquad \text{(Equation 3.1)}$$

Drag can be replaced by the following formulae:

$$D = \frac{1}{2}.C_d.A.\rho.v_x^{\ 2} \qquad \text{(Equation 3.2)}$$

Based on the underlying principles a constant resistive factor (C_R) that is the ratio of the resistive force to the velocity squared is introduced for each glide interval which incorporates the drag coefficient, water density and the maximum cross sectional area.

$$C_R = \frac{1}{2}.C_d.A.\rho \qquad \text{(Equation 3.3)}$$

The resistive force in Equation (3.2) can be replaced by a constant resistive factor (C_R) times the velocity squared.

$$D = C_R.v_x^{\ 2} \qquad \text{(Equation 3.4)}$$

Replacing the resistive force from Equation (3.4) in to Equation (3.1) the differential equation of motion in the horizontal direction(x), can be written as:

$$M.\frac{dv_x}{dt} = -C_R.v_x^{\ 2} \qquad \text{(Equation 3.5)}$$

Based on the assumptions of rectilinear glide, the resistive factor and virtual mass would remain fairly constant for a relatively a short glide interval. Transferring all the constants to one side of the equation, we have:

$$\frac{dv_x}{v_x^{\ 2}} = -C_R.\frac{dt}{M} \qquad \text{(Equation 3.6)}$$

Integrating two sides of Equation (3.4) to v_x and t we have:

$$\int\frac{dv_x}{v_x^{\ 2}} = \int -C_R.\frac{dt}{M} \qquad \text{(Equation 3.7)}$$

This will give us:

$$\frac{1}{v_x} = \frac{C_R}{M}.t + K_1 \qquad \text{(Equation 3.8)}$$

K_1 in Equation (3.8) is the constant of the integral, and needs to be found using the initial velocity condition for each glide interval.

$$v_x(0) = V_{x0}$$ (Equation 3.9)

Using initial velocity condition (Equation 3.9) and applying to Equation (3.8), we have:

$$K_1 = \frac{1}{V_{x0}}$$ (Equation 3.10)

Replacing the constant value (K_1) in Equation (3.8), the velocity can be found as a hyperbolic function of time:

$$v_x = \frac{1}{\frac{1}{V_{x0}} + \frac{C_R}{M}.t}$$ (Equation 3.11)

Equation (3.9) represents the horizontal velocity of a body during a rectilinear glide interval as a function of time and three constant parameters including the initial horizontal velocity (V_{x0}), the resistive factor (C_R), and the total virtual mass (M).

By fitting a curve represented by Equation (3.11) to the velocity-time data of a glide interval the constant parameters including the initial velocity and the ratio of the virtual mass to the resistive factor can be determined.

3.2.6. Procedures to Ensure Accuracy of the Quantified Parameters

3.2.6.1. Using raw displacement:

In previous studies (Klauck and Daniel, 1976; Bilo and Nachtigall, 1980, and Naemi and Sanders, 2004) derived velocity data has contained large fluctuations. Thus it is more desirable to work with the original displacement data that can be obtained directly from

the digitising procedure. For this reason Equation (3.11) that addresses the instantaneous horizontal velocity should be used to find the instantaneous horizontal displacement equation.

Horizontal velocity is the derivative of the horizontal displacement.

$$v_x = \frac{dx}{dt} \qquad \text{(Equation 3.12)}$$

Replacing the horizontal velocity from Equation (3.12) into Equation (3.11) we have:

$$\frac{dx}{dt} = \frac{1}{\frac{1}{V_{x0}} + \frac{C_R}{M}.t} \qquad \text{(Equation 3.13)}$$

Integrating the new differential equation we have:

$$\int dx = \int \frac{1}{\frac{1}{V_{x0}} + \frac{C_R}{M}.t}.dt \qquad \text{(Equation 3.14)}$$

This will give us:

$$x = \frac{M}{C_R}.Ln[\frac{1}{V_{x0}} + \frac{C_R}{M}.t] + K_2 \qquad \text{(Equation 3.15)}$$

K_2 in Equation (3.13) can be calculated using the initial displacement condition.

$$x(0) = 0 \qquad \text{(Equation 3.16)}$$

Using the initial displacement condition (Equation 3.16) and applying it in to Equation (3.12), we have:

$$K_2 = \frac{M}{C_R} Ln V_{x0} \qquad \text{(Equation 3.17)}$$

Replacing K_2 from Equation (3.17) in to Equation (3.15), the horizontal displacement can be found as a logarithmic function of time:

$$x = \frac{M}{C_R}.Ln\,[\frac{C_R}{M}.V_{x0}.t + 1] \qquad \text{(Equation 3.18)}$$

As the virtual mass and the resistive factor appear as a ratio in Equation (3.18), fitting a parametric curve represented by this equation to the displacement data enables the ratio to be quantified. The ratio of the virtual mass (M) to the resistive factor (C_R) is introduced as the glide factor (C_G):

$$C_G = \frac{M}{C_R} \qquad \text{(Equation 3.19)}$$

Then Equation (3.18) can be rewritten as:

$$x = C_G.Ln[\frac{V_{x0}}{C_G}.t + 1] \qquad \text{(Equation 3.20)}$$

It is obvious that Equation (3.20) represents the horizontal displacement of a gliding body as a logarithmic function of time and two constants as the initial velocity (V_{x0}) and the glide factor (C_G). Equation (3.20) can be fitted to the displacement-time data of a horizontal rectilinear glide interval, and the glide factor and the initial velocity can be found on the basis of each fit.

3.2.6.2. Eliminating the noise in the displacement data:

Random errors as a result of digitising the human body motion happen at different frequencies. Because the human motion possesses low frequency content, it is generally possible to eliminate the high frequency noise by filtering the data at frequencies higher than the one corresponding to the movement.

Because of fluctuations of the drag forces even in the steady state experiments (Howe *et al.* 2001), and the instabilities in drag as a result of the vortex shedding at different frequencies, surface pressure fluctuations generated by transitional, separated and turbulent boundary layers, and the free stream turbulence (Wang *et al.* 2003), instabilities in the resistive force at different stages of the glide are anticipated. These instabilities happen at wide frequency ranges and cause fluctuations in the displacement data of a gliding body.

Due to the high frequency content of the glide's transitional motion as a result of the mentioned instabilities in flow, filtering displacement data with a low pass filter to reduce the random noise would result in eliminating the real displacement signal.

Thus the unfiltered (raw) displacement data was used from each digitized joint that incorporated both the fluctuations from the random error and also the real signal fluctuations. In order to minimize the effect of random noise on the data that represents the whole body displacement data another strategy was required that would be able to retain the signal corresponding to the real displacement data and eliminate the noise.

In a rectilinear glide each digitized marker on the body travels at the same speed and therefore can be used as the representative of the whole body's motion. For minimizing the effect of random errors, the raw displacements of different markers were averaged to represent the raw displacement of the whole body. This process minimises any random error by cancelling the random fluctuations against each other, while the fluctuations

corresponding to the real signal would not be cancelled as they show simultaneous fluctuations of the same body.

3.2.6.3. Finding the optimal glide interval duration:

Choosing the optimum glide interval duration was important. As the drag and added mass coefficients may change with the Reynolds number, fitting Equation (3.20) to the whole glide sequence of a trial results in error. On the other hand a glide interval should be long enough to include enough points in order to produce a reliable fit and reducing errors in predicting the best fit.

The curve fitting toolbox calculates a confidence bound along with a certainty level for each calculated glide factor. The difference between the lower and upper values determines the width of the confidence bound by which the actual glide factor is confined to within the specified level of certainty. The confidence bound width for 95% certainty level, indicates the range within which the actual value of the glide factor would occur 95 times out of 100.

The greater the number of data points to which the displacement function (Equation 3.20) is fitted, the narrower the confidence bound at any certainty level. However, the error due to the change in the velocity increases with increasing the glide interval. Therefore, an appropriate compromise must be found.

The optimum number of points in each glide was determined through the pilot work by testing a male and a female subject in a setup similar to the main data collection. Different numbers of frames in each glide interval were tried to find the possible minimum number of points to which the curve could be fitted with acceptably small error. For the initial setup 4 frames that include 8 points (one per field) were considered, and the number of frames then increased by one in each setup. For each setup the errors associated with the changes in the glide factor due to changes in velocity together with the standard error of calculation based on the confidence bounds for the calculated glide

factors were determined. Further details on calculating these parameters are presented in Appendix A.

It was found that increasing the number of frames in each glide interval resulted in a narrower confidence bound while increasing the error associated with the assumption of a consistent glide factor across a glide interval. There was generally a positive gain by increasing the number of frames up to 10 as the decrease in error associated with the reduction in the confidence bound width was higher than the increase in the error associated with the glide factor consistency assumption. By increasing the number of frames beyond 10 the increase in error associated with the consistency of the glide factor over a glide interval superseded the reduction in error due to the decrease in the confidence bound width. Further details on how these sources of error changed against each other were presented in Appendix A.

Glide intervals were selected for each individual from the acceptable glide sequences of each trial to be considered as independent rectilinear glide intervals. Due to the differences in the velocities at which each subject was able to maintain a rectilinear glide under the required conditions in the designated data collection area, the total numbers of glide intervals were different for each individual ranging from 23 to 27.

3.2.6.4. Using advanced parametric curve fitting techniques:

Matlab curve fitting toolbox was used to fit a curve representing the displacement-time equation (Equation 3.20) to the raw displacement-time data of the body. The Trust-Region algorithm that can solve nonlinear problems more efficiently than the conventional least square methods was used for minimizing the summed square of the residuals, and downweight the outliers according to the Bisquare method. The Bisquare weight is a robust least square regression scheme that downweight the outliers (the extreme values due to error) based on the assumption that error is distributed normally

and the extreme values are rare (Matlab manual, 2004). This scheme minimizes the weighted sum of squares, where the weight given to each data point depends on how far the point is from the fitted curve. Points near the fitted curve are accorded the full weight, while farther points are accorded a reduced weight. This scheme uses an iteratively reweighted least square algorithm to find the best fit and was preferred to the other methods since it simultaneously seeks to find an appropriate curve using the usual least square method and it minimizes the effect of the outliers.

The goodness of fit was evaluated based on the residuals and the goodness of fit statistics like the Sum of Squares due to Error (SSE), the R-square and the Root Mean Squared of Errors (RMSE). The fit goodness can address how closely the model (Equation 3.20) calculates the raw displacement data gathered from the glide intervals.

3.2.7. Quantifying the Glide Factor and Calculating the Corresponding Average Horizontal Velocity for each Interval

By fitting a curve representing the displacement-time equation (Equation 3.20) to the raw displacement-time data of the body, the glide factor (C_G) and the initial velocity (V_{x0}) was found for each glide interval. Because each glide factor was found for each glide interval during which the velocity is not constant, the average velocity during each interval corresponds to the particular glide factor. The average velocity (V_{ave}) can be calculated as the ratio of the distance travelled in each interval(x) calculated by Equation (3.20) to the duration of the glide interval (T).

$$V_{ave} = \frac{C_G}{T}.Ln[\frac{V_{x0}}{C_G}.T + 1] \qquad \text{(Equation 3.21)}$$

For the glide intervals in this study, duration of the glide interval (T) can be replaced by 0.38 s (that is the time interval between the first and the 20^{th} point equal to duration of 19 fields of 0.02 s), knowing the initial velocity (V_{X0}) and the glide factor (C_G), the average velocity for each glide interval was calculated using Equation (3.21).

3.2.8. Verifying the Size-related and the Shape-related Glide Efficiencies

The glide factor was defined as the ratio of the virtual mass to the resistive factor. As the virtual mass and the resistive factor are influenced by the body mass and the cross sectional area respectively, the quantified glide factor reflects the combined effect of the body size as well as the body shape characteristics. By separating the size-related glide efficiency of a body that incorporates the body mass and the maximum cross sectional area from the glide factor the shape-related glide efficiency of a body was quantified.

Since the added mass of water can be considered as a fraction of the mass of the body (Vogel, 1994), the virtual mass can be replaced by a virtual mass coefficient (that is dependent on the body shape characteristics) times the body mass of subject.

$$M = C_m.m \qquad \text{(Equation 3.22)}$$

Replacing the virtual mass (M) and the resistive factor (C_R) from Equations (3.22) and (3.3) in to Equation (3.19), we have:

$$C_G = \frac{C_m.m}{\frac{1}{2}.C_d.A.\rho} \qquad \text{(Equation 3.23)}$$

Equation (3.23) can be re-written as:

$$C_G = \frac{m}{1/2 . A . \rho} . \frac{C_m}{C_d}$$ (Equation 3.24)

The first term on the right side of the Equation (3.24) that incorporates the known constant parameters including the body mass(m), the maximum cross-sectional area (A) and the water density (ρ), was defined as the glide constant (λ):

$$\lambda = \frac{m}{1/2 . A . \rho}$$ (Equation 3.25)

Glide constant (λ) is a constant parameter that determines the size-related glide efficiency and depends on the mass and the cross-sectional area of the body independent from the shape characteristics. The glide constant (λ) was calculated for each subject knowing the body mass, the maximum cross-sectional area and the water density values.

The second term on the right side of Equation (3.24) that is the ratio of the virtual mass coefficient (C_m) to the drag coefficient (C_d) was defined as a dimensionless glide coefficient (C_g).

$$C_g = \frac{C_m}{C_d}$$ (Equation 3.26)

The glide coefficient (C_g) represents a dimensionless coefficient, which is the ratio of two important dimensionless parameters including the virtual mass and the drag coefficients. The glide coefficient provides information on the shape-related glide efficiency by enabling the combined effects of the inertia and resistance to be assessed independent of the body size.

The glide coefficient (C_g) can be found for each interval, knowing the glide factor (C_G) quantified by the curve parameters, and knowing the glide constant (λ) calculated based on Equation (3.25).

$$C_g = \frac{C_G}{\lambda} \qquad \text{(Equation 27)}$$

As a dimensionless parameter the glide coefficient is not influenced by the body's size including the mass and cross-sectional area. This will help in comparing the shape-related glide efficiency between individuals, and to determine whether the differences are due to body size or if it is as a result of the body shape characteristics. To compare the glide coefficients against another dimensionless number the average Reynolds number can be calculated for each glide knowing the extended length (L), the average velocity (V_{ave}) and the dynamic viscosity (υ) of water according to the following formulae.

$$\mathrm{Re}_{ave} = \frac{V_{ave}.L}{\upsilon} \qquad \text{(Equation 3.28)}$$

3.2.9. Sample

Figure (3.3) shows a sample curve being fitted to the raw displacement data of a horizontal rectilinear glide. The Sum of Squares due to Error (SSE) was 1.058×10^{-4}, the R-square vale was 0.9999 and the Root Mean Squared of Errors (RMSE) was found to be 0.0024 that determines how good the curve is fitted to the data. On the basis of each parametric fit for each glide interval a glide factor that is the ratio of the virtual mass to the resistive factor was evaluated. The glide factor was quantified with 95% certainty within the confidence bound of between 4.417m to 4.835m. This confidence bound width corresponds to 9.03 % of the calculated glide factor (4.626 m). In other words there is only 5% possibility that the actual glide factor would be less than 4.417 m or more than 4.835 m. This indicates that the chance of calculating the glide factor within

the confidence bound is 95%. A relative standard error of calculation was calculated as the confidence bound width divided by four, which would be equal to 2.26 % of the calculated glide factor.

Also the initial velocity was quantified with 95% certainty in a confidence bound between 2.341 m/s and 2.364 m/s as 2.353 m/s.

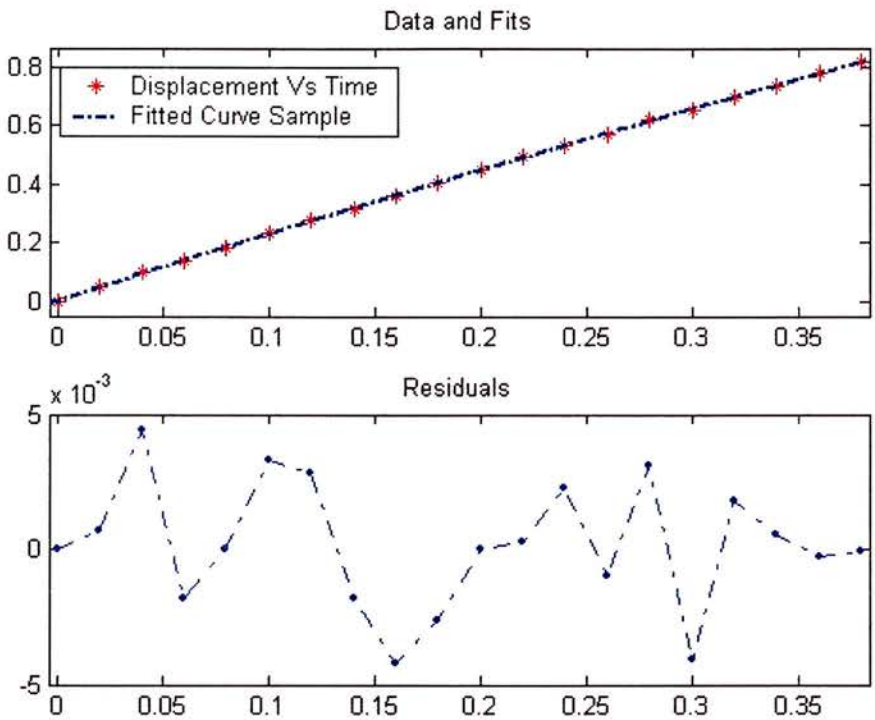

Figure 3. 3. A sample raw displacement data of a horizontal rectilinear glide and the corresponding fit based on Equation (3.20) together with the plot of the residuals.

An example of the glide factors of a male subject (KRS) plotted against the average velocity obtained from a number of glide intervals with a range of average velocities is shown in Figure (3.4).

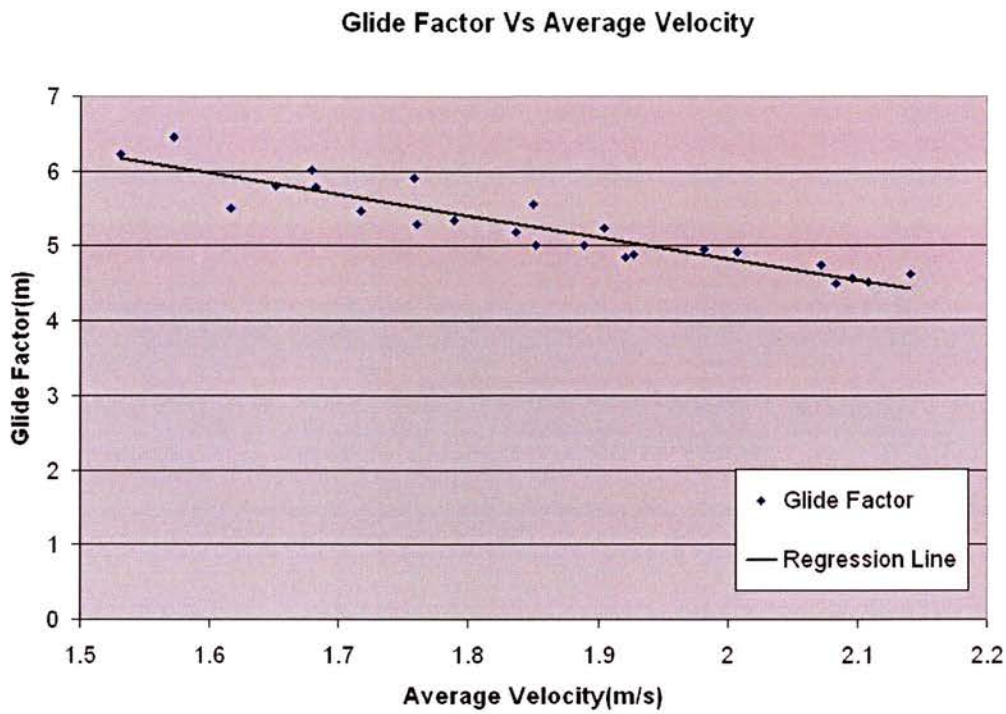

Figure 3. 4. Sample graph of the glide factor versus average velocity for a subject with the regression line.

Due to the fact that the glide factor and the average velocity were calculated based on each glide interval chosen from an acceptable glide sequence, there were no set average velocities at which each subject performed glides. However, linear regressions could be used to estimate (interpolate) the glide factor at the velocities different from the average velocities for which a glide factor was calculated. As the glide factor decreased with a linear trend by increasing average velocity (r=-0.93), a line was fitted to represent the variations (R^2=0.86). This regression line was shown in Figure (3.4).

In order to distinguish the size-related and shape-related glide efficiencies further calculations were carried out. The size-related glide constant was calculated for this subject. Based on Equation (3.25) for a body mass of 76.6 kg, a maximum cross-sectional area of 0.0832 m^2, and a water density of 996 kg/m^3, the glide constant (λ) can be calculated as 1.84 m for this subject.

The values of the glide coefficient (Cg) were calculated based on Equation (3.27) knowing the glide factor (C_G) and the glide constant (λ). For the extended length (L) of 2.593m, the average Reynolds number was calculated knowing the average velocity and the kinematic viscosity (υ) equal to 0.91×10^{-6} m^2/s according to Equation (3.28).

The glide coefficients were shown in Figure (3.5) against the average Reynolds numbers for the same male subject (KRS).

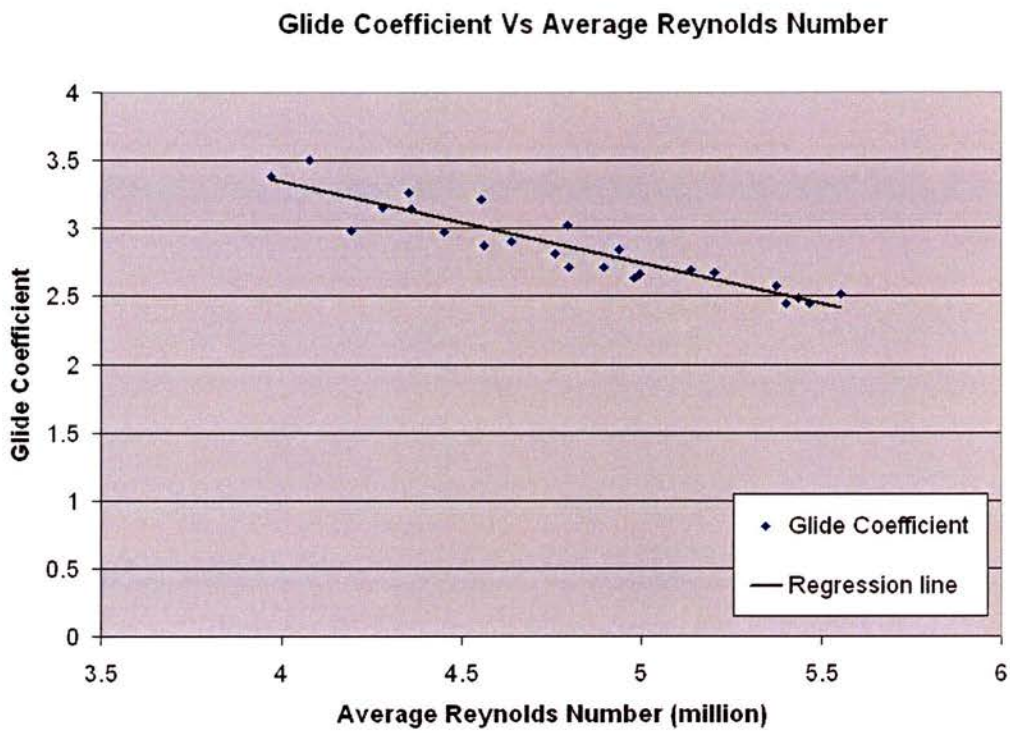

Figure 3. 5. Samples graph of glide coefficient versus average Reynolds number with the regression line.

3.2.10. Assessment of Validity, Accuracy, and Reliability of the Method

SPSS Analysis Package (ver 13.0.1, 2004) was used to perform the descriptive statistics including average and standard deviation of the parameters related to determining whether the method is valid. These include testing the logical and construct validities as well as assessing the reliability and accuracy of the method.

3.2.10.1. Testing of logical validity

One of the main tests of the logical validity was the goodness of fit of the displacement equation (Equation 3.20) to the raw displacement data. Indicators of the goodness of fit included the coefficient of determination (R-squared value), the sum of squares due to error (SSE), and the Root mean squared error (RMSE). This also indicates the extent to which the underlying assumptions and principles which were used in the process of developing the method are valid.

The fit goodness statistics indicated the R-squared value of 0.999±0.0002, the sum of squares due to error (SSE) of $3.5\pm 0.2\times10^{-5}$, and the root mean squared error (RMSE) of 0.002±0.0005. Generally residuals were randomly distributed above and below the time axis.

3.2.10.2. Testing of accuracy

In addition to the goodness of fit statistics which are an indicator of the accuracy of the method as well as the logical validity, the error associated with the assumption of the consistency of the glide factor over a glide interval as well as the confidence in the calculated glide factors was quantified.

One of the assumptions in developing the mathematical equations was the consistency of the resistive factor and the virtual mass that resulted in quantifying a constant glide

factor for a glide interval. It was found that the higher the average velocity during the glide interval the lower the glide efficiency for that glide interval. Since the average velocity during the initial stages of a glide interval is higher than during the final stages the glide factor corresponding to each stage is different. Therefore, to quantify the errors associated with the assumption of constant glide factor the regression line that represents the glide factor at each velocity (Figure 3.4) can be used to calculate the glide factor at each velocity during a glide interval. The difference between the calculated glide factor based on the regression line and the quantified glide factor based on the curve fit parameter represents the error associated with the assumption of consistency of the glide factor over a glide interval. This difference is in its maximum at the beginning and at the end of each glide interval and on its minimum at the middle of a glide interval. Further details on calculating the % error are presented in Appendix A.

As all glide factors were quantified by the curve fitting method within a certainty level of 95%, the narrower the confidence bound width, the higher the confidence in the calculated glide factors and hence the higher the accuracy. Therefore the relative confidence bound width that was defined as the ratio of the confidence bound width for a glide factor to the value of the glide factor was calculated as a measure of the accuracy. For a certainty level of 95% the confidence bound width is approximately four times the standard error of calculations. By dividing the relative confidence bound width by four a relative standard error of calculation was determined.

Within the certainty level of 95%, the relative confidence bound width was 9.8 ± 0.2% that indicated a relative standard error of the calculation equal to 2.45 ± 0.05 %. There was 2.9±1.5 m decrease in glide factor with a 1 m/s increase in the velocity. The error as a result of changes in the glide factor over a glide interval of 10 frames (0.38s) was 3.1± 0.3 %.

3.2.10.3. Testing of reliability

To investigate whether the method is reliable both the inter-day reliability known as 'stability' as well as the within day reliability known as 'internal consistency' were considered.

To test the stability (inter-day reliability) the glide factors calculated in separate sessions for a male and a female subject were investigated. For this reason the coefficient of variation of the slope and intercept of the regression lines of the best fit that represented the variation of the glide factors across average velocities on three separate sessions were calculated.

To test the internal consistency (within-day reliability) the variability of the glide factors between two glide intervals that have the same average velocities were considered. For each subject there was at least two occasions on which the average velocities of the two glide intervals were virtually the same (not more than 0.01 m/s different). The reliability coefficient was calculated as the Pearson correlation between the 16 pairs of the glide factor values (one pair for each subject). To determine the variability in the glide factors the 'relative standard error of measurement' which is the ratio of the standard error of measurement to the mean of the glide factors was calculated. The standard error of measurement (SEM) was calculated according to the following formula.

$$SEM = Sdev.\sqrt{1-r} \qquad \text{(Equation 3.29)}$$

Where Sdev represents the standard deviation of the scores and r is the reliability coefficient. As the standard error of measurement is influenced by the value of glide factor, a relative standard error of measurement was defined as the ratio of the standard error of measurement to the mean of the glide factors.

$$RSEM = \frac{SEM}{Ave} \times 100 \qquad \text{(Equation 3.30)}$$

Where RSEM is the relative standard error of measurement in percentage.

The coefficient of variation of the slope and intercept of the regression lines that represent the variations of glide factor to average velocity corresponding to three separate testing sessions for a male and female subject is presented in table (3.3) as a measure of the stability of the method (inter-day reliability).

Table 3. 2. Coefficient of variation of the regression line's slope and intercept of the male and female subject for inter-day reliability

Subject	Slope	Intercept
Female	0.12%	2.9%
Male	0.29%	1.16%

The reliability coefficient (the Pearson correlation between the pair values corresponding to the same velocity) indicating intraday reliability (internal consistency) was r = 0.988. The relative standard error of the measurement (RSEM) which is the ratio of the standard error of measurement to the mean of the glide factors was 2.94 %.

3.2.10.4. Testing of construct validity

To determine the construct validity, that is, the method's ability to distinguish between subjects in their glide efficiency, the within and between subject coefficient of variation of the glide factors at the same average velocity were compared. High construct validity would be indicated by a large coefficient of variation between the subjects relative to the coefficient of variation within the subjects.

Due to the impossibility of quantifying the glide factor for predetermined average velocities, it was not possible to compare the glide factors corresponding to the same average velocity for all the subjects. Instead the inter-individual and between individual variations of the glide factors corresponding to an average velocity bound were

considered. This velocity bound should be short enough so that the variations in the glide factors along it would be negligible and long enough to include at least three velocities at which the glide factors were calculated for each subject.

Because the ranges of attainable glide velocities were different for different subjects and gender groups the glide factors at the velocity range of 1.45 to 1.55 m/s for female and at the average velocity range of 1.65 to 1.75 m/s for male group were used.

The average and the standard deviation of the coefficient of variation of within individual glide factors and the coefficient of variation of between individual glide factors are presented in table (3.4).

Table 3. 3. Coefficient of variation of the glide factor within and between individuals for the male and female groups

Group	Between individuals	Within individuals
Female	13.2 %	1.8±0.3 %
Male	25.8 %	1.4±0.1 %

3.2.10.5. Comparing the results with the literature

Although no previous data existed for comparing the glide efficiency found in this study with previous literature, the average glide factors were calculated based on the average velocity and acceleration presented in the existing literature. The calculated values were used to make comparison with the glide factors found in this study in order to establish the validity of the results.

3.3. Results

As the glide factors changed linearly with increasing the velocity, the data for each subject was approximated by a linear fit (R^2= 0.86±0.10). The best linear fit that represents the glide factor versus the average velocity is shown in Figure (3.6) for different subjects. As it can be seen in Figure (3.6) each subject's glide factors follow a unique linear trend with a distinctive intercept and gradient that indicates how the glide factor changes across different velocities.

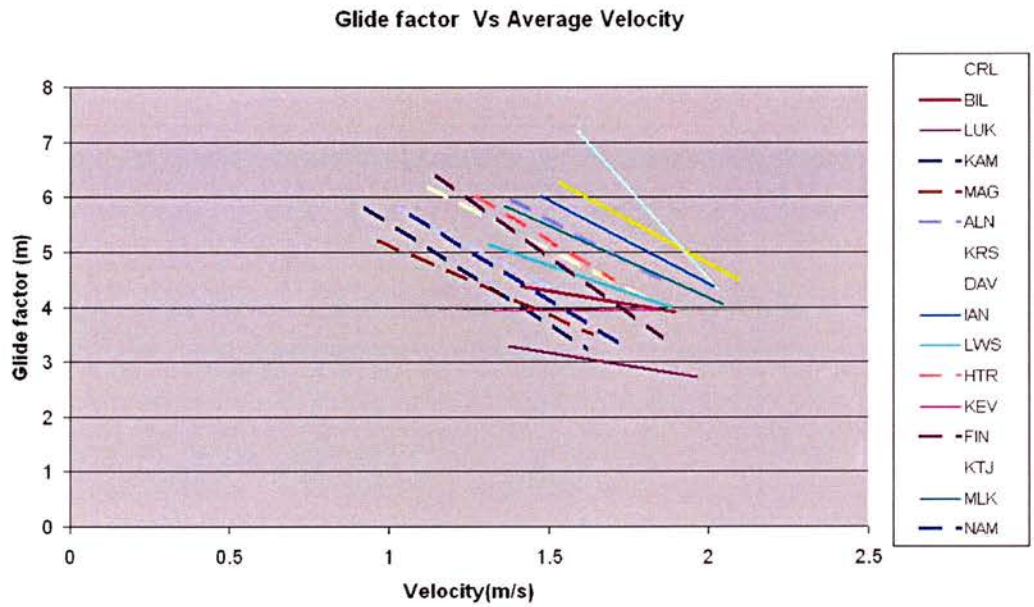

Figure 3. 6. Linear fits representing glide factor Vs average velocity for different subjects. The solid lines indicate the corresponding best linear fits for male subjects and the dashed lines represent the females' best fits.

Table 3. 4. Body mass, maximum cross-sectional area and the glide constant for each subject.

Subject	Mass (kg)	Max. Cross-sect. area (m^2)	Glide constant(m)
ALN	64.2	0.0779	1.65
CRL	65.9	0.0790	1.67
FIN	69.4	0.0847	1.64
HTR	75.1	0.0758	1.98
KTJ	70.6	0.0709	1.99
KAM	60.4	0.0687	1.76
MAG	69.0	0.0740	1.86
NAM	59.9	0.0650	1.84
BIL	73.5	0.0783	1.88
DAV	86.9	0.0966	1.80
IAN	80.1	0.0802	2.00
KEV	72.6	0.0779	1.86
KRS	76.6	0.0832	1.84
LWS	71.6	0.0807	1.78
LUK	77.4	0.0827	1.87
MLK	76.3	0.0772	1.98

The maximum cross-sectional area, the body mass and the calculated glide constant for each subject are presented in table (3.2).

The dimensionless shape-related glide coefficient was calculated for each subject at each corresponding velocity as the ratio of the glide factor to the glide constant at each corresponding velocity.

Figure (3.7) shows the glide coefficient versus average Reynolds number for each subject. Each subject's glide coefficients follow a unique linear trend with a distinctive intercept and gradient.

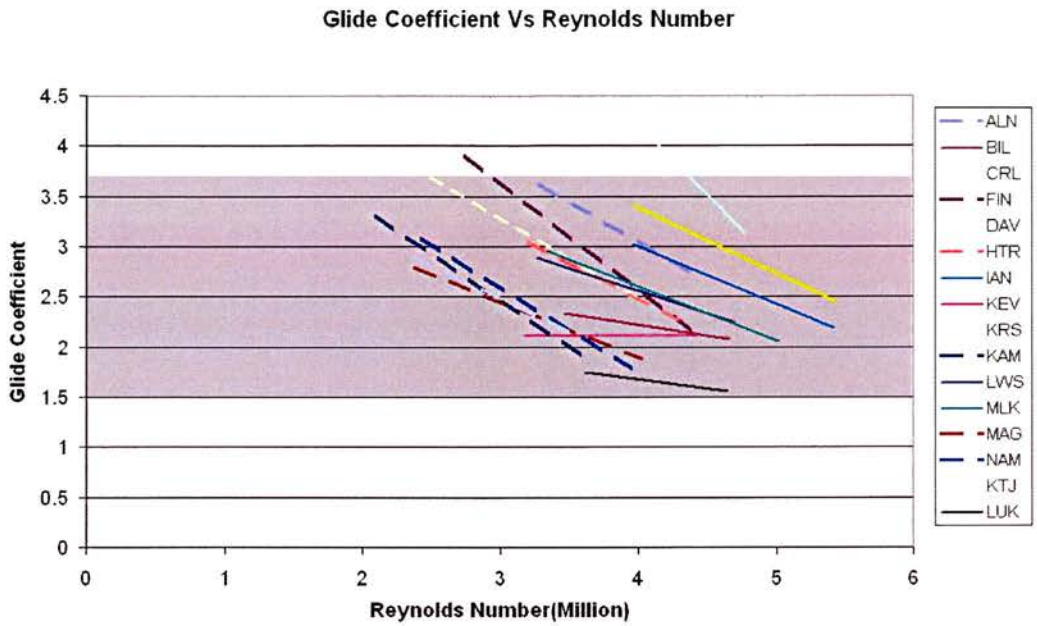

Figure 3. 7. Linear fits representing glide coefficient Vs average Reynolds numbers for different subjects. The solid lines indicate the corresponding best linear fits for male subjects and the dashed lines represent the females' data.

3.4. Discussion

Glide efficiency that relates hydrodynamic and kinematic aspects of the glide has not been determined previously despite its importance in swimming. The aim of this study was to develop and test a method of quantifying the glide efficiency in a way that accounts for both the inertial and resistive characteristics of the gliding body as well as the differences in the instantaneous velocities.

Glide efficiency has been defined in this study as the ratio of the virtual mass to the resistive factor of a gliding body during a glide interval. Glide efficiency reflects the deceleration of a body at each corresponding velocity in the sense that a body that decelerates less at each corresponding velocity glides more efficiently. The higher the ratio of the virtual mass to the resistive factor for a gliding body, the smaller the

deceleration when gliding at each corresponding velocity and therefore the higher the glide efficiency. The glide factor indicates the ratio of the velocity squared to the deceleration of a body at each instant during a glide interval thereby allowing a comparison of the glide efficiency across different velocities. The following discusses the implications and validity of the method that has been developed and tested.

3.4.1. Implications

3.4.1.1. Prediction of deceleration

In a practical context it is highly desirable to predict how a swimmer decelerates during a glide to determine how performance may be optimised. This would involve aspects such as refining body posture and the best time to initiate the post-glide phase.

In a previous study based on the fact that larger and heavier swimmers experience higher values of passive drag, it was concluded that this type of swimmer decelerates faster during glides and should start the post-glide action earlier (Benjanuvatra, *et. al.* 2001). This suggestion ignores the fact that the heavier swimmers have higher inertia, which together with the resistive force affects the changes in velocity during a glide.

In order to predict how a body decelerates during a glide, in addition to the resistive force, the value of its virtual mass that includes the body mass and the added mass of water entrained with the body should also be known. Since the value of added mass at deceleration is difficult to quantify for a human body, in the predictions based on the values of resistive force the added mass was ignored (Lyttle *et al.*, 1998). By this method the virtual mass was underestimated and assumed to be equal to the body mass. With the underestimation of the virtual mass Newton's second law of motion provided an overestimate of the deceleration (rate of changes in velocity) compared to the actual value of the deceleration of the body during a glide. Consequently, the predicted time for reaching a final velocity was shorter than that during an actual glide.

The overestimation of the rate of changes in velocity (deceleration) affects the validity of determining the exact timing to initiate the post-glide phase after the starts and turns. This results in proposing to commence the post-glide action earlier than the optimal timing. Initiating a premature post-glide action can result in increasing physiological costs and losing velocity in a higher rate compared to what could have been achieved by maintaining a passive glide. As a result of overestimation of deceleration, Lyttle *et al.*, (1998) underestimated the distance travelled in a time period compared to the real distance that could be travelled by a body during a glide.

One of the major implications of the glide efficiency is the ability to determine the velocity variations of the body during a glide. By knowing how the glide efficiency of swimmer changes across velocities, it is now possible to determine how fast he/she decelerates during a glide. This information is particularly important in predicting the exact timing for initiating the post-glide action for a particular swimmer with a distinct glide efficiency and post-glide performance. For example for each subject the glide should end when the velocity reaches the velocity which can be sustained by the post-glide actions.

Although it was possible to determine the instantaneous velocity of a body during the whole period of glide by the direct methods like video analyses, due to variations in the velocity that was mentioned earlier, and the difficulties in maintaining a consistent streamlined posture over long glide periods the instantaneous velocity data may not be valid for comparison. However, the method that has been developed enables regressions equations for glide factor as a function of velocity to be obtained. From these the predicted velocity profiles can be reconstructed based on Equation (3.11). Since the range of velocities on which the glide factor was determined for each gender group was different, the velocity was reconstructed for a different range for the male and the female groups. The reconstructed velocity variations from 2 m/s down to 1.6 m/s for the male group and the reconstructed velocity variations from 1.8 m/s down to 1.4 m/s for the female group are shown in Figures (3.8) and (3.9) respectively. By intersecting a

horizontal line that represents the velocity at which the post-glide phase can be sustained, with the curve of variations of the glide velocity for each subject the instant at which a swimmer should initiate the post-glide phase can be determined.

For example, assuming that subject MLK in the male group was able to maintain a post-glide action at the velocity of 1.6 m/s; he should end the glide and commence the post-glide action after 0.5 s from the time of the initial velocity of 2.0 m/s. Similarly if subject NAM in the female group had an initial velocity of 1.8 m/s and can maintain a post glide speed of 1.4 m/s she should glide for 0.6 s before initiating the post-glide phase.

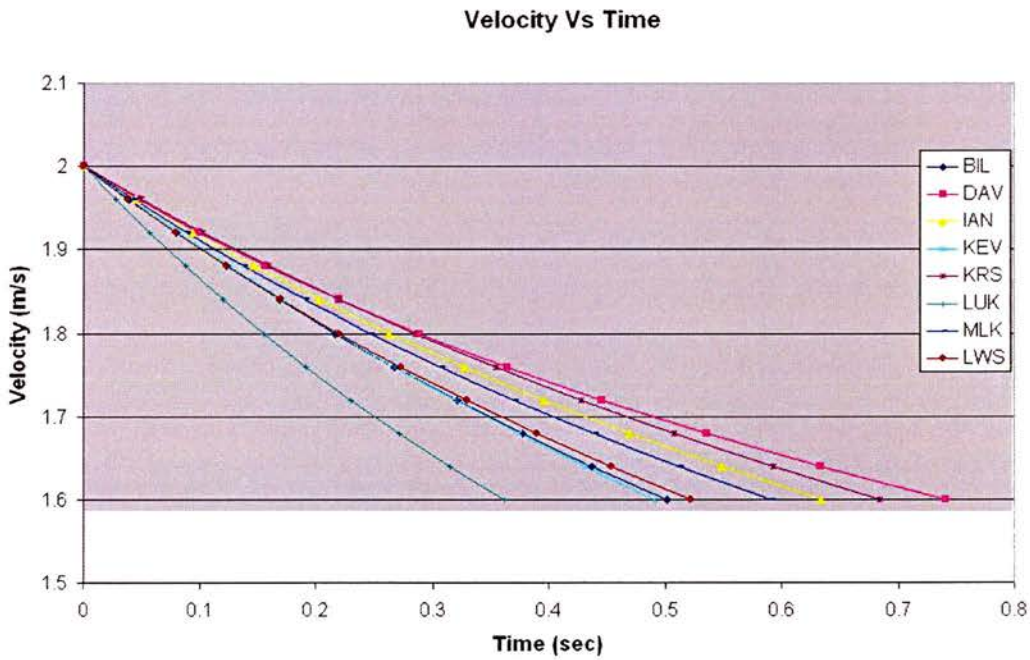

Figure 3. 8. The reconstructed velocity Vs time for the male subjects.

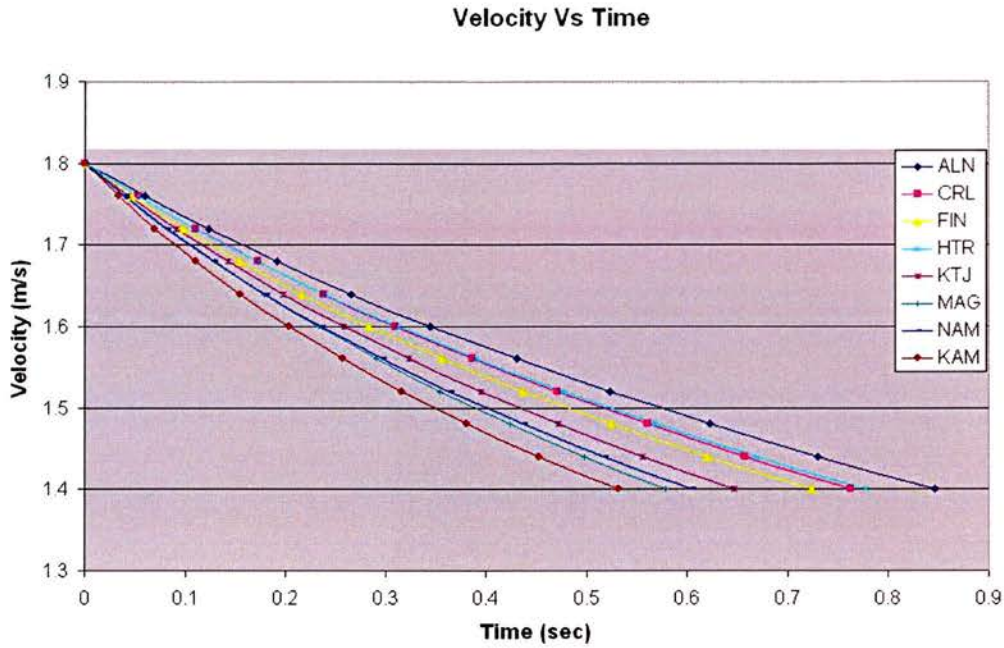

Figure 3. 9. The reconstructed velocity Vs time for the female subjects.

3.4.1.2. Glide efficiency's contribution to performance

As can be seen from the graphs in Figures (3.8) and (3.9) the velocity gradient for the subjects who possesses a higher glide efficiency is less, indicating smaller velocity decrease in a certain period of time. Also it takes longer for a subject with the higher glide efficiency to decelerate to a certain velocity compared to a subject with the lower glide efficiency.

The area below the velocity curve indicates that the distance travelled by the body with higher glide efficiency is more than the distance travelled with the body with less glide efficiency during the same time period.

In order to determine how possessing higher glide efficiency is beneficial in the swimming events, two subjects with different glide efficiency were considered while all other influential factors were controlled. In order to make the comparison valid it was

assumed that the two subjects reach a consistent posture during glides after starts and turns at the same velocity (2 m/s) and at the same distance from the wall (origin). Also the velocities at which each of the subjects is able to sustain a post-glide action with constant velocity were identical (1.6 m/s).

The distance travelled by each swimmer during the glide can be calculated based on Equation (3.20). Since each swimmer travels at a constant velocity during the post-glide action, the distance travelled during the post-glide period can be calculated as the velocity during the post-glide phase (1.6 m/s) multiplied by the time spent during this period.

The male subject with the lowest gliding efficiency (LUK) in the group with the male subject with the highest glide efficiency (DAV), were considered for this comparison. Based on their reconstructed velocities (Figure 3.8) the following scenario can be predicted and is displayed in Figure (3.10). With both starting the glide at the same position (distance from the wall) at initial velocity of 2 m/s, LUK had a velocity of 1.6 m/s after 0.36 s, while DAV had a velocity 1.75 m/s after the same period. During this period DAV travelled 0.665 m while LUK travelled 0.025 m less (0.630 m). At this time LUK started initiating the post-glide propulsive action with a constant velocity of 1.6 m/s, while DAV continued to glide. At the time of 0.74 s DAV reached the velocity to initiate the post-glide phase. LUK's total travelled distance during this period included 0.606 m as the distance travelled at the constant speed of 1.6 m/s during the time period between 0.36 s and 0.74 s, in addition to 0.630 m distance which he travelled during the glide. The distance travelled by DAV during this period was 1.282 m travelled entirely during the glide. Thus, the distance travelled by DAV was 0.046 m more than the total distance travelled by LUK during the same time.

The blue bar in Figure (3.10) represents the distance travelled during the glide with no physiological demand and the red bar represents distance travelled during the post-glide

phase that is physiologically demanding. Thus the advantage for DAV is not only in terms of distance gained but in terms of minimising physiological cost.

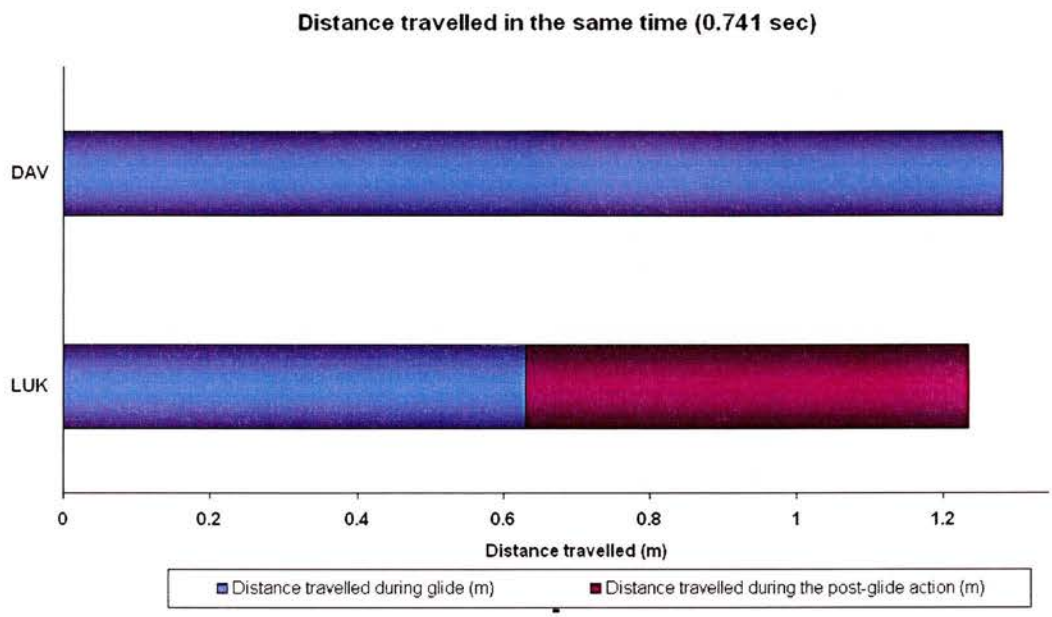

Figure 3. 10. The reconstructed distance travelled during 0.741 s.

In a 200 m race in a short course event with all else being equal, DAV finishes about 38 cm ahead of LUK, which, assuming an average velocity of 1.6 m/s (for 200 m breaststroke at this level) during a race can be translated to 0.24 s time advantage. Further, it should be noted that during a 200 m short course event DAV spends about 3 s more in the passive glide phase after starts and turns compared to LUK. This gives DAV a longer period of recovery as well as a shorter period of active swimming, which together would improve the performance.

The fact that spending more time during glide would lead to both a distance and a physiological advantage supports the findings of Hay and Guimares (1983) and D'Acquisto, *et al.* (1988) who found that swimming performance is related to the time spent during glide phase.

3.4.1.3. Shape-related Vs size-related glide efficiencies

In comparing two bodies' glide factors it is desirable to distinguish the contributions of a body's size including the mass and the cross-sectional area and other factors such as the body shape. By separating a glide factor into a glide constant and a glide coefficient the size and shape-related glide efficiencies of a body were quantified. The comparison between the glide coefficients allowed investigating the shape-related glide efficiency, while comparing the glide constants enabled determining the size-related glide efficiencies. The glide coefficient represented the ratio of the virtual mass coefficient to the drag coefficient while the glide constant represented the ratio of the body mass to the product of maximum cross-sectional area and half the water density. The glide factor is the product of the shape-related glide coefficient and the size-related glide constant.

The glide constant can be used to determine the suitability of the size of a body to enable it to glide efficiently. For example heavier swimmers with lower maximum cross-sectional areas have a better potential to glide in terms of their size compared to the swimmers with the lower body mass and higher maximum cross-sectional areas.

In comparing the subjects of our example LUK possessed a higher glide constant compared to DAV (1.87 m Vs 1.80 m). This indicated that the body size of LUK had a higher potential for more efficient glide compared to DAV's body size. Despite this his glide factor was lower than the values for DAV. This emphasises that in addition to the size, the shape of the body influence its glide efficiency.

As a dimensionless ratio the glide coefficient provided information on the shape- related glide efficiency. Since the glide coefficient was calculated as the ratio of a glide factor to the glide constant (Equation 3.27), and Reynolds number was determined as a constant (the ratio of the length to the kinematic viscosity) times velocity (Equation 3.28), the glide coefficient changed with the average Similar to the glide coefficient, the glide factor changed with the average velocity (and therefore the Reynolds number) for each individual.

The glide coefficient determines the potential of a particular body shape to glide efficiently. For example, shapes that are able to entrain a large quantity of water while minimising the drag glide efficiently. It can be seen that the superior shape of DAV that is supported by having a higher glide coefficient at each corresponding Reynolds number compared to LUK, allow him to glide more efficiently.

3.4.1.4. Performance enhancement in passive phases:

In view of the fact that passive drag values alone cannot completely predict the deceleration of a body during a glide; it can be argued that in order for a design or modification to contribute to the glide efficiency, it should be able to increase the values of the glide coefficient rather than merely decreasing the passive drag.

Since it has been established that there is a tendency for the more streamlined objects to possess a lower values of the added mass, any modification to decrease the passive drag may decrease the added mass, so that the design may not be automatically translated to a better efficiency during the glide.

This has practical applications in testing swimming suits designed to improve performance. As the effect on the ability of a body to entrain the added masses of water affects its glide efficiency and hence the swimming performance, the glide coefficient rather than passive drag coefficient should be used to address the effect of the suits on the passive glide performance.

Although previous studies on the effect swimming suits design on the passive glide performance found that in some cases these suits significantly reduce the hydrodynamic resistance (Benjanuvatra, *et al.*, 2002) and in some cases no significant difference were found (Roberts, *et al.*, 2003), these may not be adequate to determine the advantage of these suits under the realistic gliding conditions. In order to determine whether these

suits improve the passive glide performance, the hydro-kinematic method should be used to determine their effectiveness under the realistic gliding conditions.

3.4.2. Validity

3.4.2.1. Logical validity

The goodness of fit statistics indicated that the displacement equation found in this study closely represents the real displacement data of a body in a rectilinear horizontal glide. This indicates the validity of the principles and assumptions which were used in the process of finding the equation.

Contrary to the study by Sharp and Costill (1989) who did not provide any rationale on fitting the velocity variations by an exponential regression fit, the equations used in this study were derived from the equation of motion of the body during glide and were in accord with the established principles of mechanics and fluid dynamics. Also previous studies (Sharp and Costill, 1989) did not provide any information on the goodness of fit as essential information on how the recommended model fits the real kinematic data.

3.4.2.2. Accuracy

Fitting the displacement function to the displacement data increased the accuracy of the calculation, as the errors in the displacement data did not get amplified. As a result of this the fit goodness of this study (average R-squared of 0.999 and the average RMSE of 0.089) was an improvement over the previous study by Naemi and Sanders (2004) in which an average R squared value of 0.943 and an average RMSE of 0.002 were obtained. This improvement in the fit goodness parameters indicate that compared to the previous study (Naemi and Sanders, 2004) in which the velocity function (Equation 3.11) was fitted to the velocity–time data of a glide, fitting the displacement function to the displacement data produces more accurate results. Also averaging the raw displacement data of different markers to eliminate the noise compared to using the hip

kinematics provided an opportunity to eliminate the random error without affecting the real data.

Using the most advanced curve fitting technique that minimizes the summed square of residuals and downweight outliers decreased the chance of variations in the calculated glide factors caused by inaccuracies in the displacement data. The current confidence level determined by 95% certainty level together with a relative confidence bound width of 9.8 ± 0.2%, assures that there is only 5% chance that the actual glide factor would be more than about 10% different than the calculated glide factor.

The considerable changes in glide factor with the average velocity found in this study indicate the importance of calculating the glide factor for each corresponding average velocity, and the fact that one glide factor may not represent the glide efficiency of a body along the whole range of velocities. Contrary to the previous studies (Naemi and Sanders, 2004 and Klauck and Daniel, 1976), in which a function was fitted to the whole glide period, in this study the smaller intervals were considered. This helped to decrease the error as a result of consistency of the glide factor.

The high level of confidence in the calculated glide factor (relative standard error of calculation equal to 2.45 ± 0.05 %) together with the low error associated with the assumption of the consistency of the glide factor in each glide interval (3.1± 0.3 % increase in the glide factor from the beginning to the end of each interval) determine the limits of the accuracy for the method. The relatively shorter glide duration in the current study (0.38 s) compared to the previous studies (1.5 s for Starling *et al.* 1995) make it easier for a subject to maintain consistent body posture along the glide interval and contributed to the accuracy of the current study compared to the previous studies.

Despite the favourable results obtained, further improvements in the accuracy could be achieved. Increasing the sampling frequency in the future studies would allow the use of a shorter glide interval, thereby reducing the error associated with assuming a consistent

glide factor over a glide interval. Also increasing the image resolution may allow a more accurate digitizing and consequently increase the accuracy of the raw displacement data of a glide so that the confidence level in the calculated glide factor would increase.

3.4.2.3. Reliability

The results based on multiple testing of two individuals at three separate sessions indicated that the coefficients of variation of the regression lines representing the variations of the glide factor to velocity were low (less than 0.3% for the slopes and less than 3% for the intercept). This indicated that the method can be used to determine the glide efficiency with a high level of stability. The existing variability could be related to the biological variations of subjects between the test days that are not controllable.

The maximum relative standard error of measurement determined for the test-retest (the glide factors corresponding to the same velocity) was 2.94 %. This was higher than the relative standard error of calculation (2.45%) that arises in the calculation of glide factors during the curve fitting.

Since in this study other source of variability including the data collection procedure were controlled by introducing a standard procedure through the whole data collection, the remaining variability after deducing the errors as a result of calculation would be mainly due to the natural variability of conditions between tests. This could be attributed to the small variability between the postures that may not be detected under the current limits of acceptable changes that can occur during the glide intervals. Slight changes in the posture may change the flow characteristics around the body and in turn affect the resistive force and added mass values and hence affect the glide efficiency of the subject.

3.4.2.4. Construct validity

Despite the 2.94 % relative standard error of measurement, comparing the coefficient of variation of the glide factor within and between individuals at a definite velocity range indicated a small inter-individual variations compared to between individuals (1.8±0.3 % vs. 13.2 % for the female group and 1.4±0.1 % vs. 25.8 % for the male group). This indicates that the differences between individuals can be detected by this method and establishes the potential of the method in an applied context. Further studies would be followed in chapter 5 to determine the source of variability between individuals in their glide efficiency.

3.5. Conclusion

A new method dubbed the 'hydro-kinematic' has been developed that relates the hydrodynamic characteristics of a human body in a streamlined position to its glide efficiency. It was established that the glide efficiency would enable us to predict the kinematic characteristics of a body during a glide, and is more useful in studying factors that affect performance and potential performance in the glide phases than measures of passive drag alone. The glide factor was able to account for both the inertial and resistive characteristics of a body as well as the differences in the instantaneous velocity. The method showed to be able to distinguish between the individuals in their glide efficiency with an acceptable validity. The separation of glide factor to a size-related glide constant and a shape-related glide coefficient enabled the merits of the size and shape in the glide efficiency to be quantified. It was found that generally by increasing average velocity of glides the glide factor decrease and possessing higher glide efficiency at each corresponding velocity would lead to physical and physiological advantages in a race condition.

Chapter 4

Study 2: Quantifying the Human Body Hydrodynamic Parameters in a Streamlined Position Based on the Kinematics of an Underwater Glide

Nomenclature

X: Horizontal axis

Y: Vertical axis

r: Inclined axis in the direction of travel

l: Inclined axis perpendicular to the direction of travel

r: Resultant displacement of the body (m)

v: Resultant glide velocity (m/s)

$\mathbf{V_0}$.: Initial resultant velocity of the rectilinear glide interval (m/s)

D: Drag or total resistive force opposite the direction of travel (N)

L: Lift, the downward force perpendicular to drag (N)

B: Buoyancy, the hydrostatic force applies to the body in vertical direction (N)

W: Weight, gravity forces apply to the body (N)

$\mathbf{C_R}$: Resistive factor (kg/m)

$\mathbf{C_d}$: Drag coefficient (Dimensionless)

$\mathbf{C_a}$: Added mass coefficient (Dimensionless)

M: Virtual mass of the body in direction of travel (kg)

m: Mass of the body. (kg)

$\mathbf{m_a}$: Added mass of water in direction of travel (kg)

A: Maximum Cross sectional Area, Projected area in the transverse plane perpendicular to the direction of travel. (m^2)

ρ: Water density. (kg/m^3)

α: Glide angle, the angle between the rectilinear glide trajectory and the horizontal line (deg)

V: Body volume (m^3)

$\mathbf{Re_{ave}}$: Average Reynolds number over a glide interval (dimensionless)

υ: Kinematic viscosity (m^2/s)

$\mathbf{V_{ave}}$: Average velocity for each glide interval (m/s)

4.1. Introduction

Although quantifying the glide efficiency with the method established in Study 1 has the advantage of considering both the inertial and the resistive factors in conjunction with each other, the question remains as to how these two contributing factors act individually. For example, it would be of great value to quantify whether the better gliding performance of one gliding body than another is due to its low resistive forces or whether it is due to its high virtual mass. Thus it would be valuable to introduce a method that would be able to calculate the resistive and inertial parameters separately based on the kinematics of a glide. The knowledge of these two important contributing factors to glide efficiency is essential in developing an optimised streamlining position for each swimmer with the aim of minimising the resistive force and maximising the inertia. This has also specific applications in identifying flaws in gliding postures to improve performance and to identify potential in swimming (talent identification).

There is a lack of knowledge about the hydrodynamic factors of a human body in a streamlined position under a real glide condition. The methods of quantifying the hydrodynamic resistive force based on measuring resistive forces in a steady state flow may not resemble the body posture and the flow characteristics during an unrestrained glide. In an unrestrained glide the inertial and resistive force are influenced by the acceleration of the body and its entrained mass of water.

A method of calculating the resistive force based on the kinematics of a glide can produce more realistic results than the methods based on the quasi-static assumption, as the flow characteristics and the natural posture of the body during a glide would not be altered (Williams, 1987). In the existing method which used extensively in for the aquatic animals, in order to calculate the resistive force, the added mass of the body should be known beforehand.

Using existing methods of calculating the hydrodynamic resistive force applied to a human body based on the kinematics of glide has not produced accurate results since the added mass has been ignored and the virtual mass has been assumed to be equal to the body mass (Klauck and Daniel, 1976).

Due to the high degree of streamlining of the aquatic animals, their added mass value can be approximated by the added mass of the similar bodies of revolution (Landweber, 1961). Taking advantage of this approximation more realistic resistive parameters have been calculated for the aquatic animals based on the kinematics of the glide (Lang and Daybell, 1963, Feldkamp, 1987 and Stelle, *et al.*, 2000). However, due to the complex morphology of a human body, approximating the added mass with the added mass of the bodies of revolution is not valid or accurate.

The aim of this study was to develop and test a method of quantifying the hydrodynamic properties of a human body in a streamlined position during an underwater glide so that the values of the resistive factor and the virtual mass can be determined separately.

Taking advantage of the component of the net vertical force opposite the direction of travel as a constant force applied to a descending gliding body in a rectilinear path, the virtual mass and the resistive factor can be separated as independent parameters.

To determine the applicability of the method to quantify the hydrodynamic parameters of a human body in a streamlined position, the validity, accuracy and the reliability would be investigated in a similar way to what was described in Chapter 3.

Since in this study the virtual mass and resistive factor of a human body would be quantified separately, as opposed to the first study in which a ratio of these parameters were quantified as the glide factor, there is a possibility that mathematically, they 'play against each other'. Thus the independency of the calculated resistive factor and the virtual mass should be assessed.

The resistive factor and the added mass of a body are dependent on the size as well as the shape of the body. By normalising the resistive factor to control for the effect of the maximum cross-sectional area, the drag coefficients would be calculated. Also the added mass coefficient can be quantified for each body by controlling the added mass for the effect of the body volume. These two dimensionless coefficients determine the shape-related resistive and inertial characteristics of a body independent from their size.

4.2. Methods

4.2.1. Subjects

The same subjects from study1 participated in this study. As the data collection for this study was started following the completion of the pool data collection in Study 1, the same skin markings were used for each subject. The same maximum cross-sectional area and height that were calculated in study1 were used for this study.

4.2.1.1. Hydrostatic measurements

Hydrostatic weighting was used to measure the net buoyancy forces of the body when the subject inhaled maximally (Katch, *et al.*, 1969). Each subject was weighed in the hydrostatic weighting tank according to the procedure recommended by the manufacturer. Each subject was weighed three times following maximal inhalation. The net buoyancy force in the maximum inhalation would be used to calculate an upper limit for the component of the net buoyancy opposite the direction of travel during each glide.

4.2.2. Data Collection

4.2.2.1. Instruction and protocol

Prior to the pool test, the subject was instructed to push-off the wall and to adopt a streamlined position during the glides. The definition of the streamlined position was the same as in study 1, while the direction of travel was inclined towards the bottom of the pool.

A submersion, preparation and push-off protocol was taught to the subject to ensure performance of an inclined rectilinear glide at an adequate depth. This protocol included taking a moderate (normal) inhalation followed by submerging underwater while treading the water upwards to cancel the net buoyancy. While the feet were placed at push-off marks at a 30cm depth below the surface, the subject was requested to go deeper until the head reached a depth of 50 cm below the surface.

The mentioned initial push-off depth and the body orientation was considered to allow the highest part of the body (feet) to be at an adequate depth of more than 60 cm during glides where the data collection was commenced (Figure 4.1). Simultaneously the subject resumed a ready position with the arms and the trunk towards the bottom of the

pool at a point situated at 6.5m distance from the wall while the legs were bent and ready for push-off.

This distance was intended to allow a practical rectilinear inclined glide with a consistent glide angle of 15 degree so that the subject would be able to push off from the wall in a comfortable position and have an adequate depth over the part of glide path where the data were collected (Figure 4.1).

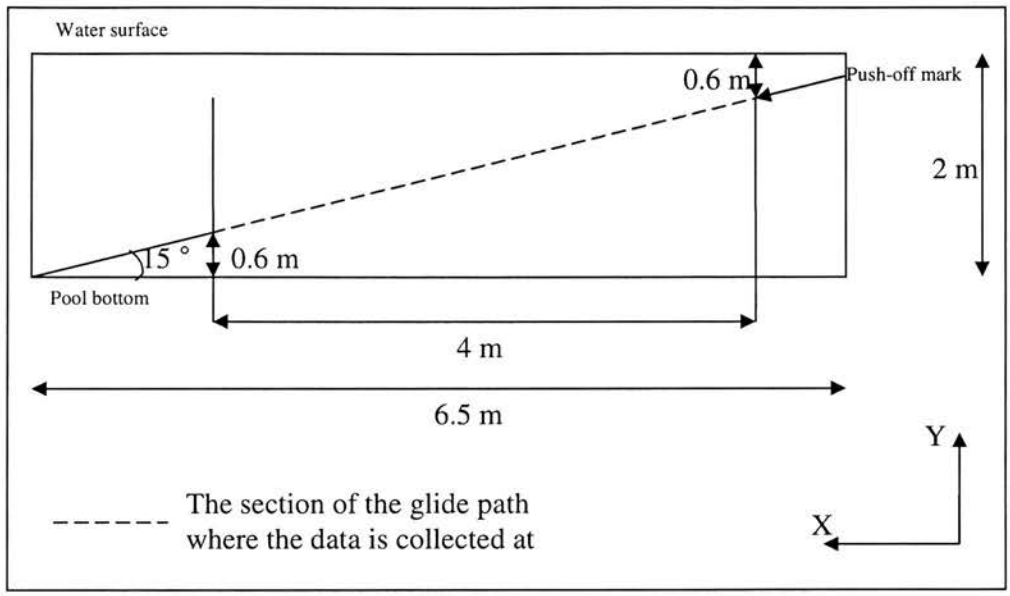

Figure 4. 1. Schematic side view of the gliding path and the designated data collection section

A moderate rather than a maximum push-off was recommended to enable adoption of a streamlined position immediately after the wall release. The subject was requested to sustain an inclined alignment during the period of the glide and to maintain the posture. It was emphasized that lateral deflection of the body (lateral sway of legs) or arching back (hyperextension) or 'twisted trunk' (misalignment of lines connecting the shoulders and the hips) should be avoided as much as possible.

4.2.2.2. Filming and feedback procedure

The filming and the feedback procedures were identical to those of study 1.

4.2.2.3. Warm-ups and the main trials

The subject participated in the warm-ups comprising 8×25 m swims starting from a static push-off from the wall and followed by a rectilinear inclined glide. After each 25 m the subject was informed about the possible changes required to improve the performance of the glides.

The main trial procedures were also the same as in Study1. Depending on the subject's ability to perform glides according to the instructions the total numbers of the glides performed by each subject were different ranging from 24 to 28 in order to achieve 15 acceptable glides.

4.2.3. Data Processing

4.2.3.1. Trimming process

In order to eliminate the possible effect of the lens distortion at the edges of the field of view, Ariel Performance Analysis System (APAS) software was used to trim the video files to the period during which the subject passed through the middle 4 meters view of the camera (Figure 4.1). This also ensured that the subjects were at an adequate depth throughout the period analyzed.

4.2.3.2. Digitizing Process

The digitizing process was identical to the procedure stated in Study1.

4.2.4. Definitions and Underlying Principles to Ensure the Logical Validity of the Method

The definitions and underlying assumptions including the passive glide, angle of attack, virtually zero angle of attack, rectilinear glide, consistency of posture and shape, consistency of maximum cross sectional area, consistency of projected area, virtually constant glide angle (α) or rectilinearity, adequacy of depth, hydrostatic balance and hydrodynamic stability, consistency of added mass, consistency of drag coefficient for limited ranges of Reynolds number, symmetry and two-dimensionality or planarity were identical to those in Study 1. In addition to these the following assumptions were necessary.

4.2.4.1. Adequacy of vertical distance from the bottom

All rectilinear glides were done in a way to prevent excess effect of the pool floor boundary on the resistive forces (Larsen, *et al.,* 1981). The body during an inclined glide should not go deeper than 1.4m as this allows a minimum 0.6 m vertical distance from the floor of the pool to prevent excess boundary effect.

4.2.4.2. Consistency of buoyancy

Consistency in body volume along each glide interval is required to ensure that the buoyancy force does not change during a glide interval. This was achieved by ensuring that the subject maintains the amount of breath during a glide. Also the changes in the body volume due to the increase in the hydrostatic pressure as a result of increase in the depth in each glide interval were negligible.

Based on these criteria the appropriate glide sequences have been selected from each trial and the sequences not complying with the criteria of the passive rectilinear inclined glide were eliminated.

4.2.5. Mathematical Model

This section describes the mathematical model and its underlying rationale for determining the resistive and inertial parameters of a swimmer during an inclined descending rectilinear glide.

Figure (4.2) demonstrates the free body diagram of a gliding subject in an inclined rectilinear glide. The body is affected by the hydrodynamic, hydrostatic and gravitational forces. In an inclined rectilinear glide the lift which might result predominantly from the shape of the body, is cancelled by the component of the net buoyancy perpendicular to the direction of travel. (Figure.4.2)

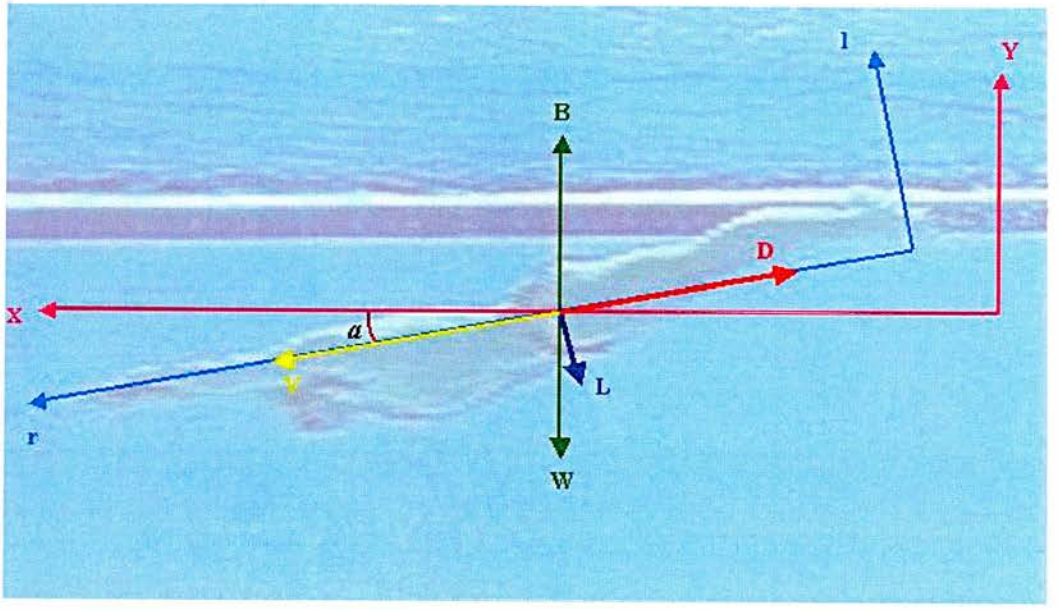

Figure 4. 2. Free body diagram of a swimmer in the streamlined position during an inclined rectilinear passive glide.

Newton's second law of motion can be applied in the direction of travel. In the absence of any propulsive force we have:

$$M.\frac{dv}{dt} = -D - (B - W).\sin(a) \qquad \text{(Equation 4.1)}$$

Drag could be replaced by the following formula:

$$D = \frac{1}{2}.C_d.A.\rho.v^2 \qquad \text{(Equation 4.2)}$$

Based on the underlying principles a constant resistive factor (C_R) that is the ratio of the resistive force to the velocity squared is introduced for each glide interval which incorporates the drag coefficient, the water density and the maximum cross sectional area.

$$C_R = \frac{1}{2}.C_d.A.\rho \qquad \text{(Equation 4.3)}$$

The resistive force in Equation (4.2) can be replaced by a constant resistive factor (C_R) times the velocity squared.

$$D = C_R.v^2 \qquad \text{(Equation 4.4)}$$

As the body volume remains constant during a rectilinear incline glide, the buoyancy represents a constant value. Since the subject perform glides in an inhaled condition, the difference between the buoyancy force and the weight that is known as the net buoyancy can be regarded as a positive constant parameter. Based on the assumption of the consistency of the glide angle (α) the component of net buoyancy opposite the direction of travel represents a constant value. For simplicity the component of net buoyancy opposite the direction of travel is replaced by a positive constant as "p".

$$p = (B - W).\sin(a) \qquad \text{(Equation 4.5)}$$

Replacing the resistive force (D) from Equation (4.4) and the net buoyancy component opposite the direction of travel (p) from Equation (4.5), into Equation (4.1), the differential equation of motion in the direction of travel (r), can be written as:

$$M.\frac{dv}{dt} = -C_R.v^2 - p \qquad \text{(Equation 4.6)}$$

Based on the assumptions, the resistive factor (C_R), the net buoyancy component opposite the direction of travel (p) and the virtual mass (M) would remain fairly constant for a glide interval. The initial velocity condition can be written as:

$$v(0) = V_0 \qquad \text{(Equation 4.7)}$$

Matlab Symbolic Math toolbox was used to solve the differential Equation (4.6), using the initial condition (4.7). The resultant velocity in the direction of travel can be found as a function of time.

$$v = \sqrt{\frac{p}{C_R}}.\tan[Arc\tan(\sqrt{\frac{C_R}{p}}.V_0) - \sqrt{\frac{p.C_R}{M}}.t] \qquad \text{(Equation 4.8)}$$

Equation (4.8) represents the resultant velocity as a function of time and four constant parameters including the initial velocity (V_0), the resistive factor (C_R), the virtual mass (M), and the net buoyancy component opposite the direction of travel (p).

4.2.6. Procedures to Ensure Accuracy of the Quantified Parameters

4.2.6.1. Using raw displacement

Because of observed fluctuations in the velocity-time data that was discussed in study 1, it was more desirable to work with the original displacement data that can be obtained directly from the digitising procedure. For this reason Equation (4.8) that addresses the instantaneous velocity should be used to find the resultant displacement-time equation.

The resultant velocity is the derivative of the resultant displacement:

$$v = \frac{dr}{dt} \qquad \text{(Equation 4.9)}$$

Replacing the velocity as the derivative of the displacement in Equation (4.8) we have:

$$\frac{dr}{dt} = \sqrt{\frac{p}{C_R}}.\tan[Arc\tan(\sqrt{\frac{C_R}{p}}.V_0) - \sqrt{\frac{p.C_R}{M}}.t] \qquad \text{(Equation 4.10)}$$

The initial displacement condition can be written as.

$$r(0) = 0 \qquad \text{(Equation 4.11)}$$

Matlab Symbolic Math toolbox was used to solve the differential Equation (4.10), using the initial condition (4.11). The displacement in the direction of travel can be found as a function of time.

(Equation 4.12)

$$r = \frac{M}{2.C_R}.\{2.Ln[\sqrt{p.C_R} + V_0.C_R.\tan(\frac{\sqrt{p.C_R}}{M}.t)] - Ln[1+\tan^2(\frac{\sqrt{p.C_R}}{M}.t)] - Ln[p.C_R]\}$$

It is obvious that Equation (4.12) addresses the resultant displacement of a rectilinear inclined gliding body in the direction of travel as a function of time and four constants including, the initial resultant velocity in the direction of travel (V_0), the resistive factor (C_R), the net buoyancy component opposite the direction of travel (p) and the virtual mass (M).

Equation (4.12) can be fitted to the resultant displacement-time data of an inclined rectilinear glide interval, and the values of the resistive factor and virtual mass can be found on the basis of each fit.

4.2.6.2. Eliminating the noise in the displacement data

Due to the similar frequency content of the random noise and the drag fluctuations that were extensively explained in Study 1 under the same heading, the average raw displacements of the different markers were used to represent the raw displacement of the whole body.

4.2.6.3. Glide interval duration

As discussed in Chapter 3, choosing the optimum glide interval duration was important. The glide duration of 0.38 s that was found in chapter 3 was chosen for this study to allow the comparison between the glide factor and the resistive factor and virtual mass. With 20 points as a glide interval, and for a certainty level of 95%, the relative confidence bound width for the resistive factor was 12.3± 0.4%, while the relative confidence bound width for the virtual mass was 3.8± 0.2% for the subjects participated in the pilot study. The errors as a result of the assumption of the consistency of the resistive factor and virtual mass over the glide interval were less than 5% and less than 2 % for the resistive factor and the virtual mass respectively for subjects in the pilot work.

Glide intervals were selected for each individual from the acceptable glide sequences of each trial to be considered as the independent rectilinear glide intervals. Due to the differences in the velocities at which each subject was able to maintain a rectilinear glide under the required conditions in the designated data collection area, the total numbers of glide intervals were different for each individual ranging from 27 to 32.

4.2.6.4. Using advanced parametric curve fitting techniques

Matlab curve fitting toolbox was used to fit a curve representing the displacement-time equation (Equation 4.12) to the raw displacement-time data of the body. The algorithm and scheme were identical to what was explained in Chapter 3 with the following exception.

In order to make sure that the parameters have been selected in a realistic range, and eliminate the possibility that the parameters play against each other some of the parameters were limited by the lower and upper limits.

A lower limit for virtual mass was set as the subject's body mass value. An upper limit for the net buoyancy component opposite the direction of travel was also set as the product of the underwater weight in the maximum inhale measured in the weighing tank and the sine of the glide angle during each glide interval (Equation 4.5). The gradient of the linear regression fit to the average coordinates of the markers in an inclined path of the glide was used to find the glide angle for each rectilinear inclined glide.

At each corresponding velocity the drag force is the product of the maximum cross-sectional area of a body and the dynamic pressure difference between its leading and trailing edges. The dynamic pressure at the leading edge of a body is $(0.5.\rho.v^2)$, and the amount of dynamic pressure at the trailing edge depends on the degree of streamlining of a body. The more streamlined a body, the more the dynamic pressure at the trailing

edge, hence less the dynamic pressure difference between the leading edge and the trailing edge of a body. On the other hand for a bluff body the dynamic pressure at the trailing edge may drop to zero. As the human body represents a shape in more streamlined shape than a bluff body it was expected that the dynamic pressure at the trailing edge to be more than zero. For this reason, an upper limit for the resistive factor was calculated when the drag coefficient was equal to one (when the dynamic pressure at the trailing edge is zero) for each subject.

Fit goodness was evaluated using the fit goodness parameters identical to what was mentioned in Study1, in order to address how closely the model (Equation 4.12) calculates the raw resultant displacement data gathered from the glide intervals.

4.2.7. Quantifying the Resistive Factor and Virtual Mass and Calculating the Corresponding Average Velocity for each Glide Interval

Because each resistive factor and virtual mass was found for each glide interval during which the velocity is not constant, average velocity during each interval corresponds to these parameters. The average velocity (V_{ave}) can be calculated as the ratio of the resultant distance(r) travelled in each interval calculated based on Equation (4.12) to the intervals duration (T).

$$\overline{V} = \frac{r(T)}{T} \qquad \text{(Equation 4.13)}$$

For the glide intervals in this study T can be replaced by 0.38 s. Knowing the initial resultant velocity (V_0), the resistive factor (C_R), the net buoyancy component opposite the direction of travel (p) and the virtual mass of body (M), an average velocity can be calculated that corresponds to the particular parameters for a glide interval.

4.2.8. Finding Drag and Added Mass Coefficients

Drag coefficient can be calculated from the values of the resistive factor knowing the maximum cross sectional area and the fluid density.

$$C_d = \frac{2.C_R}{A.\rho} \qquad \text{(Equation 4.14)}$$

Drag coefficient as a dimensionless coefficient is the indicator of the shape-related resistive characteristics. By eliminating the effects of the cross sectional area, the drag coefficient can be used to compare swimmer's ability to decrease resistance independent of their size.

The added mass (m_a) was found by subtracting the body mass (m) from the virtual mass (M).

$$m_a = M - m \qquad \text{(Equation 4.15)}$$

The body volume (V) during each glide interval can be quantified based on the net buoyancy component opposite the direction of travel which was found from the fitted curve. Based on Equation (4.5) we have:

$$B = \frac{p}{Sin\alpha} + W \qquad \text{(Equation 4.16)}$$

The buoyancy is equal to the weight of the displaced water according to the Archimedes principle.

$$B = \rho.V.g \qquad \text{(Equation 4.17)}$$

The body volume can be quantified by combining Equation (4.16) and (4.17).

$$V = \frac{\frac{p}{Sin\alpha} + W}{\rho . g} \qquad \text{(Equation 4.18)}$$

Equation (4.18) represents the body volume based on the net buoyancy component opposite the direction of travel (p), the glide angle (**α**), the weight on land (W), the fluid density (ρ) and the gravity acceleration (g). Calculating the body volume (***V***) from Equation (4.18), and obtaining the added mass from Equation (4.15) the added mass coefficient can be calculated.

$$C_a = \frac{m_a}{\rho . V} \qquad \text{(Equation 4.19)}$$

The added mass coefficient is a useful parameter that can identify the shape-related properties of the body for entraining water along independent from the size.

To compare the drag and added mass coefficients of different subjects against a dimensionless number, the average Reynolds number was calculated knowing the extended length (L), the average velocity (V_{ave}) and the dynamic viscosity (υ) of water according to the following formulae.

$$\mathrm{Re}_{ave} = \frac{V_{ave} . L}{\upsilon} \qquad \text{(Equation 4.20)}$$

4.2.9. Sample

Figure (4.3) shows a sample curve being fitted to the raw displacement data of a horizontal rectilinear glide. The resistive factor was quantified with 95% certainty within the confidence bound of between 16.2 kg/m to 18.3 kg/m. This confidence bound width corresponds to 12.1 % of the quantified resistive factor (17.23 kg/m). The virtual mass

was quantified within the confidence bound of between 79.9 kg to 84.4 kg, which corresponds to 5.4 % of the calculated virtual mass (82.16 kg).

The initial velocity for the glide interval was quantified as 2.099 m/s, within the confidence bound lower limit of 2.059 m/s and upper limit of 2.138 m/s. The component of the net buoyancy opposite the direction of travel was calculated as 1.25 N in a confidence bound of between 0.92 N to 1.58 N. The average velocity can be calculated based on Equation (4.13) as 1.85 m/s.

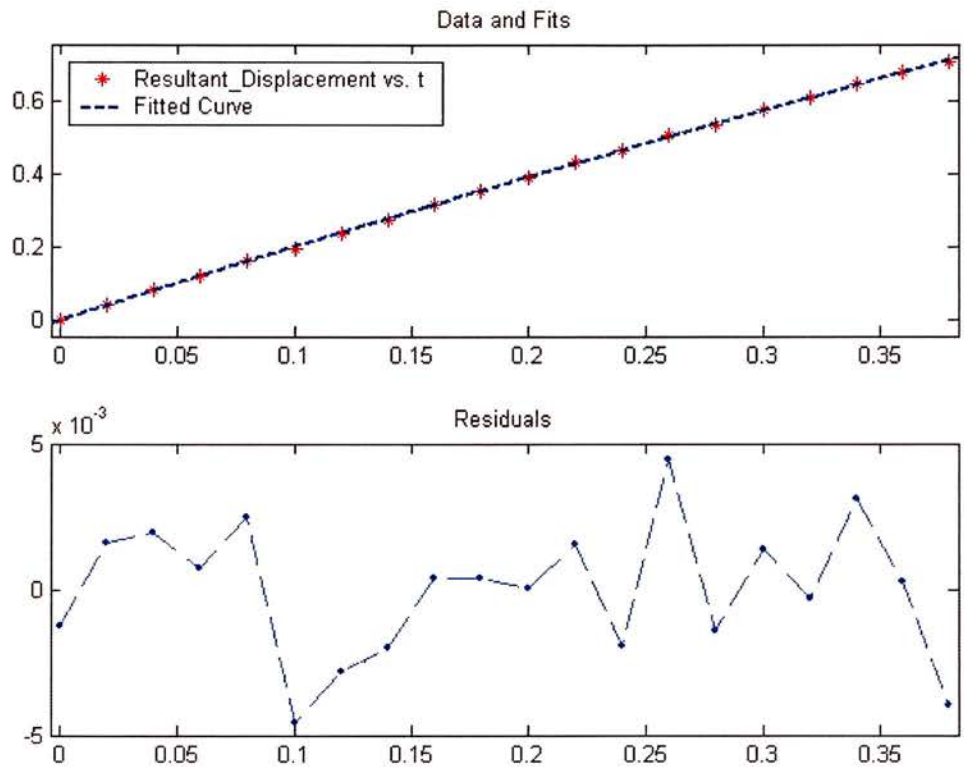

Figure 4. 3. A sample raw resultant displacement data of an inclined rectilinear glide and the corresponding fit based on Equation (4.12).

On the basis of each parametric fit for each glide interval a resistive factor and virtual mass were evaluated. The resistive factors and the virtual masses were shown in Figures (4.4) and (4.5) for the different average velocities for a female subject (FIN) with the

body mass of 69.4 kg and the maximum cross sectional area of 0.0847 m^2. Due to the fact that the glide factor and the average velocity were calculated based on each glide interval chosen from an acceptable glide sequence, there were no set average velocities at which each subject performed glides. However, linear regressions could be used to estimate (interpolate) the resistive factor and the virtual mass at the velocities different from the average velocities for which the resistive factor and virtual mass were calculated. As the resistive factor increased with a linear trend by increasing average velocity (r = 0.97), a linear line was fitted to represent the variations (R^2=0.94). Also the virtual mass showed to decrease with increasing the average velocity (r=-0.92), that allows a linear regression line to represent the variations (R^2=0.85).

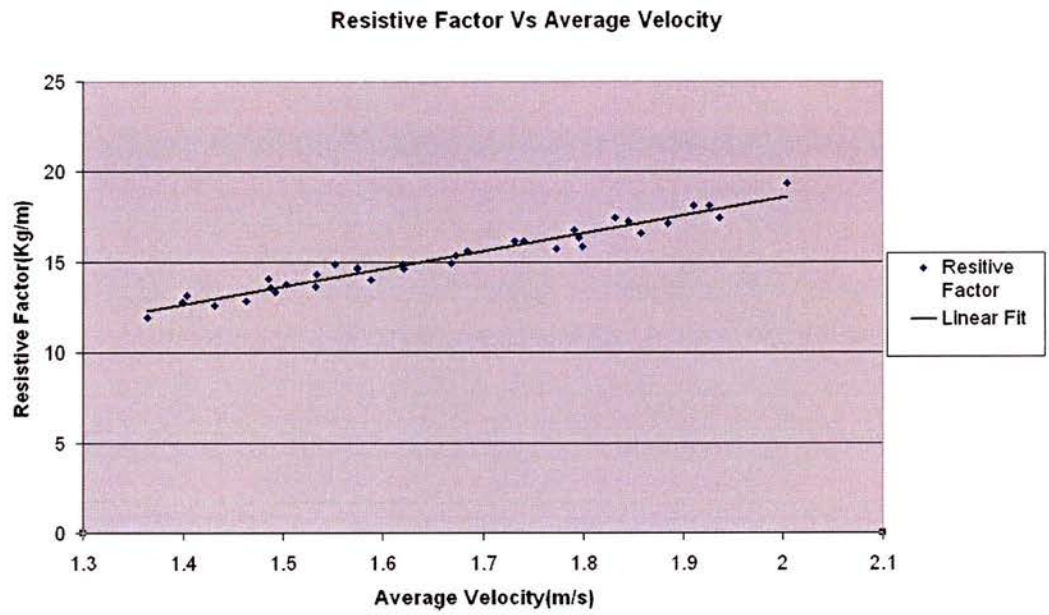

Figure 4. 4. A sample graph of resistive factor versus average velocity for a female subject.

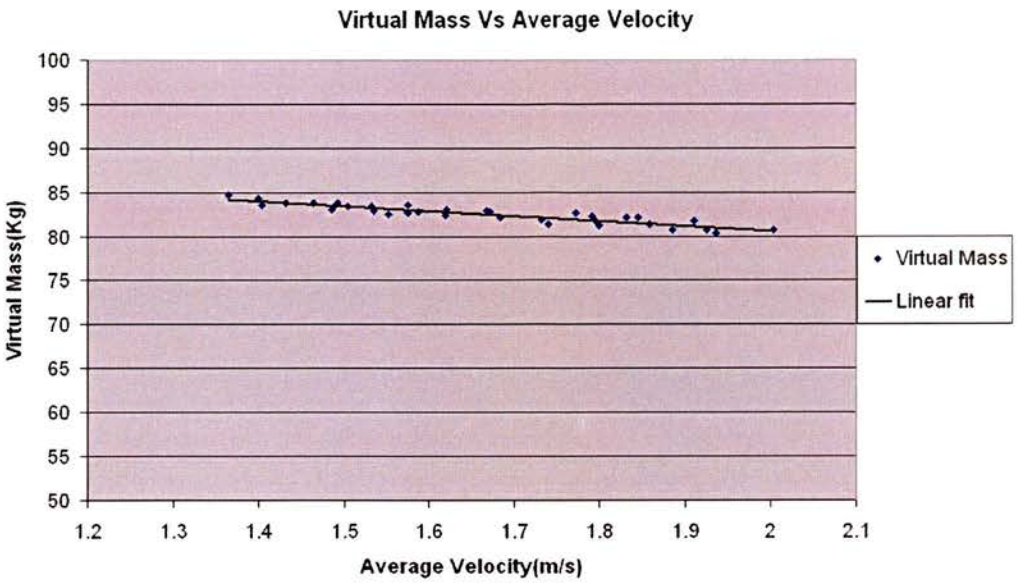

Figure 4. 5. A samples graph of virtual mass versus average velocity for a female subject.

4.2.9.1. Calculating drag and added mass coefficients

The value of the drag coefficient (Cd) at each corresponding velocity was calculated based on Equation (4.14) knowing the resistive factor (C_R), the maximum cross-sectional area (A = 0.0847 m^2) and the water density (ρ = 996 kg/m^3). For the extended length (L = 2.398 m). The average Reynolds number was calculated knowing the average velocity and the kinematic viscosity (υ) equal to 0.91×10^{-6} m^2/s according to Equation (4.20).

The drag coefficients were shown in Figure (4.6) for different average Reynolds number for the same female subject (FIN).

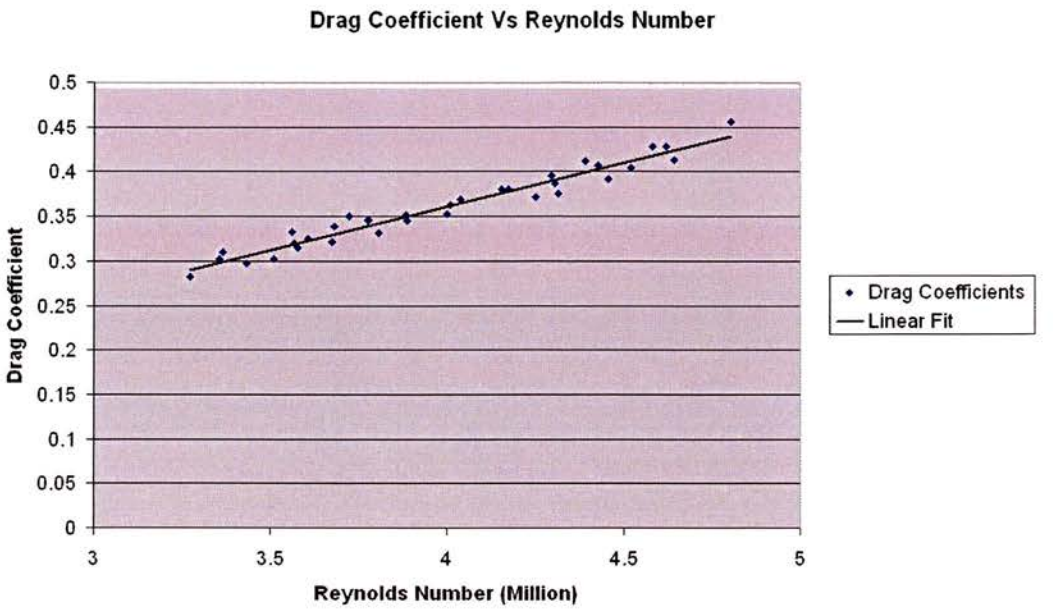

Figure 4. 6. A sample graph of drag coefficient versus average Reynolds number of a female subject.

Added mass (m_a) at each corresponding velocity was calculated based on Equation (4.15) knowing the virtual mass (M) and the body mass (m = 69.4 kg). The body volume during each glide interval was calculated based on Equation (4.18) knowing the component of the net buoyancy opposite the direction of travel (p) and the glide angle (α)-which was determined based on each glide interval-together with other constants such as the body weight (W = 680 N), the water density (ρ = 996 kg/m^3) and the gravity acceleration (g =9.8 m/s^2).

The added mass coefficient (C_a) was calculated for each velocity based on Equation (4.19). The added mass coefficients were shown in Figure (4.7) for different average velocities.

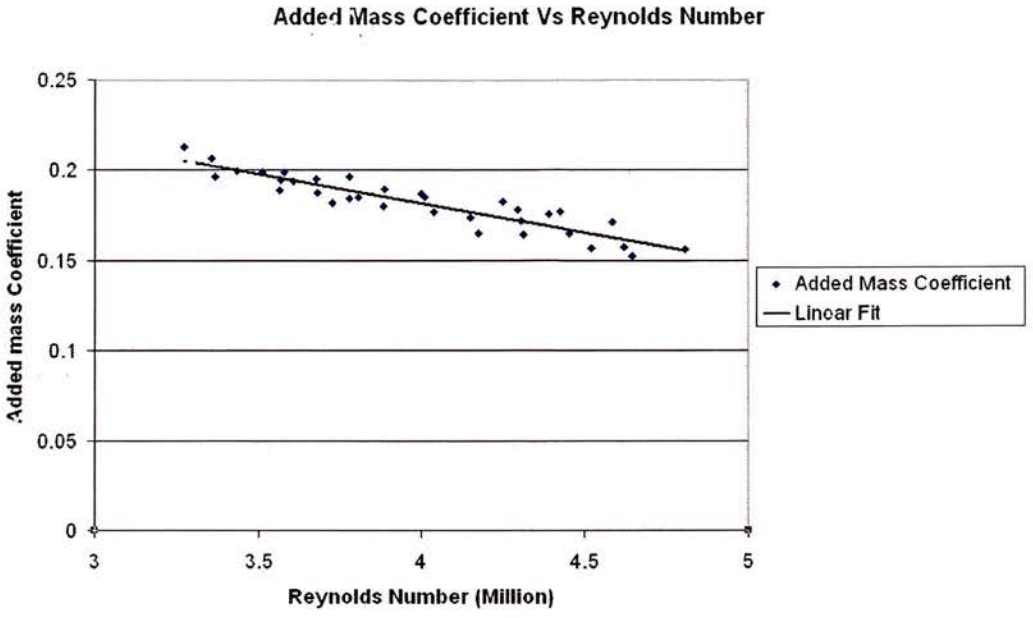

Figure 4. 7. A sample graph of added mass coefficient versus average Reynolds number of a female subject.

4.2.10. Assessment of Validity, Accuracy, and Reliability of the Method

The assessment of the logical and construct validities, accuracy and reliability in quantifying the resistive factor and the virtual mass were identical to what was described in Chapter 3 for the glide factor. More than these as in this study more parameters were quantified based on each fit, it was necessary to ensure that the parameters represent the value that they should represent. Following tests were conducted to ensure the precision of the calculated parameters.

4.2.10.1. Testing of independency of the calculated parameters

In order to ensure the independency of the virtual mass and the resistive factor from each other the Pearson product moment correlation coefficients were calculated between these two parameters.

Also the correlations between the upper limits of the resistive factor and the resistive factors calculated at different velocities were determined to ensure that the resistive factors were calculated independent from the value of the upper limit. Similarly the correlation between the body mass and the virtual mass was determined in order to make sure that the virtual mass was quantified independent of its lower limit (body mass).

Further, although the subjects were instructed to aim for a marker at the bottom of the pool at 6.5m distance from the wall (Figure 4.1), maintaining the exact angle was not possible between trials and some small variations existed. The average glide angle was 13.9±1.94 degrees. The correlation between the glide angle and the quantified resistive factor and the virtual mass should be determined to assess the independency of these parameters from the glide angle.

4.2.10.2. Testing of precision of component of net buoyancy

If the component of net buoyancy opposite the direction of travel represents the precise value, then the quantified value for this parameter should be the same when the body volume remains constant. As the subject hold their breadth and do not change the glide angle, the component of the net buoyancy should remain the same between the two intervals selected from the same trial. In order to assess to what extent the component of net buoyancy was calculated precisely, its coefficients of variation were quantified between the glide intervals of the same trial.

4.2.10.3. Comparing the results with the literature

Although no previous data existed for comparing the virtual mass found in this study with the virtual mass of a human body found in previous literature, the added mass coefficients found in this study could be compared with the values of the other objects.

This would be done in order to make sure that the calculated added mass was a reasonable value for the human body.

The resistive forces at each corresponding velocity were calculated based on the quantified resistive factors. The results of the resistive forces at each corresponding velocity from this study was compared with the results from the previous literature, to investigate whether the values obtained are similar to those of the other studies in order to further establish the validity of the method.

As the added mass of a human body has not been quantified before, it was not possible to directly compare the virtual mass results of this study with the comparative data from the literature. Instead the added mass coefficients found in this study could be compared with the values of other objects to establish whether the quantified values are reasonable and meaningful.

4.3. Results

4.3.1. Logical validity results

The fit goodness statistics indicated the R-squared value of 0.999 ± 0.0001, the sum of squares due to error (SSE) of 2.2 ± 0.07×10^{-4}, and the root mean squared error (RMSE) of 0.002 ± 0.0055. Generally the residuals were randomly distributed above and below the time axis.

4.3.2. General results

As the resistive factors changed linearly with increasing velocity, the data for each subject was approximated by a linear fit (R^2= 0.88±0.09). The best linear fit that represents the resistive factor versus average velocity has been shown in Figure (4.8) for different subjects. As it can be seen in Figure (4.8) each subject's resistive factor follows

a unique linear trend with distinctive intercept and gradient that indicates how the resistive factor changes across different velocities.

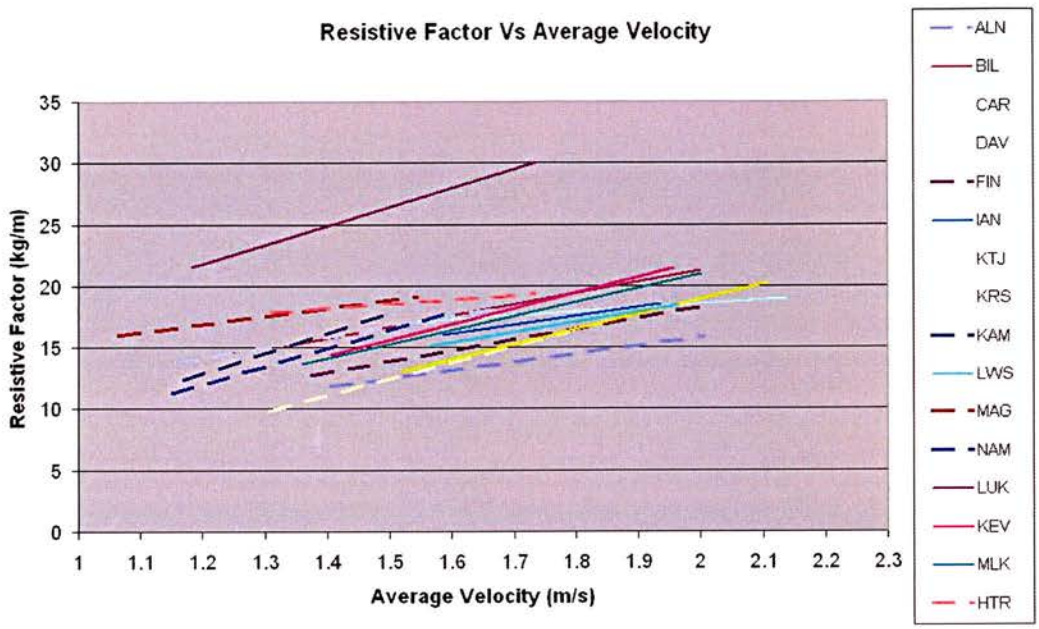

Figure 4. 8. Linear fits representing resistive factor Vs average velocity for different subjects. The solid lines indicate the corresponding best linear fits for male subjects and the dashed lines represent the females' best fits.

Similarly the variations in the virtual mass versus the average velocity can be best approximated by a linear fit for each subject (R^2= 0.85±0.09). The linear fits representing the virtual mass versus average velocity were shown in Figure (4.9) for different subjects.

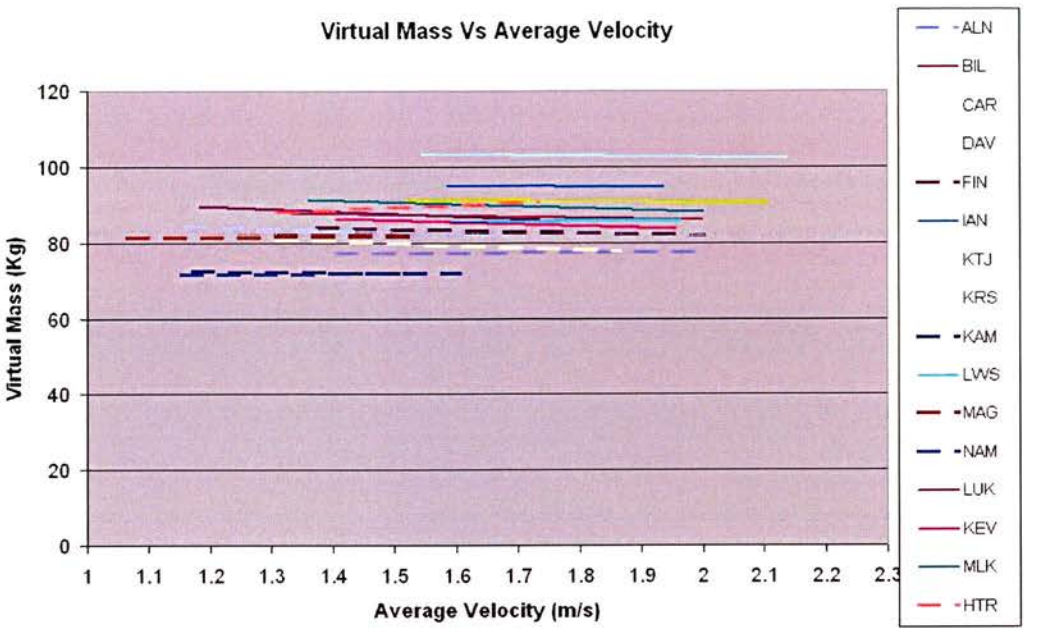

Figure 4. 9. Linear fits representing virtual mass Vs average velocity for different subjects. The solid lines indicate the corresponding best linear fits for male subjects and the dashed lines represent the females' best fits.

The maximum cross-sectional area was 0.077± 0.008 m^2 and the streamlined length was 2.45±0.14 m. The drag and added mass coefficients versus average Reynolds number were shown in Figures (4.10) and (4.11) respectively for different subjects. As it can be seen in these figures each subject possesses a unique fit with a distinctive intercept and gradient that indicates how the glide coefficient changes across the Reynolds numbers.

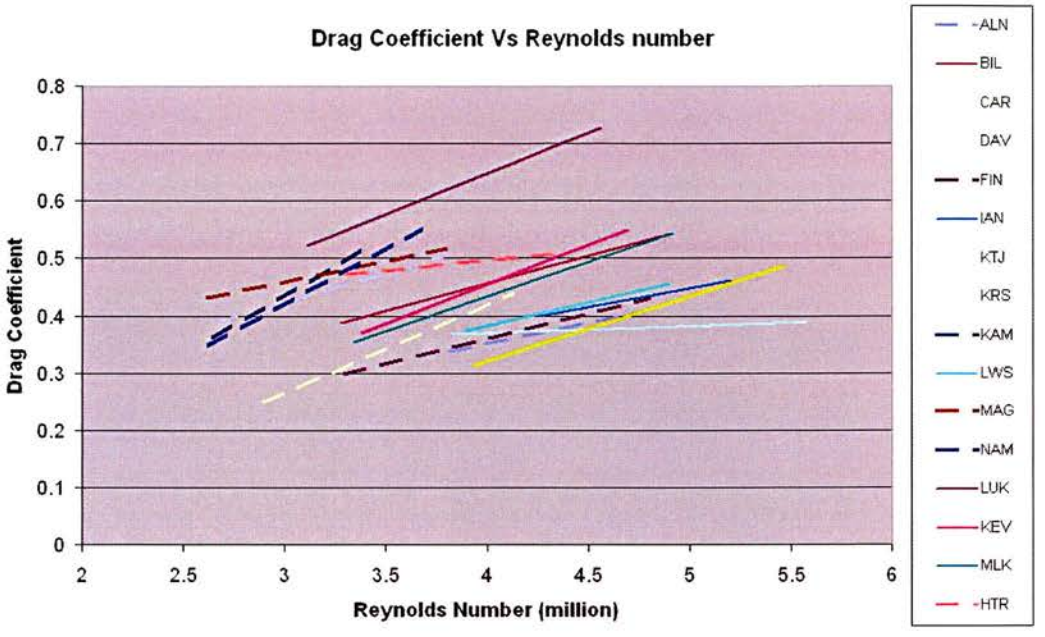

Figure 4. 10. Linear fits representing drag coefficient Vs average Reynolds numbers for different subjects. The solid lines indicate the corresponding best linear fits for male subjects and the dashed lines represent the females' data.

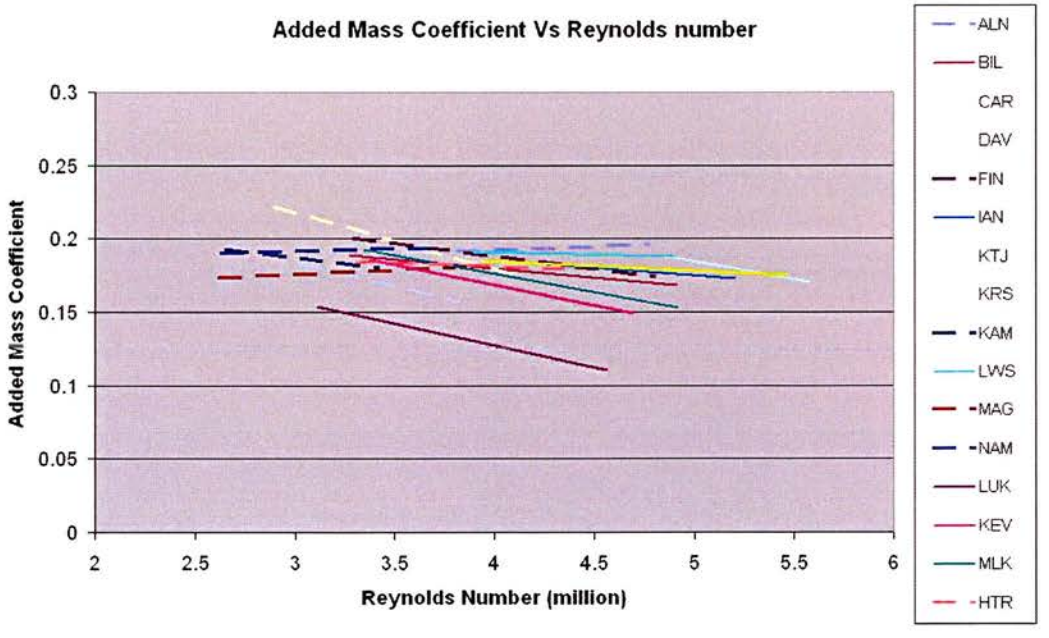

Figure 4. 11. Linear fits representing added mass coefficient Vs average Reynolds numbers for different subjects. The solid lines indicate the corresponding best linear fits for male subjects and the dashed lines represent the females' data.

4.3.3. Accuracy results

Within the certainty level of 95%, the relative confidence bound width for the resistive factor was 16.1 ± 0.7% that indicated a relative standard error of the calculation equal to 4.0 ± 0.17 %. The relative confidence bound width for the virtual mass was 5.8 ± 0.4% that indicated a relative standard error of the calculation equal to 1.45 ± 0.19 %.

There was 9.9± 4.08 kg/m increase in the resistive factor and 1.9± 3.04 kg decrease in the virtual mass with each 1 m/s increase in the average velocity. The maximum errors as a result of consistency of the resistive factor and virtual mass over a glide interval were 5.9 % and 2.0% for the resistive factor and the virtual mass respectively.

4.3.4. Reliability results

The coefficient of variation of the slope and intercept of the regression lines that represent the variations of the resistive factor to the average velocity corresponding to three separate testing sessions for a male and female subject is presented in Table (4.1) as a measure of the stability of the method (inter-day reliability) in quantifying the resistive factor.

Table 4. 1. Coefficient of variation of the regression line's slope and intercept of the resistive factor-average velocity of the male and female subject for inter-day reliability

Subject	Slope	Intercept
Female	0.41%	2.75%
Male	0.73%	0.61%

The same variables for the virtual mass were presented in Table 4.2 as a measure of the stability of the method (inter-day reliability) in quantifying the virtual mass.

Table 4. 2. Coefficient of variation of the regression line's slope and intercept of the virtual mass-average velocity of the male and female subject for inter-day reliability

Subject	Slope	Intercept
Female	0.59%	1.41%
Male	0.36%	0.54%

The reliability coefficient (the Pearson correlation between the pair values corresponding to the same velocity) indicating that the intraday reliability (the internal consistency) was r = 0.88 for the restive factor and r= 0.96 for the virtual mass. The relative standard error of measurement (RSEM) which is the ratio of the standard error of measurement to the mean was 6.68 % and 1.48 % for the resistive factor and the virtual mass respectively.

4.3.5. Construct validity results

The average and the standard deviation of the coefficient of variation of within individual resistive factors and the coefficient of variation of between individual resistive factors are presented in Table (4.3).

Table 4. 3. Coefficient of variation of the resistive factor within and between subjects for the male and female groups

Group	Between individual	Within individuals
Female	16.2 %	2.07±0.54 %
Male	22.6 %	2.46 ±0.14 %

The same variables for virtual mass were calculated and were presented in Table 4.4 as a measure of the construct validity of the method, in quantifying the virtual mass.

Table 4. 4. Coefficient of variation of the virtual mass within and between subjects for the male and female groups

Group	Between individual	Within individuals
Female	6.85 %	1.55±0.77 %
Male	4.70 %	1.03±0.41 %

4.3.6. Parameters independency results

No significant correlation was found between the virtual mass and the resistive factor. There was no significant correlation between the upper limits of the resistive factor and the quantified resistive factor between subjects. Also there was no correlation between the body mass and the virtual mass. No significant correlation was found between the glide angle and either the resistive factor or the virtual mass.

4.3.7. Volume consistency results

The net buoyancy calculated for different intervals of the same trial showed a coefficient of variation of 0.7± 0.2 %. The body volume during the trials was 0.67 ± 0.34 litre more than the volume of the body when neutrally buoyant (that was calculated as the ratio of the body mass to the water density) while it was 1.90 ± 0.67 less than the body volume in the maximum inhale.

4.4. Discussion

The aim of this study was to develop and test a method of quantifying the hydrodynamic resistive and inertial parameters of a body in a streamlined position. A parametric equation was developed that represents the kinematic behaviour of a body during a rectilinear inclined glide. By restricting the parameters to be chosen in the acceptable limits, the resistive force and the virtual mass were quantified by fitting the parametric curve to the displacement data of an inclined rectilinear glide interval.

This method is an advancement over the conventional methods of quantifying hydrodynamic resistive force based on the kinematics of a glide that require the added mass values to be known beforehand. Furthermore, the method quantified the value of the added mass during the deceleration that has not been quantified for a human body before despite its practical importance in the glide phase of swimming.

4.4.1. Implications

4.4.1.1. Contribution of resistive factor and virtual mass to glide efficiency

Quantifying the resistive factor and virtual mass allows assessing the hydrodynamic parameters that contribute to the glide efficiency of a body separately. Since high glide efficiency can be achieved by high virtual mass and/or a low resistive factor, it was valuable to determine the contribution of each of these parameters.

In Chapter 3 it was found that glide factor decrease with increasing velocity, while at that stage it was not possible to determine how the virtual mass and the resistive factor change separately by an increase in velocity. In this study it was found that there was an increase in the resistive factor and a decrease in the virtual mass by an increase in the average velocity. This emphasises that by decreasing velocity from the initial to final stages of a glide the quantity of water body entrains increases while the resistive factor decreases.

4.4.1.2. Prediction of resistive force velocity relationship

In this study, it was found that the resistive factor changes linearly with velocity. Thus at each velocity the resistive factor can be quantified by the equation of the regression line.

$$C_R = S.v + I \qquad \text{(Equation 4.21)}$$

Where S is the slope of the linear regression line (9.9 ± 4.0 kg.s/m^2) and I is the intercept (1.4 ± 6.4 kg/m). Replacing the resistive factor from Equation (4.21) to Equation (4.4) the resistive force can be calculated as:

$$D = A.v^3 + B.v^2 \qquad \text{(Equation 4.22)}$$

Thus the relationship between the resistive factor and the velocity can best be explained by sum of a cubic and quadratic function (Equation 4.22). It can be argued that although the formulae for the different sources of drag like the skin friction, the pressure drag and the wave drag incorporates the velocity, the velocity squared and the cubed velocity respectively, since the coefficients that determine the equality of formulas like the friction drag coefficient, pressure drag coefficient and wave length themselves change when the velocity changes, the variations in each source of drag would be different than when the coefficients that determine these variations are held constant. Thus it should be emphasised that the fact that sum of a cubic and quadratic function best approximates the resistive force does not imply that the sources of drag are the wave and form drags.

This trend of changes in the resistive force with the velocity is also different than the previous findings which propose a quadratic relationship (Vennell, *et al.*, 2005) or a linear relationship (Lyttle, *et al.*, 1998) between the resistive force and velocity when the wave drag is not presented. This can be related to the fact that the force data in the previous studies were averaged, and then the variations with velocity were fitted by a function. Averaging the data would remove the important aspect of the between individuals variability, and cause the relationship to be different than when the data related to each subject were fitted separately.

4.4.1.3. Ability to determine the resistive force at any velocity

The other advantage of this method is that based on the regression line that determines the variations of the restive factor and the added mass with velocity these parameters can be interpolated at any velocity. This allows comparing the drag forces at velocities other than the velocities which the drag forces were quantified at.

The average resistive force of 85 N (86.7 N for the male and 83.3 N for the female group) at velocity of 2 m/s was lower than the value of 93.55 N which was calculated by Rumyantsev (1982) as cited by Vorontsov and Rumyantsev (2000) for a gliding body in the streamlined position when the wave drag is not presented. The higher values of the resistive force found by Rumyantsev (1982) are likely to be due to the relatively higher average maximum cross-sectional area (0.096 m^2), compared to the average maximum cross sectional area in the present study (0.078 m^2).

The results of the present study is comparable with the Maiello *et al.* (1998) who measured the drag forces of 11 female swimmers at 50 cm below the surface in a flume and reported the average resistive forces of 54.3 N and 65.9 N at the velocities of 1.76 m/s and 1.91 m/s respectively. The average resistive forces for female group in this study were 57.2 N and 72.7 N at the corresponding velocities slightly higher than the values found by Maiello *et al.* (1998). Since there is no information presented on the maximum cross-sectional area it is not possible to discuss the source of the discrepancy.

In comparison the average restive forces found for the velocities of 1.6 m/s and 1.9 m/s in this study were 22% and 7% lower than what was found by Lyttle (1999). Conversely the values of the resistive force calculated at a velocity of 2.2 m/s were 8% higher than the corresponding value found with Lyttle (1999).As the average chest girth for the subjects are comparable (103.6 cm for the present study and 101.8 cm for the study by Lyttle (1999)), the discrepancy is likely to be due to the differences in the morphological characteristics of the body. This would further be discussed under the 'shape-related resistive characteristics' heading.

The slight difference in the resistive forces found in this study compared to the methods based on the direct force measurement can also be attributed to the differences in the body posture. As the flow is steady during a towing experiment, and unsteady during a glide, the body is expected that adapt a different posture to balance the different forces and moments in each condition. Also since during towing the drag force can be

measured over a longer period of time at each corresponding velocity, a subject has more time to adapt to the flow compared to glides that happen at a relatively shorter period.

4.4.1.4. Performance enhancement in passive phases

As what was discussed in Chapter 3, a design to enhance performance should consider both the components of glide factor including the resistive factor and the virtual mass. This method provides practical applications in testing the swimming suits designed to improve performance, as the suit effect on the ability of a body to entrain the added mass of water as well as its ability to reduce the drag may be quantified separately. Further, as the morphological characteristics of each swimmer is different a certain body suit may affect the values of the resistive factor and the added mass differently, so that the gained advantage related to the glide phase as a result of wearing the same suit would be different among individuals. Being able to quantify these parameters separately helps in having a deeper insight in to the underlying hydrodynamic parameters related to the glide efficiency.

Shape-related resistive and added inertia characteristics

In comparing two bodies' resistive factor and added mass it is desirable to distinguish the contributions of a body's size including the volume and the cross-sectional area and other factors such as the body shape. By quantifying the drag and added mass coefficients the shape-related resistive and added inertia characteristics of a body were quantified.

It was found that the drag coefficient increases with a linear trend with increasing the Reynolds number, while the added mass coefficient decreases. The variations in the drag coefficient is similar to what were established by Clarys (1978a) and Clarys (1979) who found a linear trend between the drag coefficient and the Reynolds number at the range of 1 to 4 million for the towed swimmers at a depth of 60 cm below the surface.

Although having lower maximum cross-sectional areas gives a swimmer a better potential to create less resistance during a glide, but in determining the resistive force the shape of the body should also be considered. In comparing the subjects of our example HTR possessed a lower maximum cross-sectional area compared to FIN (0.0758 m^2 Vs 0.0847 m^2). This indicated that the body size of HTR had a higher potential for creating less resistance when gliding through water compared to FIN's body size. Despite this HTR's resistive factor (19.2 kg/m) was higher than the values for FIN (15.6 kg/m). This emphasises that in addition to the size, the shape of the body influence its resistive force.

The drag coefficient determines the potential of a particular body shape to posses less resistance while gliding through water. For example, shapes that are able to allow the water to flow over the body with minimal disturbance minimise the drag. In comparison of these two subjects the superior shape of FIN that is supported by having a lower drag coefficient (0.38) allow her to glide more efficiently compared to HTR with a drag coefficient of (0.51).

The drag coefficient of 0.3 at a Reynolds number of 4 million calculated based on the results of Vennell *et al.* (2006) for a submerged mannequin fixed in a flume is comparable to the minimum drag coefficient of 0.32 at the same Reynolds number. The differences may be due to the differences in the pliability of the skin between mannequin and the live subject. Also as the mannequin was reconstructed based on the scan of a body in an upright streamlined position; it might not reflect the body's morphological characteristics during the underwater streamlined position.

The added mass of water entrained with the body in a glide depends on the body volume as well as the shape characteristics of the body to entrain the added mass of water along. Thus subjects who possess a higher volume are expected to be able to entrain more water along compared to the swimmers with the lower body volume.

In comparing two other subjects in this study, KTJ possess a lower added mass (11.7 kg)

compared to ALN (13.0 kg) despite KTJ larger body volume (70.6 lit) compared to ALN (65.4 lit). This is a result of the superior shape of ALN to entrain more water along that is determined by the added mass coefficient of 0.19, higher than the added mass coefficient of 0.16 for KTJ.

Due to lack of previous data on the added mass of the human body in deceleration no comparison can be made with the literature, but it is possible to compare the values obtained in this study with the added mass coefficient of the other bodies of revolution. Also the added mass coefficient of the aquatic animals that can be approximated by the added mass of the bodies of revolution (Landweber, 1961) may be compared with the corresponding values for a human body.

The average added mass coefficient found in this study was equal to 0.18 that is much higher than 0.05 as the added mass of a spheroid with a length to diameter of 6 that is close to the subject's average ratio of the chest breadth to the extended height in this study. For dolphins the added mass coefficient has been approximated between 0.045 and 0.067 (Lang and Daybell, 1963). As a more streamlined body posse less added mass coefficient, it can be seen that the higher value of the added mass for a human body is in line with its relatively poor streamlining. This further confirmed that the added mass values of a human body were calculated reasonably.

4.4.2. Validity

4.4.2.1. Logical validity

The fit goodness statistics indicated that the displacement equation which was found in this study closely represents the real displacement data of a body in a rectilinear inclined glide. This indicates the validity of the principles and assumptions which were used in the process of finding the equations. As the displacement equation was based on the equation of motion of a body, the fact that the displacement equation predicts the real displacement data closely indicates that the underlying principles and assumptions that

were employed to develop the equation of motion were realistic and feasible. As otherwise the displacement function would not be able to approximate the real displacement data closely. This establishes the logical validity of the method.

This is an improvement over the previous methods of calculating the resistive forces based on the kinematics of glide, as they did not provide any information on the goodness of the fit as essential information on how the recommended model fits the real kinematic data (Klauck and Daniel, 1976 and Oppenheim, 1997).

4.4.2.2. Accuracy

Fitting the displacement function to the displacement data increased the accuracy of the calculation, as the errors in the displacement data did not get amplified. As a result of this the model was better fitted to the data than the previous studies (Klauck and Daniel, 1976). Also averaging the raw displacement data of different markers to eliminate the noise compared to using the hip kinematics provided an opportunity to eliminate the random error without affecting the real data.

Using the most advanced curve fitting technique that minimizes the summed square of the residuals and downweight the outliers decreased the chance of the variations in the calculated resistive factors and virtual mass caused by the inaccuracies in the displacement data. The current confidence level determined by 95% certainty level together with a relative confidence bound width of 16.1 ± 0.7% for the resistive factor and 5.8 ± 0.4% for the virtual mass assures that there is only 5% chance that the actual resistive factor and the virtual mass would be outside the confidence bounds.

The considerable changes in the resistive factor and the virtual mass with the average velocity found in this study indicate the importance of calculating the resistive factor and the virtual mass for each corresponding average velocity, and the fact that one resistive factor and virtual mass may not represent the inertial and resistive characteristics of a body along the whole range of velocities. Contrary to the previous studies (Klauck and

Daniel, 1976 and Oppenheim, 2000), in which a function was fitted to the whole glide period, in this study the smaller intervals were considered. This helped to decrease the error as a result of the consistency of the resistive factor and virtual mass.

The high level of confidence in the calculated resistive factor and virtual mass (the relative standard error of calculation equal to 4.0 ± 0.17 % and 1.45 ± 0.19 % respectively) together with the low error associated with the assumption of the consistency of the resistive factor and virtual mass in each glide interval (5.9± 0.6 % decrease in the glide factor, and 2.0± 0.2 % increase in the virtual mass from the beginning to the end of each interval) determine the limits of the accuracy for the method. The relatively shorter glide duration in the current study (0.38 s) compared to the previous studies (2 s for Klauck and Daniel, 1976 and more than 10s Oppenheim, 1997) made it easier for a subject to maintain consistent body posture along the glide interval, which contributed to the accuracy of the current study compared to the previous studies.

Despite the favourable results obtained, further improvements in the accuracy could be achieved. Increasing the sampling frequency in the future studies would allow the use of a shorter glide interval, thereby reducing the error associated with assuming a consistent resistive factor and virtual mass over a glide interval. Also increasing the image resolution may allow a more accurate digitizing and consequently increase the accuracy of the raw displacement data of a glide so that the confidence level in the calculated resistive factor and virtual mass would increase.

4.4.2.3. Reliability

The results based on multiple testing of two individuals at three separate sessions indicated that the coefficients of variation of the regression lines representing the variations of resistive factor and virtual mass to velocity were low (less than 1% for the slopes and less than 3% for the intercept). This indicated that the method can be used to determine the hydrodynamic parameters of the body during a glide with high level of

stability. The existing variability could be related to the biological variance and the learning effect between sessions that may not be controlled for.

The maximum relative standard error of measurement determined for the test-retest (the glide factors corresponding to the same velocity) were 6.68 % for the resistive factor and 1.48% for the virtual mass. This was higher than the relative standard error of calculation (4.0% and 1.45% respectively) that arises in the calculation of the resistive factor and virtual mass during the curve fitting.

Since in this study by introducing a standard procedure through the whole data collection other sources of variability including the data collection procedure were controlled, the remaining variability after deducing the errors as a result of calculation would be mainly due to the natural variability of conditions between the tests. This could be attributed to the small variability between the postures that may not be detected under the current limits of acceptable changes that can occur during the glide intervals. Slight changes in the posture may change the flow characteristics around the body and in turn affect the drag and added mass coefficient values and hence affect the resistive force and the virtual mass of subject.

The results of the reliability can be compared with the results from Lyttle (1999) reported a coefficient of variation of 1.7% for retesting a subject at the velocity of 1.9 m/s. The coefficient of variation for a test-retest of a subject in the current study at a velocity close to 1.9m/s is equal to 2.82 %. The higher values of variations in the current method compared to the towing method used by Lyttle (1999) could be related to the fact that the towing data were collected over a longer period of time compared to the duration of glide, the higher internal consistency (intra-day reliability) was expected.

4.4.2.4. Construct validity

Comparing the coefficient of variation of the resistive factor and the virtual mass within and between individuals at a definite velocity range indicates a small inter-individual variations compared to between individuals'. The average within individual coefficient of variation of the virtual mass was four times the coefficient of variation of between individuals, while this quantity was eight times for the resistive factor. This indicates that the differences between individuals can be detected by this method that establishes the construct validity of the method.

Previous method did not take in to account the important aspect of the construct validity, as most of them treated the pool data as a whole (Karpovich, 1933; Counsilman, 1955; Kent and Atha 1971; van Manen and Rijken, 1975; Jiskoot and Clarys, 1975; Clarys and Jiskoot, 1975; Clarys *et al.*, 1974; Clarys 1978a; Clarys 1978b and Clarys, 1979; Lyttle, 1999,; and Chatard *et al.*, 1990). By doing so the important aspect of between individual's variability was eliminated, and the practical applications were restricted.

The method proposed in this study is able to detect the differences between individuals and has a great potential in an applied context. Further studies would be followed in chapter 5 to determine the source of variability between individuals in their glide efficiency.

4.4.2.5. Parameters independency

The lack of significant correlation between the virtual mass and the resistive factor indicates that these parameters do not play against each other. Lack of significant correlation between the upper limit of resistive factor and the quantified resistive factor and between the body mass (as the lower limit of the virtual mass) and the virtual mass indicate that these parameters were quantified independent of the lower and upper limits for each individual. This further emphasize that the application of these limits were to prevent the parameters to choose unreasonable values.

Also the fact that there was no correlation found between the values of the resistive factor and the virtual mass with the glide angles indicate that the change in glide angle would not affect the quantified values.

Net buoyancy consistency

The net buoyancy was found to stay consistent across different intervals during each trial (CV_{ave}=0.7%) confirming the hydrostatic nature of this parameter and the method's ability to quantify this as a constant parameter. This indicates that the component of the net buoyancy opposite the direction of travel was quantified precisely with this method.

4.5. Conclusion

A new method dubbed the 'hydro-kinematic' has been developed that quantifies the hydrodynamic characteristics of a human body in a streamlined position. The method showed to be able to distinguish between individuals in their hydrodynamic parameters with acceptable validity. Calculating the drag and added mass coefficients enabled the contribution of the shape characteristics to the hydrodynamic parameters related to a glide to be quantified.

Chapter 5

Study 3: An Investigation into the Relationships between the Size and the Shape Characteristics of the Human Body and its Glide Efficiency and Hydrodynamic Parameters

Nomenclature

X: The longitudinal axis perpendicular to the transverse plane

Y: The frontal axis perpendicular to the frontal plane

Z: The sagittal axis perpendicular to the sagittal plane

x: The inferior-superior coordinate (m).

y: The anterior-posterior coordinate (m).

z: The medial-lateral coordinate (m).

$\mathbf{h_c}$: The vertical distance between each level and the superior level for each zone (m)

$\mathbf{h_z}$: The height of each zone or the total height of body in the streamlined position(m)

$\mathbf{P_s}$: The relative position of cross-section (dimensionless).

$\mathbf{d_{nom}}$: Nominal diameter (m)

FR: Fineness ratio (dimensionless)

CR: Cross-sectional ratio (dimensionless)

TI: Taper index (m^2/m)

m: Body mass. (kg)

A_c: Cross sectional Area. (m^2)

ρ: Water density. (kg/lit)

V: Body volume (lit)

θ_h: Segmental angle of attack for a horizontal rectilinear glide (degrees)

θ_i: Segmental angle of attack for an inclined rectilinear glide (degrees)

φ: Joint angle (degrees)

α: Glide angle, the angle of rectilinear glide path to the horizontal (degrees)

5.1. Introduction

As glide performance during starts and turns is related to the swimming performance (Hay and Guimares, 1983 and D'Acquisto, *et al.*, 1988), determining the size and the shape characteristics of bodies that are correlated to their glide efficiency and hydrodynamic parameters is valuable for identifying body characteristics that may contribute to swimming performance.

In study 1 it was established that the glide factor as an indicator of the glide efficiency is the product of a glide constant that incorporates the size-related parameters of the body like the body mass and the maximum cross-sectional area; and a glide coefficient which is related to the body's shape characteristics (Figure 5.1). Despite the fact that in theory an advantage in gliding can be gained by increasing either or both of these two parameters namely the glide constant and/or the glide coefficient, in practice the relationship between each of these two parameters and the glide factor is unknown. Since the glide efficiency is a new concept introduced in Study 1, it is obvious that no previous study investigated the relationships between either the body size or the shape characteristics and the glide efficiency parameters.

In Study 2 the resistive factor was shown to be proportional to the product of the maximum cross-sectional area related to the size of the body and the drag coefficient related to the body shape (Figure 5.2). Despite the fact that in theory a decrease in the resistive force can be gained by decreasing either or both of these two parameters, namely the maximum cross-sectional area and/or the drag coefficient, it is not known how in practice the resistive factor of the swimmers would be related to either of these two parameters. Also in Study 2 the added mass of the body was found to be proportional to the product of the body volume that is related to the size of the body and the added mass coefficient related to the body shape (Figure 5.2). Despite the fact that in theory an increase in the amount of the added mass can be gained by increasing either or both of these two parameters namely the body volume and/or the added mass coefficient, it is not understood how in practice the added mass of the swimmers would be related to either of these two parameters.

While several studies reported the effect of the size and the shape characteristics on the resistive parameters (Clarys et. al., 1974; Clarys, 1979; Clarys; 1986, Chatard *et al.*, 1990; Lyttle *et al.,* 1998 and Benjanuvatra *et al.,* 2001), as the added mass of a body during a glide was not quantified previously, there is no existing literature on the relationship between the size and the shape characteristics of the body and its added mass during a glide.

In order to quantify the relationship between the size of the body and its hydrodynamic resistance, anthropometric parameters of the body related to an upright position with the hands on side were considered. From these parameters head and thorax circumferences together with thorax depth and breadth have been found to have a significant correlation with the drag values (Clarys et. al., 1974). Also, the chest girth and maximum cross-sectional area, body surface area, mass and the height were found to be correlated to the drag values (Chatard *et al.*, 1990; Lyttle *et al.,* 1998; Benjanuvatra *et al.,* 2001). These studies measured the anthropometric characteristics of the body while the subject stands in an upright position with the hands on the side, a position different from the

streamlined position in which the hydrodynamic parameters of the body were measured. In other words the anthropometric measures of the body in an upright position with the hands on the side do not reveal the actual size-related parameters of the body. For example, positioning the arms at the side of the body would increase the maximum cross-sectional area compared to the streamlined position. For these reasons relationships between the size of the body and its hydrodynamic and glide efficiency parameters can be expected to be different from the actual anthropometric measures of a body in a streamlined position. Thus it is essential to investigate the anthropometric characteristics while the body maintains the streamlined position. This helps in having a deeper insight into the relationships between the actual anthropometric variables and the glide efficiency and hydrodynamic parameters.

On the other hand the shape-related parameters including the glide coefficient, the drag coefficient and the added mass coefficient are influenced by the specific shape of the body in a streamlined position (Figure 5.1 and Figure 5.2). Unlike the glide constant, the maximum cross-sectional area and the body volume that are directly quantifiable using the anthropometric measures of the body in a streamlined position, the shape of a body is not a quantifiable entity. Instead, features of the shape characteristics that influence the glide, drag and added mass coefficients could be defined considering the fluid dynamic principles.

To quantify the shape feature important in resistive characteristics of the body, the morphological indices, were adapted from naval architecture and from the hydrodynamic studies of aquatic animals (Clarys, *et al.*, 1974). From these indices some have been found to be correlated to the resistive parameters of the human body (Clarys *et al.* 1974; Clarys, 1978b; Clarys, 1979; and Lyttle, *et al.* 1998). Despite these due to the difference between the shape of the body in a streamlined position and that of the other objects, there is a need to more specifically adapt the existing parameters and define new morphological indices which are better able to identify the merits of the shape characteristics of the human body in a streamlined position.

Similar to the anthropometric measurements in previous studies, the morphological indices were not defined for the specific streamlined position. For example, the fineness ratio of a body calculated in a position with the hands on the side underestimates the fineness ratio of a body in a streamlined position. This is a result of a lower length and higher maximum cross-sectional area of the body when the arms are positioned alongside the body compared to a streamlined position. Therefore a different relation between the actual morphological indices and the resistive characteristics of the body may be found. Thus it would be extremely valuable to determine the relationships between the specifically adapted morphological indices of the human body in a streamlined position and the glide efficiency and hydrodynamic parameters.

In addition to the morphological indices, the shape of the body changes with variations in the body posture. Alley (1952) found that 'dropping' the legs as a result of hip flexion, increases the hydrodynamic drag forces. Also, head position was found to play an important role in the amount of the resistance encountered by a swimmer (Miyashita and Tsunoda, 1978). Additionally the correlation between joint laxity and drag force indicates the ability of subjects with higher flexibilities to adopt a superior streamlining position that creates less resistance (Chatard *et al.*, 1990). Despite the fact that these indicate the effect of posture on the resistive characteristics of body, no study has ever determined the relationship between postural angles during glide and the resistive characteristics. Thus it is valuable to investigate if there is a relationship between the postural angles and the glide efficiency and hydrodynamic parameters.

The development of the new method for quantifying the glide efficiency and hydrodynamic parameters based on the kinematic of a glide presented in Chapters 3 and 4, and separation of the glide efficiency and hydrodynamic parameters to the parameters related to the size and to the parameters related to the shape characteristics of the body, offer an opportunity to investigate the relationships between the anthropometric

measures, morphological indices and postural angles on the glide efficiency and the hydrodynamic parameters in a more robust way than previously.

Thus the first aim of this study was to determine the relationship between the size-related parameters including the glide constant, the maximum cross-sectional area and the body volume of a human body in a streamlined position with the glide factor, the resistive factor and the added mass of a body during a streamlined glide.

The second aim of this study was to determine the relationship between each of the shape-related parameters including the glide coefficient; drag coefficient and added mass coefficient and the glide factor, the resistive factor and the added mass of a body in a streamlined position.

The third aim of this study was to determine the relationship between each of the morphological indices including fineness ratios, cross-sectional ratios, taper indices, and relative position of cross-sections and the shape-related parameters including the glide coefficient; the drag coefficient and the added mass coefficient in a streamlined position.

The last aim of this study was to determine the relationship between postural parameters including the joint and segmental angles and the shape-related parameters including the glide coefficient; the drag coefficient and the added mass coefficient of a human body in a streamlined position.

5.1.1. Models

The deterministic models in Figure (5.1) and (5.2) were developed based on the findings of Study 1 and Study 2.

5.1.1.1. Glide efficiency model

In Study 1, the glide efficiency was quantified as a parameter incorporating the glide constant and a glide coefficient. While the glide constant incorporates body mass and the maximum cross-sectional area, it is related to the size of the body. On the other hand the glide coefficient, being the ratio of the virtual mass coefficient to the drag coefficient, depends on the shape of the body (Figure 5.1).

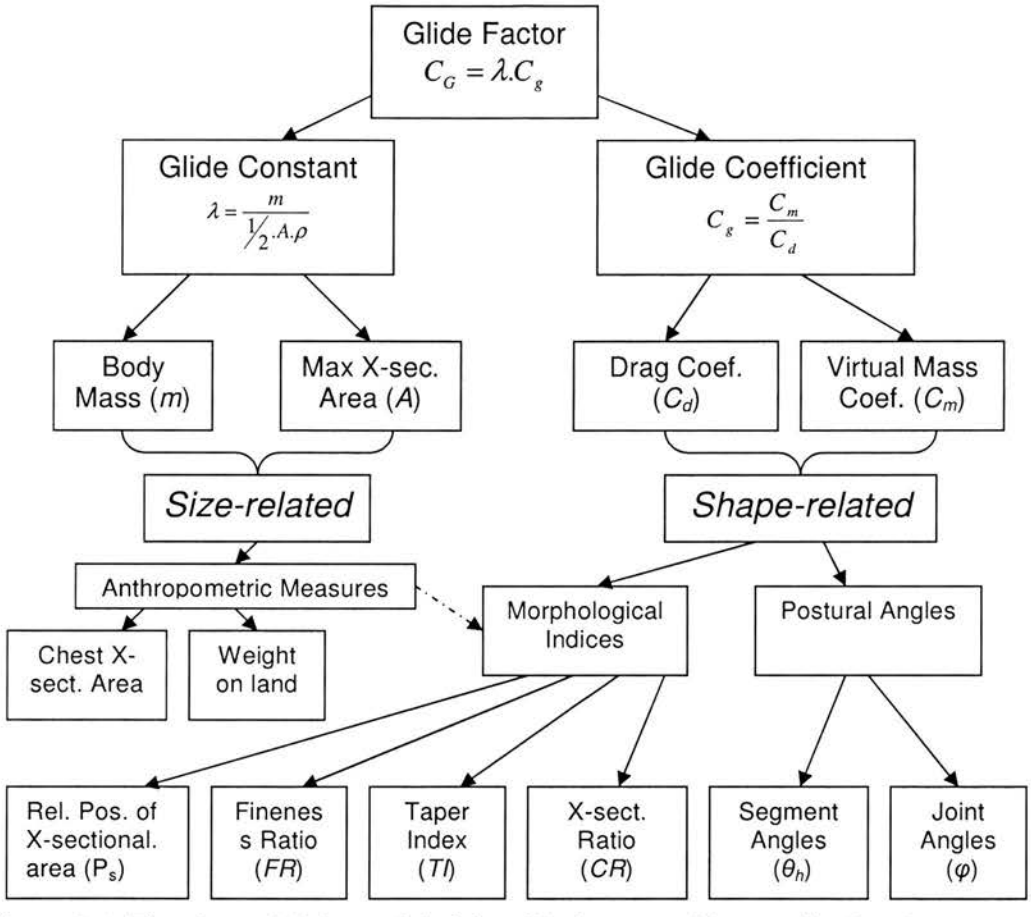

Figure 5. 1. The deterministic model of the glide factor and its contributing shape-related and size-related parameters based on study 1.

5.1.1.2. Model of the hydrodynamic parameters related to the glide efficiency

In study 2, the virtual mass and the resistive factor as the components of the glide efficiency were quantified separately. The virtual mass is the sum of the body mass and the added mass. The body mass is regarded as a parameter related to the size of the body. The added mass incorporates the body volume related to size and the added mass coefficient related to shape of the body. On the other hand the resistive factor incorporated the drag coefficient and the maximum cross-sectional area, in which the former relates to the shape of the body while the later is related to the size of body in a streamlined position (Figure 5.2).

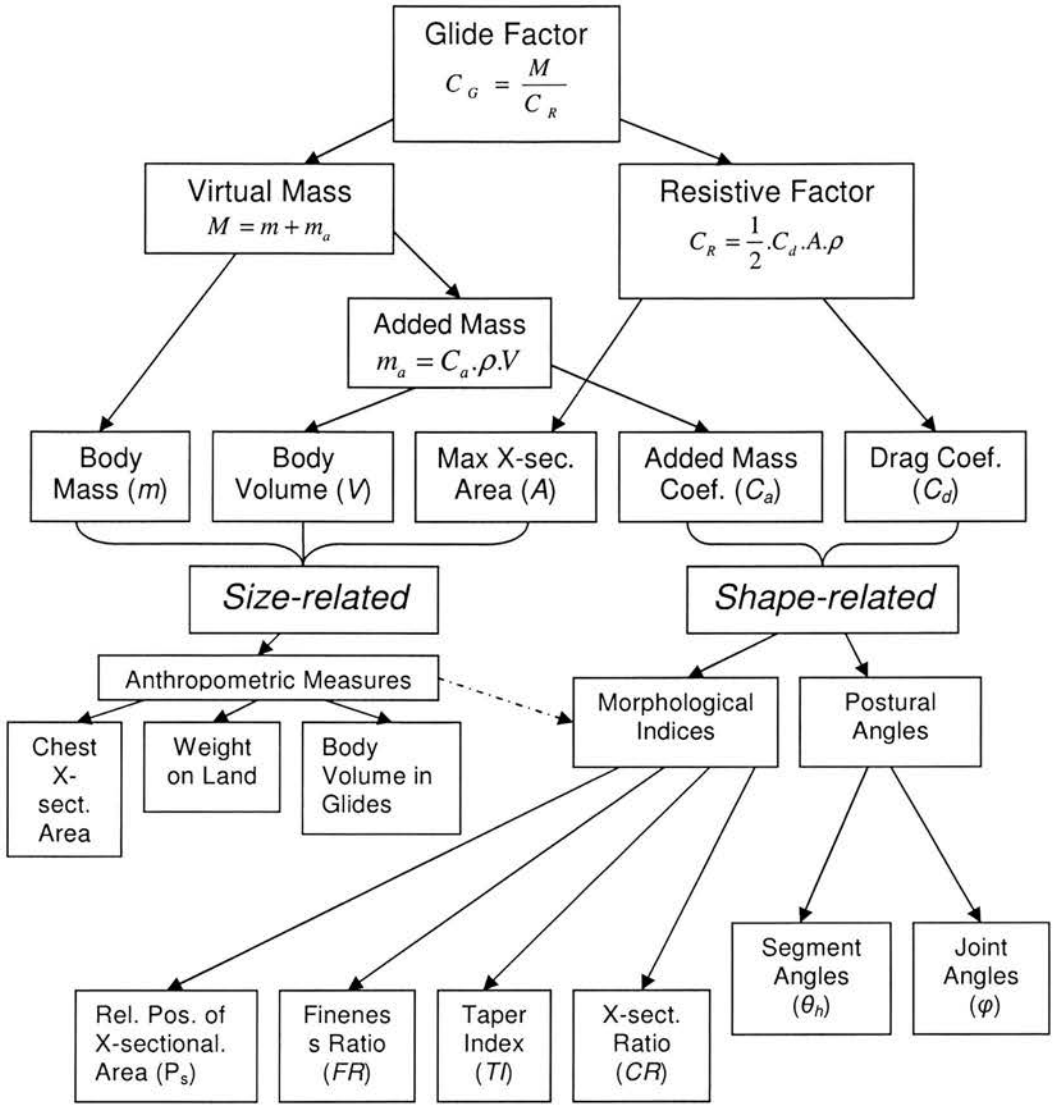

Figure 5. 2. The deterministic model of the glide factor and its contributing shape-related and size-related parameters based on study 2.

5.1.1.3. Note

It should be mentioned that since in Study 1 it was not possible to quantify the resistive factor and the virtual mass separately, these parameters do not appear in the first model (Figure 5.1). However in both models the parameters at the first level depend on the maximum cross-sectional area; body mass and drag coefficient at the third level of both

models (Figure 5.1 and Figure 5.2). As the virtual mass coefficient incorporates the added mass coefficient and the body volume (Equation 2.15, chapter 2), instead of the virtual mass coefficient in Figure 5.1, the added mass coefficient and the body volume are shown in Figure (5.2). Thus all the parameters at the third level refer to the same concept from two different overviews, and may be divided in to 'shape-related' and 'size-related' parameters.

5.1.1.4. Size and the shape characteristics

The size of the body is influenced by the specific anthropometric measures of a body in a streamlined position. These include the body mass quantified by weight of the body on land, the maximum cross-sectional area that is represented by the chest cross-sectional area in a streamlined position and the body volume quantified by the body volume during the glide. The shape characteristics of the body can be determined by the morphological indices and postural angles. Four morphological indices including the relative position of cross-sections, fineness ratio, cross-sectional ratio and taper index can be quantified using the specific anthropometric measures of the body in a streamlined position. The postural angles are categorized as the joint angles and the segmental angles of attack.

5.2. Methods

5.2.1. Subjects

The participants in this study were the same as in Study 1 and 2.

5.2.2. Quantifying Body's Size and Shape Characteristics

Since measurement of the human body's anthropometric parameters was not possible during an underwater glide, the anthropometric variables were measured for the subject

on land in an upright position simulating as closely as possible the streamlined position adopted during the underwater glide. The anthropometric measures from these measurements were also used to calculate the morphological indices. Posture was quantified based on the body joint angles during the underwater glides.

Due to the difference in velocities attainable common to members of the group of males and the group of females these common velocities were different across males and females. Female subjects possessed a lower average velocity range across the trials compared to their male counterparts. For this reason the correlations between resistive factor, added mass and glide factor with the anthropometric measures, morphological indices and postural angles were determined for the male and female groups separately.

5.2.3. Selection of the Body Shape Characteristics

In order to choose the body shape characteristics that may be related to the added mass, drag and glide coefficients, an understanding of the phenomena that affect these coefficients along with how body shape may affect those phenomena is necessary.

5.2.3.1. Phenomena that affect the drag; added mass and glide coefficients

For a body gliding underwater at a depth adequate to avoid wave drag, the main sources of resistive force are friction and pressure drag. Also, as elaborated in the review of literature, the added mass in the absence of wave drag could be considered to result from flow separation, that is, the wake-related added mass as well as the 'skin-related added mass' due to the presence of the boundary layer. Thus, the distribution of the areas vulnerable to high shear stress that affect the boundary layer thickness and the areas vulnerable to flow separation that determine the size of the wake together determine the drag and added mass coefficients. Consequently, the glide coefficient of a

body, as the ratio of virtual mass coefficient to the drag coefficient (Figure 5.1), would be affected by the same phenomena as the boundary layer and the flow separation, and may be determined by the boundary layer thickness and the size of the wake.

5.2.3.2. Note

Although both the drag and added mass coefficients are affected by the separation and the boundary layer phenomena, the extent to which each of these are affected depends on the shape of the body. For example, an increase in the size of the wake may increase the added mass coefficient at a rate different from the rate of increases in the drag coefficient. Similarly, the changes in the thickness of the boundary layer may affect the drag and added mass coefficients to a different extent. The fact that the more streamlined bodies have lower added mass coefficients is valid for bodies with a regular shape (i.e. spheres Vs spheroids). However, due to irregularities in the body shape and of a human body it was expected that the drag and added mass coefficients would not be affected to the same extent by the boundary layer and separation phenomena. The correlation between the drag and added mass coefficients were determined to investigate this possibility (Figure 5.2).

5.2.3.3. Selection of parameters which affect the drag added mass and glide coefficients

The body contours affect how the water flows over the body; it influences the distribution of shear force on the body surface that determines the thickness of the boundary layer at different parts of the body. Further, the areas of flow separation that determine the size of the wake are influenced by the body contours. Since the boundary layer thickness and size of the wake contribute to both the added mass and drag coefficients, the body contour that influences these coefficients should be considered as an aspect of the shape important from hydrodynamics point of view. By influencing drag and added mass coefficients, the body contour may affect the glide coefficient and hence the glide efficiency of a body. In determining the body contours the amount of change in

the cross-sectional areas as well as the position of these changes are important. These were quantified as the morphological indices while the orientation of each cross-section relative to the flow was quantified as the postural angles (Figure 5.1 and Figure 5.2).

Morphological indices

In order to quantify the body contour two existing morphological indices were specifically adapted for the human body. These include the 'relative position of maximum cross-sectional area' and the 'fineness ratio'. Two new morphological indices including the 'taper index' and the 'cross-sectional ratio' were defined as well.

Adapting the existing morphological indices

Unlike the body of aquatic animals, the human body in a streamlined position does not represent a single streamlined fuselage. The variations in the cross-sectional area and the presence of limbs and the joint attachments complicate the flow characteristics and thus the definition of morphological indices in the case of a human body is not straight forward. For this reason, the body was considered as two zones attached at the waist. The upper zone consisted of the arms and the upper part of the trunk to the waist. The lower zone included the lower trunk below the waist and the legs. The head was treated separately.

Like streamlined bodies each part has a gradual increase in the cross-sectional area followed by a gradual decrease. In the case of the upper zone, which excludes the head, the cross-sectional area increases from the dactylion to the chest area and from there decreases to the waist. For the lower zone the cross-sectional area increases from the waist to the hip level and then decreases down to the akropodion.

By dividing the body into these two different zones it became possible to define a more specific hydrodynamic characteristic for each zone. This allowed the fineness ratio to be defined for each zone as well as for the whole body. Since the head represents a place of sudden change in the profile of a human body in a streamlined position, its position

relative to the leading edge of body (dactylion) is important. Also although in a streamlined position the swimmer tries to cover the head with the arms, parts of the head can not be covered completely with the arms. As a result the vertex may be in direct contact with the upcoming flow. As the head is the only relatively bluff segment which encounters with the flow, the position of the maximum cross-sectional area of the head is an important consideration.

Relative positions of cross-sections

The positions of the each cross-section for different parts of the body are also important as they determine the potential places where the flow would be separated from the body. These include the position of each cross-section such as the chest and buttocks (at hip level) both relative to each zone as well as to the whole body. The position of minimum cross-sectional area at the trunk in the waist area can also be considered as important. As a result of adverse pressure gradients, the flow decelerates past the chest area and it reaches the waist which has the lowest cross-sectional area in the trunk region with a low momentum. After passing the waist the flow accelerates and increases its momentum due to a favourable pressure gradient resulting from an increase in the cross-sectional area from waist to hip. Thus the position of the waist to the whole body is important as it determines where the flow has the lowest momentum in the trunk region. The formula for calculating the relative position of each cross-section is presented in 'calculating morphological indices' section.

Fineness ratio

Dividing the body into two zones enables the fineness ratios to be defined for the lower and upper zones. The fineness ratios, defined for the aquatic animals with almost circular cross-sectional areas as the ratio of body length to maximum diameter (Fish and Hui, 1991), need to be adapted for the human body. A human body's cross-sectional area is elliptical rather than circular (Wicke and Lopers, 2003). Thus, in this study a nominal diameter was defined for each cross-section as the diameter of the circle that has the same area as the cross sectional area as the ellipse that approximates the cross-

section of body. The formula for calculating the fineness ratios is presented in 'calculating morphological indices' section.

Defining new morphological indices

Two new morphological indices including cross-sectional ratio and taper index were defined in order to quantify the changes in the body contours.

Taper index

A 'taper index' can be defined as the gradient of changes in the cross-sectional area of the body when they pass from one to another. This determines the magnitude of the direction changes as the particles in the flow pass from one cross-sectional area to another (Figures 5.1 and 5.2). The areas behind the buttocks and back are vulnerable to flow separation. Therefore, the taper indices from the chest to waist, waist to hip and hip to thigh are useful in quantifying the potential for flow separation in these areas. The formula for calculating the taper index is presented in 'calculating morphological indices' section.

Cross-sectional ratio

The ratios of the cross-sectional areas determine the pressure gradient and the possibility of flow separation and therefore the wake size of the body. The closer to 1 the ratio of two adjacent cross-sectional areas, the less the change in the direction of flow of the particles when they pass from one part to the other (Figures 5.1 and 5.2). The formula for calculating the cross-sectional ratios is presented in 'calculating morphological indices' section.

Determining Postural angles

The shape characteristic of a body is also affected by the postural angles. These affect the relative position of limbs to the flow and to each other which in turn affect the hydrodynamic and glide efficiency parameters of body. Thus, to quantify the posture, the segmental angles of attack and joint angles were measured. The formulas for

calculating the joint angles and segmental angles of attack are presented in 'calculating postural angles' section.

5.2.4. Calculation of Variables

The glide efficiency parameters including glide factor, glide coefficient, and the hydrodynamic parameters including resistive factor, drag coefficient, added mass and added mass coefficient, were the main dependent variables. These were calculated for each subject at the corresponding velocity or Reynolds number based on the regression lines of the best fit that were found in Study 1 and Study 2.

As the glide efficiency and hydrodynamic parameters change with velocity, the correlations should be found at identical velocities between subjects. Because of the differences in the attainable glide velocities between the gender groups, the glide factor, glide coefficient, added mass, added mass coefficient, resistive factor and drag coefficient were all calculated at the velocities of 1.4, 1.5 and 1.6 m /s for the female and at the velocities of 1.6, 1.7 and 1.8 m /s for the male group.

As the shape-related glide efficiency and hydrodynamic parameters change with the Reynolds number, the correlations should be found at identical Reynolds numbers across subjects. Because of the differences in the streamlined length, as well as the attainable glide velocities between the gender groups, the glide coefficient, drag coefficient and the added mass coefficient were calculated at a Reynolds number of 3.5 million for the female subjects and at a Reynolds number of 4.5 million for the male subjects.

The anthropometric data were obtained for a body in a streamlined position using the photogrammetric method described in Chapter 3. The morphological indices were calculated based on the anthropometric measures. The body volume data were obtained from the body volume during glides calculated in chapter 4. For calculating the joint

angles the coordinates of joints during horizontal and inclined glides in Chapter 3 and 4 were calculated.

5.2.4.1. Anthropometric measurements

The photographic method for anthropometric measurement was preferred to the direct measurement using tapes and callipers as a faster and more practical option. As different sections of the body should have been measured in a streamlined position, the subject would have spent exhaustive time in the streamlined position. By using the photogrammetric method the subject possess the streamlined position for a shorter period of time close to the period of an underwater glide. Also by using the photogrammetric method inaccuracies resulting from excess contraction of the limb with the measurement device were eliminated.

The procedure of taking the photos from the subjects in an upright streamlined position and digitizing the outline of the images was the same as what was described in Study 1. The same anatomical landmarks were also used in this study.

Thicknesses and breadths of the areas of interest at each measurement level were calculated from the digitized outline. These are further explained in the 'measurement level' section.

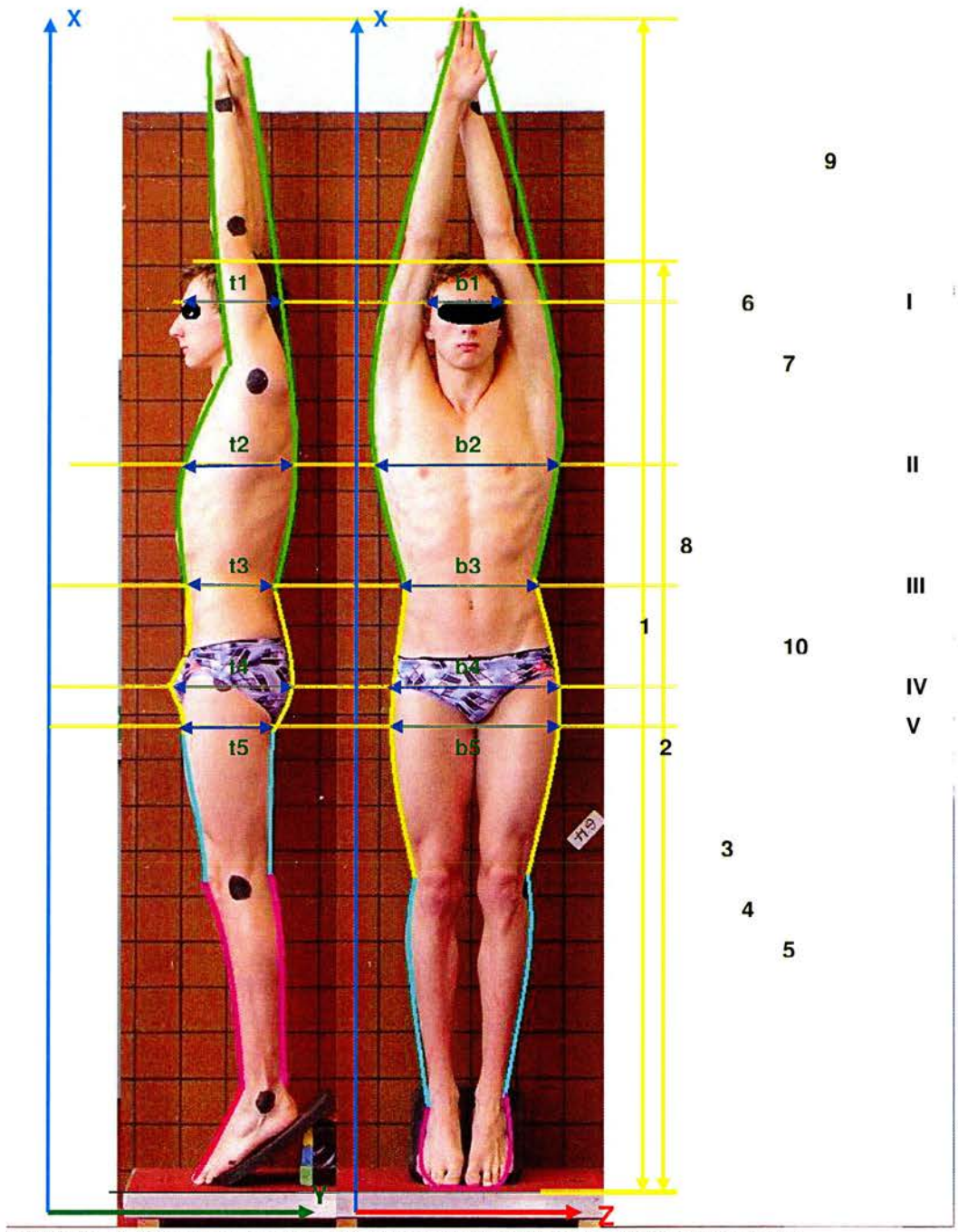

Figure 5. 3. Sample photograph of the subject from front and side views

In the female subjects, the fibrus septa of the breast is attached to the deep fascia overlying the pectoralis major, and none of the muscles beneath the breast including

pectoralis minor and serratus anterior are in isometric contraction in a streamlined position. Thus the breast thickness is much less in this position compared to anatomical posture with hands on side. The existing thickness is further flattened by the tight swimming suit. For these reasons the breasts were included in the depth of chest.

On the basis of the assumption that cross sectional area of a human body could be well replaced by the appropriate ellipse (Jensen, 1978) the cross sectional areas of these parts were calculated. Heights were also measured as the vertical distance between the corresponding levels.

Measurement levels:

Five measurement levels were determined as follows:

I-Forehead level: Horizontal level immediately superior to glabella (portions of the frontal bone between the supraorbital ridges).

II-Chest level: At the level of mesosternale.

III-Waist level: At the level of minimum girth around the waist

IV-Hip level: At the level of the greatest posterior protuberance of the buttocks.

V-Thigh level: At a level 2 cm below the gluteal fold.

Heights:

Heights were defined between the corresponding levels as follows.

1-Streamlined height: The vertical distance between akropodion (the most superior point of the foot that may be the first or second digit) and dactylion (the most distal point of the third digit of the hand).

2-Head height: The vertical distance between akropodion (ground level) and vertex (the most superior point on the skull) of the head.

3- Chest Height: The vertical distance between akropodion (ground level) and the chest level.

4- Waist Height: The vertical distance between akropodion (ground level) and the wait level.

5- Hip Height: The vertical distance between akropodion (ground level) and the hip level.

6-Chest to top distance: The vertical distance between the chest level and dactylion (top level).

7- Waist to top distance: The vertical distance between the waist level and dactylion (top level).

8- Waist to chest distance: The vertical distance between the waist level and the chest level.

9- Head to top distance: The vertical distance between the head level and dactylion (top level).

10- Hip to waist distance: The vertical distance between the hip level and the waist level.

Zones:

Two different zones were defined as follows:

The upper zone: Is defined from the waist level to dactylion.

The lower zone: Is defined from the knee level to the waist level.

5.2.4.2. Obtaining joint position data

The vertical and horizontal positions of each joint, measured during Study 1 were used to quantify the joint angles during the horizontal rectilinear glide in the first study. Similarly, the joint coordinates in Study 2 were used to calculate the joint angles during the inclined glides.

5.2.5. Calculating Anthropometric Measures, Morphological Indices and Postural Angles

5.2.5.1. Anthropometric measures

The intersect point of the level line with the body contour curve was found at each level for the front and side views. The intersect points were named as the left and right intersect points in the frontal view while at the side view these were known as anterior and posterior points.

Breadth

Breadth for each section was calculated as the distance between the right and left intersect points in the front view.

$$B = z_l - z_r \qquad \text{(Equation 5.1)}$$

Thickness

Thickness for each section was calculated as the distance between the anterior and posterior intersects points in the side view.

$$T = y_p - y_a \qquad \text{(Equation 5.2)}$$

Cross-sectional area

Based on the assumption that the cross-sectional area of a human body could be well replaced by an appropriate ellipse (Jensen, 1978 and Wicke and Lopers, 2003) the area of each cross-section was calculated at each level.

$$A_c = \frac{\pi}{4} \times B \times T \qquad \text{(Equation 5.3)}$$

The cross-sectional areas were shown in Table (5.2).

Table 5. 1. The average and standard deviation of the cross-sectional areas of each segment.

Cross-sectional area (m^2)	Female		Male		Pooled	
	Ave	Stdev	Ave	Stdev	Ave	Stdev
Head	0.023	0.002	0.024	0.001	0.024	0.002
Chest	0.073	0.006	0.081	0.007	0.077	0.008
Waist	0.043	0.005	0.045	0.003	0.044	0.004
Hip	0.070	0.006	0.076	0.005	0.073	0.006
Thighs	0.062	0.007	0.059	0.005	0.060	0.006

Height and vertical distance

As in a streamlined position the legs are positioned side by side to each other, thighs were considered as attached segments representing a nominal cross-sectional area double the cross-sectional area of each segment. Cross-sectional area of eight sections of the body including head, chest, waist, hip, thighs, knees, calves and ankles were calculated using Equation (5.3).

Heights and the vertical distances were calculated as the vertical distance between each corresponding inferior and superior levels.

$$H_{s-i} = x_s - x_i \qquad \text{(Equation 5.4)}$$

The streamlined height, vertex height, chest height, waist height, hip height chest to dactylion, waist to dactylion, head to dactylion, waist to chest and hip to waist were calculated based on Equation (5.4).

The heights of each level and the vertical distances between different levels were presented in Table (5.3).

Table 5. 2. The average and standard deviation of heights for male, female and the pooled group.

Distance (mm)	Female		Male		Pooled	
	Ave	Stdev	Ave	Stdev	Ave	Stdev
Streamlined Height	2353	105	2542	102	2447	140
Vertex Height	1873	80	1973	114	1923	109
Chest Height	1456	65	1595	59	1525	94
Waist Height	1232	55	1285	81	1259	72
Hip Height	1128	210	1081	50	1105	149
Chest to dactylion	897	54	946	50	922	56
Waist to dactylion	1120	56	1256	45	1188	85
Waist to Chest	223	20	310	49	267	57
Head to dactylion	480	63	569	83	524	84
Hip to waist	220	99	204	42	212	74

5.2.5.2. Calculating morphological indices

Based on the calculated heights and cross-sectional areas a series of ratios and indices were defined as follows.

The relative position of cross-section

The relative position of each cross-section with regards to each zone's length or the whole body length was defined as:

$$P_s = \frac{h_c}{h_z} \qquad \text{(Equation 5.5)}$$

The relative position of the head to the whole body, the relative position of the chest to the upper body and the whole body, the relative position of the hip to the lower body and the relative position of the waist to the whole body were calculated based on Equation (5.5).

Fineness ratio

The nominal diameter (d_{nom}) was calculated for each cross-section based on Equation (5.6):

$$d_{nom} = \sqrt{\frac{4.A_c}{\pi}} \qquad \text{(Equation 5.6)}$$

The nominal diameter of cross-sectional areas at chest and hip were calculated as represented the maximum cross-sectional areas of the upper and lower zones.

The fineness ratio was defined as the ratio of height to the nominal diameter:

$$FR = \frac{h_z}{d_{nom}} \qquad \text{(Equation 5.7)}$$

Knowing the heights of lower, upper and the whole body, based on Equation (5.4) and the nominal diameters based on Equation (5.6), the fineness ratios of the upper, lower and the whole body were calculated based on Equation (5.7).

Taper index

A taper index was defined as the ratio of changes in the cross-sectional area to the distance between the two consequent cross-sections as follows:

$$TI = \frac{A_{c1} - A_{c2}}{x_{c1} - x_{c2}} \qquad \text{(Equation 5.8)}$$

The chest to waist, waist to hip and hip to thigh taper indices were calculated based on Equation (5.8).

Cross-sectional ratio

The ratio of two cross sectional areas as C_1 and C_2 can be calculated as follows:

$$CR = \frac{A_{c1}}{A_{c2}} \qquad \text{(Equation 5.9)}$$

The chest to waist, waist to hip and hip to waist cross-sectional ratios were calculated based on Equation (5.9).

The positions of maximum cross-sectional areas, fineness ratios, taper indices and cross-sectional ratios were presented in Table (5.4) for different zones as well as for the whole body.

Table 5. 3. The average and standard deviation of the position of maximum cross-sectional area, fineness ratio, tapering indices and cross-sectional ratios for male, female and the pooled group.

	Female		Male		Pooled	
Morphological Indices	Ave	Stdev	Ave	Stdev	Ave	Stdev
Position of head to the whole body	0.2	0.02	0.22	0.03	0.21	0.03
Position of chest to the whole body	0.38	0.01	0.37	0.01	0.38	0.01
Position of waist to the whole body	0.48	0.01	0.49	0.02	0.49	0.02
Position of chest to the upper-body	0.8	0.02	0.75	0.04	0.78	0.04
Position of hip to the lower-body	0.15	0.02	0.16	0.03	0.15	0.02
Fineness ratio of the whole body	9.83	1.99	10.1	2.34	9.97	2.12
Fineness Ratio of upper-body	4.68	0.84	4.99	0.96	4.83	0.78
Fineness Ratio of lower-body	3.37	0.69	3.08	0.14	3.23	0.50
Hip to thigh taper index (m)	0.05	0.04	0.12	0.07	0.08	0.07
Chest to waist taper index (m)	0.13	0.04	0.12	0.04	0.13	0.04
Waist to hip taper index (m)	-0.13	0.04	-0.13	0.02	-0.14	0.03
Chest to Hip Cross section	1.05	0.13	1.07	0.09	1.06	0.11
Hip to waist Cross section	1.62	0.14	1.69	0.16	1.65	0.15
Chest to waist Cross section	1.7	0.25	1.79	0.16	1.75	0.21

5.2.5.3. Calculating postural angles

Segmental angles of attack

Segmental angles were calculated based on the joint centre's coordinates during glide intervals. For each segment with two joints at the superior and inferior ends the segmental angle was calculated according the following formulae.

$$\theta_h = \frac{180}{\pi} \times Arc\tan\frac{y_s - y_i}{x_s - x_i} \qquad \text{(Equation 5.10)}$$

Seven segments were considered including hand, arm (forearm and upper arm together), trunk, thigh, shank, foot and head. As the elbow's axis of rotation was not parallel to the optical axis of the camera, the forearm and upper arm were considered together.

Equation (5.10) was used to calculate each segmental angle to the horizontal. From the hydrodynamic point of view, the segmental angles of attack to the upcoming flow are important. For horizontal glides the segmental angle to the horizontal reflects segmental angle of attack and no further calculation is required. For an inclined glide each segmental angle should be considered relative to the rectilinear inclined glide path in order to reflect the segmental angle of attack.

For an inclined glide each segmental angle were corrected for the glide angle according to the following formulae, to calculate the segmental angle of attack.

$$\theta_i = \theta_h - \alpha \qquad \text{(Equation 5.11)}$$

Joint angles

The segmental angles of the adjacent segments were used to calculate the joint angles.

$$\varphi = \theta_n - \theta_{n-1} \qquad \text{(Equation 5.12)}$$

Each joint angle was adjusted for supplementary pair to reflect the angles shown in Figure (5.4.) Six joint angles including wrist, shoulder, neck, hip, knee and ankle were calculated.

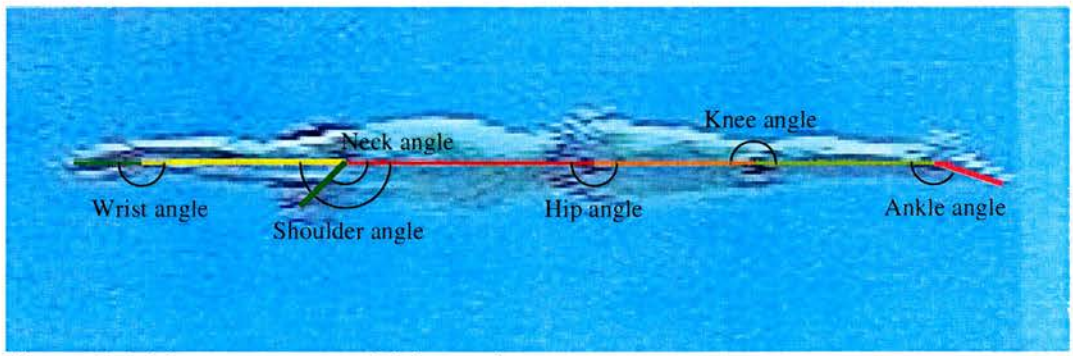

Figure 5. 4. The segments and joint angles

According to the condition of the consistency of posture described in Chapters 3 and 4 each subject performed glides with a specific and consistent segmental and joint angle throughout the glide intervals. As the body posture may be different during horizontal and inclined glides these values were calculated separately.

The segmental angle of attack and the joint angles were shown for the horizontal and inclined glides in Table (5.5) and Table (5.6) respectively. A positive segmental angle of attack indicates that the posterior side of the limb is facing the oncoming flow, and a negative value indicates that the anterior side of the limb is facing the oncoming flow during the glides.

Segmental angles of attack and joint angles during the horizontal glides

Table 5. 4. The average and standard deviation for different segmental and joint angles for male, female and the pooled group for horizontal glides.

Segment/Joint	Female		Male		Pooled	
Angle (◦)	Average	Stdev	Average	Stdev	Average	Stdev
Hand	1	7	-2	4	-1	5
Wrist	170	5	177	5	173	6
Arm	11	4	1	5	6	6
Shoulder	163	7	176	7	169	9
Head	53	14	39	9	46	14
Neck	121	17	138	10	129	16
Trunk	-7	3	-3	3	-5	3
Hip	189	5	186	3	188	4
Thigh	3	2	3	2	3	2
Knee	182	3	181	5	181	4
Shank	1	2	3	4	2	3
Ankle	168	3	166	4	167	4
Foot	-11	2	-11	3	-11	3

Segmental angles of attack and joint angles during the inclined glides

Table 5. 5. The average and standard deviation for different segmental and joint angles for male, female and the pooled group for inclined glides.

Segment/Joint	Female		Male		Pooled	
Angle (◦)	Average	Stdev	Average	Stdev	Average	Stdev
Hand	0	7	-1	5	-1	6
Wrist	170	6	177	6	173	7
Arm	9	4	2	4	6	5
Shoulder	163	5	174	7	169	8
Head	44	13	40	9	42	11
Neck	128	12	136	9	132	11
Trunk	-7	3	-3	3	-5	3
Hip	192	5	188	4	190	5
Thigh	5	3	4	3	5	3
Knee	181	3	179	5	180	4
Shank	4	3	5	3	5	3
Ankle	167	5	166	3	167	4
Foot	-9	3	-8	5	-9	4

5.2.6. Data Analyses

SPSS Analysis Package (ver 13.0.1, 2004) was used to determine the descriptive statistics including means and standard deviations.

The following Pearson product moment correlations were calculated between the following parameters, with alpha levels of $p<0.05$ regarded as significant.

5.2.6.1. Size and shape

Correlations between the following parameters averaged across the velocities of 1.4, 1.5 and 1.6 m /s for the female group and velocities of 1.6, 1.7 and 1.8 m /s for the male group were obtained.

The glide factor, glide coefficient, resistive factor, drag coefficient, added mass and added mass coefficient for the male and the female groups are presented in Table (5.1).

Table 5. 6. The average and standard deviation of the glide factor calculated for the male and female groups at corresponding velocities

	Female			Male		
	1.4 m/s	1.5 m/s	1.6 m/s	1.6 m/s	1.7 m/s	1.8 m/s
Glide Factor (m)	4.93±0.70	4.59±0.70	4.25±0.69	4.98±1.30	4.73±1.12	4.49±0.95
Glide Coefficient	2.77±0.53	2.58±0.51	2.39±0.50	2.66±0.73	2.53±0.62	2.40±0.52
Res. Fact.(kg/m)	14.9±2.74	15.8±2.64	16.88±2.60	17.71±4.31	18.70±4.50	19.70±4.71
Drag Coefficient	0.41±0.09	0.43±0.09	0.46±0.10	0.43±0.10	0.46±0.11	0.48±0.12
Added mass (kg)	13.08±1.1	12.98±1.07	12.88±1.21	13.68±2.01	13.40±2.18	13.11±2.35
Add. mass Coef.	0.19±0.01	0.19±0.01	0.19±0.01	0.18±0.02	0.17±0.03	0.17±0.03

The glide constant was 1.80 ± 0.14 m for the female group and 1.88 ± 0.08 m for the male group. The glide coefficient was 2.59 ± 0.54 at Reynolds number of 3.5 million for the female group and 2.47 ± 0.61 at Reynolds number of 4.5 million for the male group. The maximum cross-sectional area was 0.0745 ± 0.0063 m^2 for the female group and 0.0821 ± 0.0063 m^2 for the male group. The drag coefficient was 0.44 ± 0.09 at

Reynolds number of 3.5 million for the female group and 0.48 ± 0.11 at Reynolds number of 4.5 million for the male group.

The body volume was 67.49 ± 5.36 Lit. for the female group and 77.56 ± 5.03 Lit. for the male group. The added mass coefficient was 0.181 ± 0.014 at Reynolds number of 3.5 million for the female group and 0.169 ± 0.027 at Reynolds number of 4.5 million for the male group.

The relationship between size and glide efficiency and hydrodynamic parameters

The correlations between the glide factor and the glide constant; the resistive factor and the maximum cross-sectional area; and the added mass and the body volume were determined.

The relationship between shape and glide efficiency and hydrodynamic parameters

The correlations between the glide factor and the glide coefficient; the resistive factor and the drag coefficient; and the added mass and the added mass coefficient were determined.

5.2.6.2. Relationship between the shape characteristics and glide efficiency and hydrodynamic parameters

The correlations between the following parameters at the Reynolds number of 3.5 million for the female and at the Reynolds number of 4.5 million for the male group were determined.

The relationship between morphological indices and the glide efficiency and hydrodynamic parameters

The correlations between glide coefficient and all morphological indices; between drag coefficient and all morphological indices and between added mass coefficients and all morphological indices were found.

The relationship between postural angles and the glide efficiency and hydrodynamic parameters

The correlations between glide coefficient and all joint angles and segmental angles of attack; between drag coefficient and all joint angles and segmental angles of attack; and between added mass coefficients and all joint angles and segmental angles of attack were found.

5.2.6.3. Relationship between the drag coefficient and the added mass coefficient

In order to determine to what extent the drag and added mass coefficients were related the correlation between these two parameters at the Reynolds number of 3.5 million for the male and at a Reynolds number of 4.5 million for the male group were calculated.

5.3. Results

Some of the anthropometric measures, morphological indices and postural parameters were correlated significantly with the glide and hydrodynamic parameters.

5.3.1. The relationship between size and glide efficiency and hydrodynamic parameters

5.3.1.1. Glide factor and glide constant

No significant correlation was found between the glide factor and the glide constant for either male or the female group at either velocity (Figure 5.5).

5.3.1.2. Resistive factor and maximum cross-sectional area

Resistive factor at either velocity did not show any correlation with the maximum cross-sectional area (Figure 5.6).

5.3.1.3. Added mass and the body volume

There was no significant correlation between the added mass and the body volume for either the male or the female groups at either velocity (Figure 5.7).

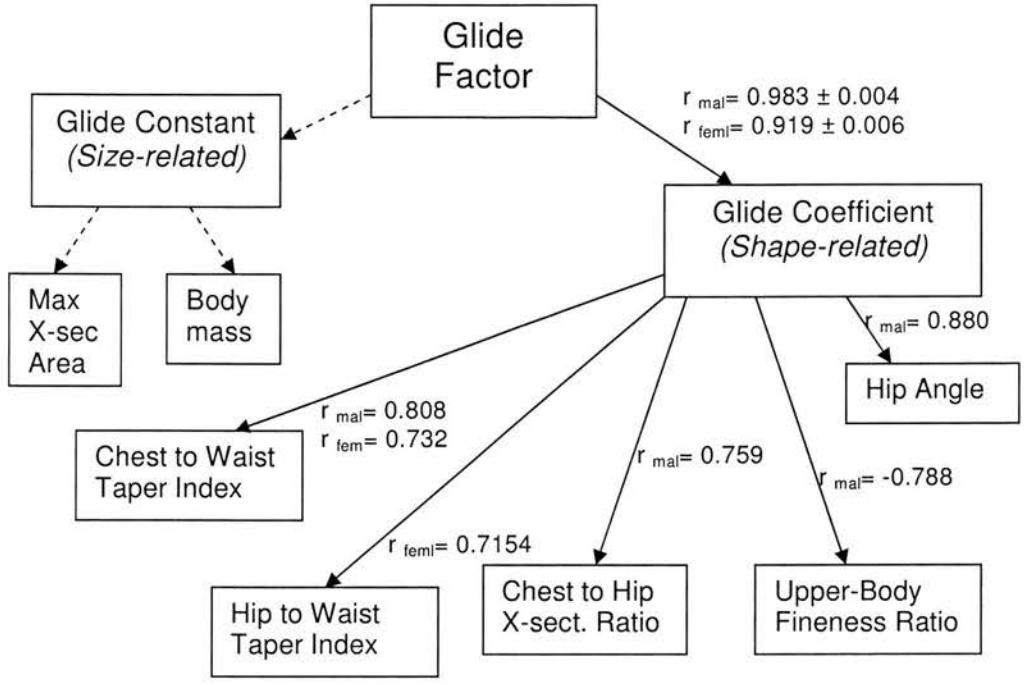

Figure 5. 5. The contributing parameters to the glide factor. The solid arrows indicate a significant correlation and the dashed arrows indicate an insignificant correlation. r_{mal} and r_{fem} represent the correlation for the male and female groups respectively

5.3.2. The relationship between shape and glide efficiency and hydrodynamic parameters

5.3.2.1. Glide factor and glide coefficient

The glide factor was significantly correlated with the glide coefficient for the male group (r= 0.983 ± 0.004) and for the female group (r=0.919 ± 0.006) at all the corresponding velocities (Figure 5.5).

5.3.2.2. Resistive factor and drag coefficient

The resistive factor was significantly correlated with the drag coefficient for male group (r=0.972 ± 0.001) and for the female group (r=0.950 ± 0.003) at all corresponding velocities (Figure 5.6).

5.3.2.3. Added mass and the added mass coefficient

The added mass was significantly correlated with the added mass coefficient for the male subjects (r= 0.944 ± 0.007) at all corresponding velocities, while no significant correlation was found for the female group at any velocity (Figure 5.7).

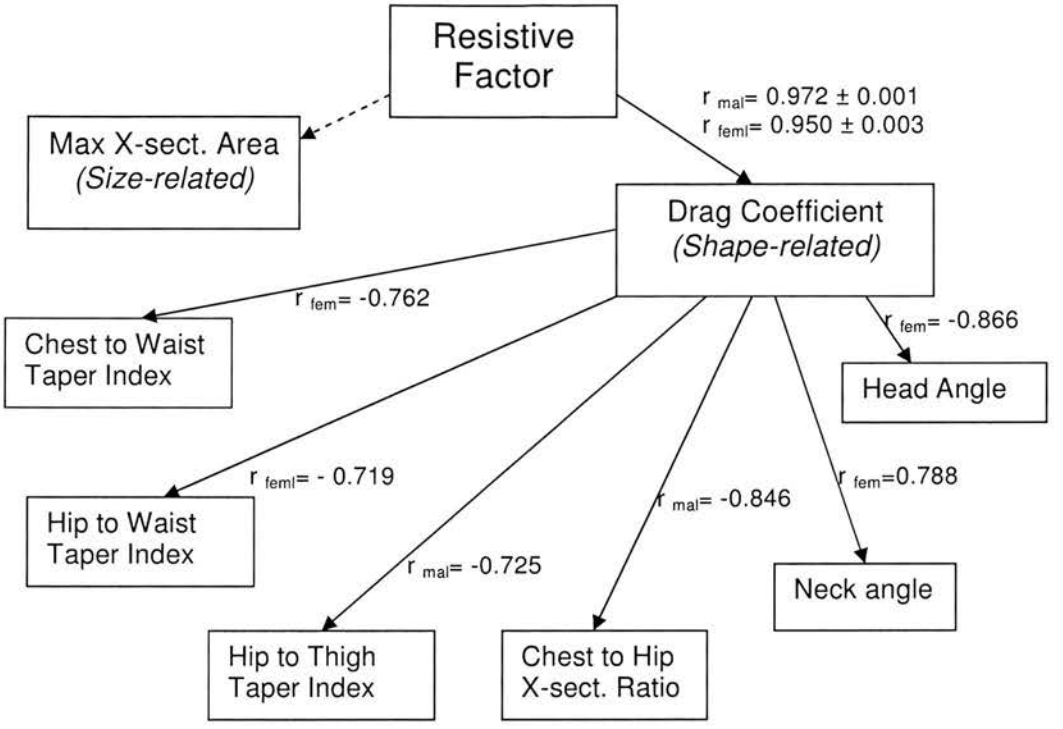

Figure 5. 6. The contributing parameters to the resistive factor. The solid arrows indicate a significant correlation and the dashed arrows indicate an insignificant correlation. r_{mal} and r_{fem} represent the correlation for the male and female groups respectively

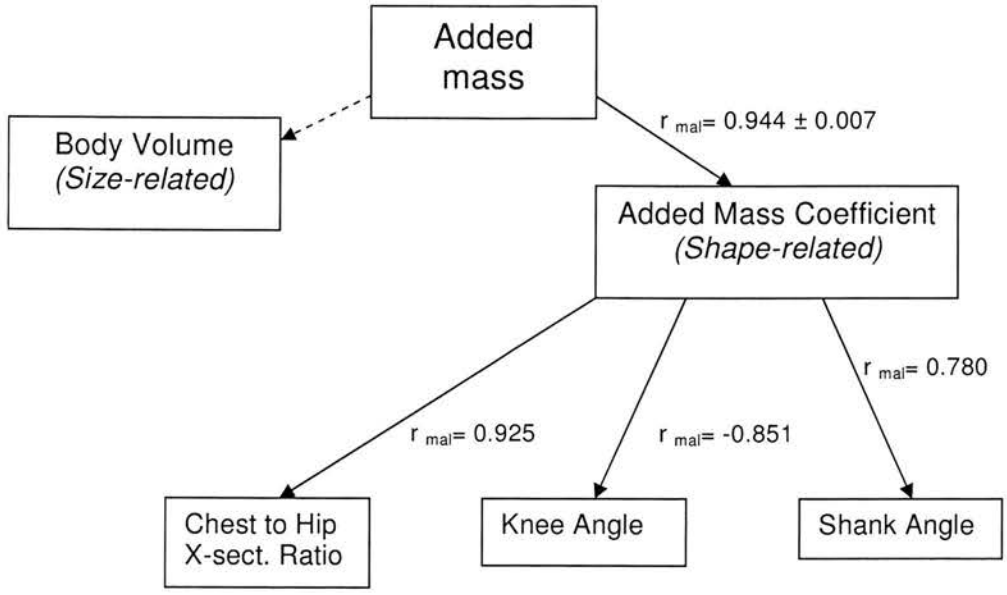

Figure 5. 7. The contributing parameters to the added mass. The solid arrows indicate a significant correlation and the dashed arrows indicate an insignificant correlation. r_{mal} and r_{fem} represent the correlation for the male and female groups respectively.

5.3.3. Relationship between the shape characteristics and shape-related glide efficiency and hydrodynamic parameters

Some of the morphological indices were significantly correlated to the shape-related glide efficiency and the hydrodynamic parameters.

5.3.3.1. The relationship between morphological indices and the shape-related glide efficiency and hydrodynamic parameters

Correlation between the glide coefficient and the morphological indices

Chest to waist taper index was significantly correlated to the glide coefficient for both the male and the female groups (r= 0.808 and r= 0.732). Hip to waist taper index was also significantly correlated to the glide coefficient for the female group (r= 0.7154). The upper body fineness ratio was negatively correlated to glide coefficient in the male group (r=-0.788). There was a significant correlation between the glide coefficient and the ratio of chest to hip cross sectional areas for the male group (r= 0.759) (Figure 5.5).

Correlation between the drag coefficient and the morphological indices

Chest to waist and hip to waist taper indices for female and hip to thigh taper index for male subjects were significantly correlated to the drag coefficient (r= -0.762 and r= -0.719 for female and r= -0.725 for the male subject) (Figure 5.6). The ratio of chest to hip cross-sectional area was negatively correlated to drag coefficient (r = -0.846) (Figure 5.6).

Correlation between the added mass coefficient and the morphological indices

The ratio of chest to hip cross-sectional area was positively correlated to the added mass coefficient (r= 0.925) for the male subjects (Figure 5.7).

5.3.3.2. The relationship between postural angles and the shape-related glide efficiency and hydrodynamic parameters

Some of the joint angles and segmental angles of attack were significantly correlated to the shape-related glide efficiency and the hydrodynamic parameters.

Correlation between the glide coefficient and the joint angles and segmental angles of attack

There were significant strong correlations (r= 0.880 respectively) between hip angle with the glide coefficient for the male subjects (Figure 5.5).

Correlation between the drag coefficient and the angles and segmental angles of attack

Head segment's angle of attack was significantly and negatively correlated to the drag coefficient for female group (r= -0.866). Neck angle was correlated to the drag coefficient for female subjects (r= 0.788) (Figure 5.6).

Correlation between the added mass coefficient and the angles and segmental angles of attack

Knee angle was correlated negatively with the added mass coefficient (r= -0.851) for the male group. The shank angle was also positively correlated to the added mass coefficient for the male group (r=0.78) (Figure 5.7).

5.3.4. Relationship between the drag coefficient and the added mass coefficient

No significant correlation was found between the added mass coefficient and the drag coefficient for either the male or the female group at the corresponding Reynolds numbers.

5.4. Discussion

The relationship between the size and the shape characteristics of a body in a streamlined position and its glide efficiency and hydrodynamic parameters has not been determined previously. The first aim of this study was to investigate the correlation between the size and the shape characteristics quantified by the anthropometric measures, morphological indices and postural angles of a body in a streamlined position and the hydrodynamic and the glide efficiency parameters.

Although the existence of a significant correlation does not necessarily imply a cause and effect between two parameters, it enables us to determine the size and the shape characteristics of bodies with superior gliding efficiency and hydrodynamic parameters.

5.4.1. Size versus Shape

The results indicate that the shape-related hydrodynamic and glide efficiency parameters contribute more to the glide and hydrodynamic characteristics than the size-related parameters. Specifically it can be concluded that subjects with superior shape (determined by higher glide coefficient) tend to glide more efficiently than the subjects with a superior size (that is determined by higher glide constant). The same statement was true for the resistive factor. The correlations indicate that the bodies with a more streamlined shape determined by a lower drag coefficient encounter lower resistive forces compared the bodies with smaller size determined by a lower maximum cross-sectional area. These facts emphasise the relative importance of the shape-related

parameters compared to the size-related parameters when considering the hydrodynamic and glide efficiency of a body.

Contrary to the previous findings that claimed the maximum cross-sectional area to be correlated to passive drag (Lyttle, *et al.*, 1999), in this study there was no correlation between the drag values and the maximum cross-sectional area. This difference is likely to be due to the differences between the ranges of velocity at which drag was quantified. In the study by Lyttle *et al.* (1999) the resistive forces at velocities of 1.6 to 3.1 m/s were measured. Thus, it is possible that at higher velocities other anthropometric variables become significant.

A significant correlation between the added mass and added mass coefficient with no correlation between the added mass and the body volume indicated that the bodies with an appropriate shape to entrain more water had higher added mass than the bodies with a larger volume.

While mathematically increasing either the glide constant or the glide coefficient would increase the glide factor, the correlations indicated that the disadvantage in a glide of having an inappropriate size may be compensated by an appropriate shape. The same statement is applicable for the resistive and inertial characteristics of the body. This may be the answer the questions as to how the best elite level swimmers with greater chest cross-sectional areas that would be expected to create a high resistive force, perform better than many with smaller cross sectional areas.

5.4.2. Relationship between the Shape Characteristics and Glide Efficiency and Hydrodynamic Parameters

Some of the morphological indices and joint and segmental angles were correlated significantly with the glide, drag and added mass coefficients of the body in a streamlined position.

5.4.2.1. Morphological indices

Relative position of cross-sections

As the relative position of each cross-section to the whole length of a body for aquatic animals determines the point where the boundary layer separation is expected to occur, an increase in the relative position is associated with a decrease in passive drag (Mordvinov, 1972). The fact that no correlation was found between the relative position of the maximum cross-sectional area and the drag coefficient indicated that this assumption might not be applicable to human bodies. This might be as a result of difference between shape characteristics of a human and the more streamlined shapes due to the irregularities of the human body that make the possible flow separation not to happen in the positions of the maximum cross-sectional areas.

Fineness ratio

Fineness ratio of the upper body as an indicator of the degree of streamlining of the upper-body was correlated negatively with the glide coefficient for the male group. The upper-body fineness ratio range (4.99 ± 0.96) was higher than the optimal fineness ratio of 4.5 (Hertel, 1966). In this range the drag coefficient was expected to increase with increasing fineness ratio. This may justify the negative correlation between the upper body fineness ratio and the glide coefficient.

Contrary to the results of Clarys (1978), who found that there was a negative correlation between passive drag and fineness ratio, there was no correlation between the fineness ratio of the whole body and any of the hydrodynamic and glide efficiency parameters. This discrepancy could be due to the fact that Clarys (1978) used the values of body height instead of streamlined height to calculate the fineness ratios. Also, as in most of the previous studies, the swimmers were tested on the water surface. In these cases wave drag may cause other parameters to be different and the results may not be comparable with the results based on measurement of a submerged body.

Taper index

The taper indices were positively correlated with the glide coefficient. This can be justified by the fact that the taper indices were negatively correlated with the drag coefficient, while no correlation was found between the taper indices and the added mass coefficient. As these taper indices determine the gradient of changes in two consecutive cross-sectional areas of the body, it seems that bodies with faster changes of cross-sectional areas have a lower drag coefficient that would help them to glide more efficiently.

Although it should be emphasised that it is possible that abrupt changes in the cross-sectional area that would result in high values of taper index may increase drag excessively and result in a high drag coefficient, it seems that the taper indices for subjects in this study were lower than those values. Within the existing range of taper indices, the greater change in cross-sectional ratios may allow the flow to remain attached to the body further downstream and create less separation. It should be emphasised that since there is no previous literature on the optimum taper index, no comparison can be made.

Cross-sectional ratio

Male subjects with a higher ratio of chest to hip cross-sectional area showed a better streamlining characteristic by having a significantly lower drag coefficient. This can be

justified by assuming that during glides the lower zone 'drafts' the upper zone. As the chest and hip cross-sectional areas represent the maximum cross-sectional areas of the upper and the lower zones of body respectively, the lower the ratio of the maximum cross-sectional area of the drafting zone to the maximum cross-sectional area of the leading zone, the more the drafting zone would be able to take advantage of drafting and reduce resistive force. This may decrease the drag coefficient and consequently increases the glide coefficient that can justify the positive correlation between the ratio of chest to hip cross-sectional area and the glide coefficient.

5.4.2.2. Postural angles

The significant correlation between neck angle and drag coefficient indicate that the head is in its best streamlining position when the neck is slightly flexed. Extension of the head may result in upper arms being further apart from each other that creates a less streamlined shape that may be responsible for an increase in the drag coefficient. The increase in resistive factor as a result of increase in neck angle agrees with the findings of Miyashita and Tsunoda (1978) who found significantly higher resistive force values associated with a higher head position. As they considered the resistive forces on the water surface, this study extended their findings for the drag values underwater.

Male subjects with their hips hyperextended had higher glide efficiencies than the male subjects with extended hips. This is in keeping with the fact that the subjects with higher hip angles (hyperextension) had lower drag coefficients. However, in the latter case the values were not significant. It can be argued that the hyperextension of the hip causes the thigh and trunk to be aligned along each other in a more streamlined manner so that the water flows around the body with less disturbance than when the hip is extended.

On the other hand male subjects with more flexed knees had a higher added mass coefficient. As the shank angle shows the same correlation with the added mass, it can be concluded that by flexing the knee the amount of water entrained with the body known increases.

5.4.3. Relationship between the Added Mass and Drag Coefficients

The fact that no significant correlation was found between the added mass coefficient and the drag coefficient for either the male or the female group indicates that the added mass and drag characteristics are not related to each other. However, they may both be affected by the separation point and boundary layer. Unlike more regular bodies, human bodies with irregular humps and hollows do not behave similarly. Thus, the phenomena of flow separation and boundary layer affect the added mass and drag coefficients to varying extents across subjects.

5.4.4. Comparison with Ideal Shapes

The shape-related glide efficiency and hydrodynamic parameters of a human can be compared with the corresponding values of aquatic mammals that have a superior morphological characteristic compared to human body. .

The drag coefficient at Reynolds number of 2.5 million for a 85 kg subject of this study (0.35) was more than three times the reported drag coefficient of a harbour seal of similar mass at identical Reynolds number (0.11 reported by Williams and Kooyman, 1987) . At the Reynolds number 5.5 million the drag coefficient of Steller sea lions was found to be 0.08 (Stelle *et al.*, 2000), almost one fifth of the drag coefficient of the most streamlined male subject in this study (0.38). The average drag coefficient of the subjects at the Reynolds number of 2.5 million was 0.3, which was almost five times the average drag coefficient of California sea lions reported by Feldkamp (1987).

The large difference between drag coefficients of aquatic mammals and humans demonstrates the relatively poor streamlined shape of humans compared to aquatic animals. Limb internalization in the aquatic mammals and the presence of a tapered

shape help them to have lower drag coefficients than humans. This indicates the poor streamlining of a human body shape compared to the most streamlined shapes. A human body even in a streamlined position represents interference between different body segments and the existence of humps, bumps and hollows create local areas of pressure gradient. This makes the human body react to the flow in a complicated way compared to the well streamlined shape of the aquatic mammals that evolved with drag reducing shape characteristics (Aleyev, 1977 and Fish and Rohr, 1999).

Shape imperfections of a human body in a streamlined position like the gaps between forearms and the head, the interface between the legs, and concave areas of the body such as the areas under the chin create sudden changes in the flow direction (Clarys, 1979). The existence of these critical areas which generally are not present in aquatic animals is the reason for the major differences between drag coefficients of a human body compared to the aquatic mammals.

In contrast, the average added mass coefficient of the subjects of this study (0.18) was much higher than the added mass coefficient of California sea lions (0.05 as reported by Feldkamp, 1987). It should be noted that being less streamlined helps the human body to entrain more water as it decelerates. Although this has advantages during a glide by increasing the virtual mass of the human body, it cannot supersede the disadvantage of the increased drag coefficient. It should be emphasised that an identical increase in the added mass and drag coefficient would lead to a decrease in the glide coefficient. Since the glide coefficient is the ratio of virtual mass coefficient to the drag coefficient, an increase in the added mass coefficient from 0.1 to 0.2 (100 % increase) increases the virtual mass coefficient from 1.1 to 1.2 (only 9 % increases). Thus, doubling both the drag and added mass coefficients would decrease the glide coefficient by more than 45 %.

Comparison of the glide coefficient of 15 at Reynolds number of 2.5 million for the sea lion's based on the values reported by Feldkamp (1987), with the average glide

coefficient of the subjects participating in the current study (3.5), again emphasises the relative importance of drag coefficient compared to the added mass coefficient on glide efficiency.

5.4.5. Implications

5.4.5.1. Talent identification

The results of this study have practical applications in talent identification with the aim of selecting novice swimmers with a potential of performing at high level. As discussed in Chapters 3 and 4, superior glide efficiency and hydrodynamic parameters of a body contributes to swimming performance. The results of this study indicate that in talent identification the evaluation should be based on the shape of the body rather than its size. For example, a swimmer with a large streamlined body is more likely to be able to glide more efficiently than a small swimmer with poorly streamlined body. Even if the higher maximum cross-sectional area of the larger swimmer cancels his lower drag coefficient, yielding an identical resistive factor, the advantage of having higher virtual mass as a result of higher body mass enables the larger streamlined swimmer to glide more efficiently compared to the small poorly streamlined swimmer.

The relationship between morphological indices and the hydrodynamic and glide efficiency parameters also have practical applications for identifying the streamlining degree of a body without the requirement for measuring drag forces directly. For example, subjects who possess a higher chest to waist taper index are more likely to be able to glide more efficiently than the subject with a lower chest to waist taper index.

5.4.5.2. Posture optimization

The results of the correlation of certain joint angles with the hydrodynamic and glide efficiency parameters are helpful in developing an optimised streamlined posture with the aim of enhancing glide efficiency and hence the swimming performance. In developing such a streamlined posture specific attention needs to be paid to the joint

angles which were found to be significantly correlated to the glide efficiency and hydrodynamic parameters in this study including neck, hip and knee angles. To determine the effects of the angles and their optimal values for each subject further studies must be conducted.

5.4.5.3. Swimming suit design

The results of this study have important applications in designing swimming suits for improving performance. As the correlation was found between the hip to waist taper index and the gliding efficiency, it is possible that designing a swimming suit that compresses the waist area to further decrease its cross-sectional area with a consequent increase in the taper index may help to improve performance. Further studies are required to determine the optimal range of taper index for each individual. The tension characteristics of the suit should be evaluated so that suits for each individual can be designed.

5.4.6. Future Studies

Although some of the investigated morphological indices and postural angles account for part of the variation in the hydrodynamic behaviour of the body, more specific parameters are needed to account for the exact shape characteristics of body during a streamlined position.

Three dimensional body scanning can provide more detailed information on the exact changes of the body contour in order to define the shape parameters that would be able to quantify the body contour of a human body. In this case other parameters may be found to be significantly correlated with the glide's hydrodynamic and efficiency parameters.

Also, due to the difference between the posture adopted on land and the posture during a streamlined glide, slight differences between the anthropometric variables measured in

the upright streamlined position compared to the streamlined position underwater may exist. Modifying the 3D scan of the body to replicate the exact streamlined posture of the body during a glide would enable the morphological parameters to be measured realistically. Future technology might enable underwater cameras that are able to reconstruct the whole body contour during glides. It is possible that by using the mentioned techniques in the future studies, other important shape characteristics would be determined.

5.5. Conclusion

Subjects with superior shape characteristics, rather than subjects who had a large body mass with a low cross-sectional area were able to glide more efficiently. Also subjects with superior shapes encountered lower resistance and were able to entrain more added mass of water than the subjects with higher maximum cross-sectional area or a higher body volume respectively. Thus, the difference of hydrodynamic and glide efficiency parameters between two bodies depends predominantly on the differences in shape characteristics including morphological indices and postural angles. The results indicated that some of the morphological indices and joint angles investigated in this study were correlated to the glide efficiency and hydrodynamic parameters. The assumption that the more streamlined objects possess a lower added mass coefficient seems not to be applicable to the human body.

Chapter 6

Summary, Conclusion and Future Directions

6.1. Summary

Hydrodynamic parameters of a human body in a streamlined position determine its glide efficiency and therefore the swimming performance. Despite the importance of the resistance and inertia parameters, no study has been conducted to examine these under real glide conditions including natural posture and the specific flow characteristics. The studies in this thesis were conducted to develop methods of quantifying the glide efficiency and the hydrodynamic parameters based on the kinematics of a gliding body, and to investigate to what extent they can reflect the differences as a result of variations in anthropometric and morphological characteristics between individuals.

The aim of the first study was to develop and test a method of quantifying glide efficiency in a way that accounts for both the inertial and resistive characteristics of the gliding body as well as the differences in the instantaneous velocities. In this study, a method of investigating the combined effect of resistance and inertia on the glide efficiency of a streamlined human body in a horizontal rectilinear glide was established. A glide factor that addresses glide efficiency as the ratio of virtual mass to resistive factor was introduced as a new concept in hydrodynamics. A parametric horizontal displacement-time equation was found based on the equation of motion of a body in a horizontal rectilinear glide where body is affected by the drag force in horizontal direction. By fitting the curve representing this parametric equation to the displacement-time data of a horizontal rectilinear glide gathered from video analyses, glide factor and

initial velocity were quantified for each glide interval. Results indicated that the glide factor generally increases with decreasing velocity, and these changes follow a linear trend for each subject. Separating the glide factor to a size-related glide constant and a shape-related glide coefficient allowed identifying the size-related and shape-related advantage of each individual during a glide. The validity and applicability of the method were established.

It was valuable to investigate whether, the advantage of a body during a glide was due to its ability to reduce resistance or whether it is related to its ability to entrain more water and have higher added mass. Thus, the purpose of Study 2 was to develop and test a method of quantifying the hydrodynamic properties of a human body in a streamlined position during an underwater glide so that the values of the resistive factor and the virtual mass can be determined separately. A new parametric resultant displacement-time equation was developed based on the equation of motion of a body in a rectilinear inclined glide considering the component of net buoyancy opposite the direction of travel as a constant force in addition to the drag. By fitting the parametric equation to the displacement-time data of a rectilinear inclined glide, and restricting the parameters to be chosen to a realistic range, the resistive force and virtual mass were extracted separately. Results indicated that this method is valid and able to calculate the hydrodynamic parameters. By calculating the drag and added mass coefficients, investigating the hydrodynamic characteristics of a body independent from body size became possible.

The aim of the third study was to determine the true relationship between the size and the shape characteristics of the body and its hydrodynamic and glide efficiency parameters. To achieve this, the correlations between anthropometric and postural parameters and the calculated glide and hydrodynamic parameters in the first and second studies were investigated. Some morphological indices and joint and segmental angles which are considered being important from hydrodynamic point of view were examined.

Some of theses parameters were significantly correlated with hydrodynamic and glide parameters.

The results of these studies indicated that in study of glide efficiency, both the resistive force and the inertial characteristics of a body can and should be considered as separate entities affecting glide performance.

6.2. Conclusion

This thesis yielded the following advancements in the study of performance in passive glides among swimmers:

6.2.1. Study1: Underwater Glide Efficiency of a Human Body in a Streamlined Position.

1. A 'glide factor' was defined as the ratio of virtual mass to resistive factor and quantified by fitting a parametric curve to the displacement-time of a horizontal rectilinear glide.
2. The glide factor can be used to predict the deceleration rate during glides.
3. A 'glide constant' was defined as a parameter incorporating the ratio of body mass to the maximum cross-sectional area.
4. A 'glide coefficient' was defined as the ratio of virtual mass coefficient to drag coefficient and was calculated as the ratio of the glide factor to the glide constant.
5. Improving the glide efficiency rather than decreasing the drag alone should be the aim of swimmers seeking to improve performance.
6. The developed mathematical model accurately fitted the kinematic data of a body in a horizontal rectilinear glide, indicating the logical validity and accuracy of the method.
7. The relative standard error of calculation equal to 2.45 ± 0.05 % together with the low error associated with the assumption of the consistency of the glide

factor in each glide interval (3.1± 0.3 %) determine the limits of the accuracy for the method.

8. The coefficients of variation of the slopes and the intercept of the regression lines representing the variations of the glide factor to velocity were less than 0.3% and less than 3% respectively indicating the level of inter day reliability (stability) of the method.
9. The maximum relative standard error of measurement determined for the test-retest was 2.94 % determining the internal consistency (intraday reliability).
10. A small inter-individual variations compared to between individuals (1.8±0.3 % vs. 13.2 % for the female group and 1.4±0.1 % vs. 25.8 % for male group) indicated that the differences between individuals can be detected by this method.

6.2.2. Study2: Quantifying the Human Body Hydrodynamic Parameters in a Streamlined Position Based on the Kinematics of an Underwater Glide.

11. The resistive factor and the virtual mass were quantified by fitting a parametric curve to the displacement data of a rectilinear inclined glide while restricting the parameters to a realistic range.
12. The relationship between the resistive factor and velocity for each individual could best be explained by sum of a cubic and quadratic function.
13. The mathematical model developed based on the free body diagram fitted accurately the kinematic data of a body in an inclined rectilinear glide, indicating that the model is realistic (R2 =0.999±0.0001).
14. The developed mathematical model fitted perfectly the kinematic data of a body in an inclined rectilinear glide, indicating the logical validity and accuracy of the method.
15. The relative standard error of calculation equal to 4.0 ± 0.17 % for the virtual mass and 1.45 ± 0.19 % for the resistive factor together with the 5.9± 0.6 % and 2.0± 0.2 % error associated with the assumption of the consistency of the

resistive factor and virtual mass indicated the limits of the accuracy of the method.

16. The coefficients of variation of the slopes and the intercept of the regression lines representing the variations of the resistive factor and the virtual mass to velocity were less than 1% and less than 3% respectively indicating the level of inter day reliability (stability) of the method.
17. The maximum relative standard error of measurement determined for the test-retest were 6.68 % for the resistive factor and 1.48% for the virtual mass determining the internal consistency (intraday reliability).
18. The average within individual coefficient of variation of the virtual mass was four times the coefficient of variation of between individuals, while this quantity was eight times for the resistive factor establishing the construct validity of the method.

6.2.3. Study3: An Investigation into the Relationships between the Size and the Shape Characteristics of the Human Body and its Glide Efficiency and Hydrodynamic Parameters.

19. The shape-related hydrodynamic and glide efficiency parameters contribute more to the glide and hydrodynamic characteristics than the size-related parameters.
20. As no significant correlation was found between the added mass coefficient and the drag coefficient it can be concluded that the added mass and drag characteristics are affected to different degrees by the boundary layer and flow separation phenomena.
21. Among male subjects the ratio of chest to hip cross-sectional area was significantly correlated with drag coefficient (r=-0.846), and added mass coefficient (r=0.925) indicating that having a big chest relative to the hips is an advantage during glides.

22. The taper indices in the trunk area were significantly correlated with drag coefficients. This may be attributed to an increase in the favourable pressure gradient as a result of increasing taper index within the existing limits of variations.
23. The ratio of chest to hip cross-sectional area was significantly correlated to glide and added mass coefficients and negatively correlated to drag coefficient. This may be the result of a decrease in the drag force encountered by the lower zone of body that drafts along the leading upper zone, when this ratio increase.
24. Male subjects with their hips hyperextended had higher glide efficiencies than the male subjects with extended hips.
25. Male subjects with more flexed knees showed a higher added mass coefficient than those with less flexed knees indicating a tendency to increase the amount of water entrained with the body by knee flexion.
26. Fineness ratio of the upper body as an indicator of the degree of streamlining of the upper-body was correlated significantly with the glide coefficient for the male group. The fact that the fineness ratio ranged higher than the optimal value for a minimum drag may justify the recognized correlation.
27. The significant correlation between neck angle and drag coefficient indicated that the head is in its best streamlining position when the neck is slightly flexed. Extension of head may result in upper arms to be further apart from each other that create a less streamlined shape and may be responsible for an increase in the drag coefficient.
28. The large difference between drag coefficients of aquatic mammals and humans demonstrates the relatively poor streamlined shape of humans compared to aquatic mammals.

6.3. Future Directions

As the method of calculating glide and hydrodynamic parameters is based on fitting an appropriate curve to the displacement data of a rectilinear glide, any inaccuracy in the

kinematic data would produce errors in calculating the values. Using higher image resolution and decreasing the size of the skin markers may improve the accuracy of the raw displacement. Increasing the sampling frequency would also increase the accuracy of the calculated glide and hydrodynamic parameters by allowing the mathematical model to be fitted to higher number of points in a shorter interval.

As splitting the frames separates the odd and even fields, the shape of the marker would be different based on which interlaced lines are eliminated. Since most automatic digitizing software digitize the centre of the area with higher contrast, the inconsistency in shape of the marker viewed in each field is a source of error in the kinematic data. Digitizing frames instead of field would decrease the chance of error as a result of this deficiency.

Despite the practical values of the methods of calculating the glide and hydrodynamic parameters from the glide kinematics of a body in streamlined position, during a race or training swimmers do not maintain a rectilinear glide. In practice the glides after starts and turns happens over a curvilinear path with a variable depth. A method that would be able to consider these changes during the glides in an uncontrolled condition would be valuable for more practical applications.

Also as during glides after turns the swimmers twist while maintaining a streamlined position, the methods of acquiring the kinematics data by digitizing the skin markers, may not produce accurate data. Using accelerometer with high sampling frequency is another option of getting data, but the equations based on fitting an acceleration-time data with an appropriate fit needs to be developed. Also attaching the accelerometers to body in a proper place so that the vibration of soft tissues does not affect the measurements is another issue that need to be considered properly.

Method of direct velocity measurement like swim-meter have the advantage of high sampling frequency, but the fluctuations in velocity decreases the accuracy of the calculated parameters. Also the calibration of the system to convert the voltage to velocity, the point of attachment of the wire to the body and maintenance of the

appropriate pre-tension in the wire are critical issues that need to be considered beforehand.

As a futuristic speculation, methods based on the Doppler Effect may be able to have a more accurate measurement of the displacement of the body during glide, but the applications of these devices in swimming research are yet to be developed.

The classical morphological parameters that reflect the hydrodynamic characteristics of streamlined shape of aquatic animals are not completely adaptable to the complex human morphological structure. In case of human new morphological concepts that account for the humps, bumps and hollows of a human body in a streamlined position is required to reflect the hydrodynamic value of human body. Methods based on three-dimensional scan of body can account for the changes in the body contour. When anthropometric parameters can be defined more accurately and specifically based on these values new parameters may be found to be correlated to the hydrodynamic and glide efficiency parameters.

Although the 'Hydro-kinematic' method can quantify the hydrodynamic values of a body in streamlined glide position, it is not able to determine critical areas responsible for the observed resistive and inertial properties. Also the method is not able to distinguish between different drag sources. CFD analysis of a realistic 3-D scan of a human body in streamlined position is able to reveal more details about the critical area of separation and to identify the different sources of drag encountered by a swimmer during glide. The simulation would be realistic if the model would be run under transient flow condition resembling those during a glide. This may only be achieved knowing the exact changes in the instantaneous velocity of body which can be determined thanks to 'Hydro-kinematic' method.

References

Aleyev, Y. G. (1977). *Nekton.* The Hague: Dr VV. Junk b. v. 435pp.

Alley, L. E. (1952). An analysis of water resistance and propulsion in swimming the crawl stroke. *Research Quarterly, 23*, 257-270.

Amar, J. (1920). *The human motor.* London: G. Routledge & Sons, ltd.

APAS (2001). Ariel Performance Analysis System. Ariel Dynamics, Inc: USA.

Batchelor, G. K. (1967). *An Introduction to Fluid Dynamics.* Cambridge University Press, Cambridge.

Benjanuvatra, N., Blanksby, B. A., & Elliott, B. C. (2001). Morphology and hydrodynamic resistance in young swimmers. *Paediatric Exercise Science, 13*(3), 246-255.

Benjanuvatra, N., Dawson, G., Blanksby, B. A., & Elliott, B. C. (2002). Comparison of buoyancy, passive and net active drag forces between Fastskin TM and standard swimsuits. *Journal of Science and Medicine in Sport, 5*(2), 115-123.

Bilo, D. & Nachtigall, W. (1980). A simple method to determine drag coefficients in aquatic animals. *Journal of Experimental Biology, 87*, 357-359

Chatard, J. C., Lavoie, J. M., Bourgoin, B., & Lacour, J. R. (1990). The contribution of passive drag as a determinant of swimming performance. *International Journal of Sports Medicine, 11*(5), 367-372.

Chatard, J. C., Chollet, D., & Millet, G. (1998). Performance and drag during drafting swimming in highly trained triathletes. *Medicine and Science in Sports and Exercise, 30*(8), 1276-1280.

Chatard, J. C., & Wilson, B. (2003). Drafting distance in swimming. *Medicine and Science in Sports and Exercise, 35*(7), 1176-1181.

Chow, J. W., Hay, J. G., Wilson, B. D., & Imel, C. (1984). Turning technique of elite swimmers. *Journal of Sport Sciences, 2*(3), 241-255.

Clarys, J. P. (1978a). An experimental investigation of the application of fundamental hydrodynamics to the human body. In B. Eriksson & B. Furberg (Eds.),

International Series on Sport Sciences, Volume 6; Swimming Medicine IV (pp. 386-394). Baltimore, USA: University Park Press.

Clarys, J. P. (1978b). Relationship of human body form to passive and active hydrodynamic drag. In E. Asmussen & K. Jorgenson (Eds.), *Biomechanics VI-B* (pp. 120-125). Baltimore, USA: University Park Press.

Clarys, J. P. (1979). Human morphology and hydrodynamics. In J. Terauds & E. W. Bedingfield (Eds.), *International Series on Sports Science, Volume 8; Swimming III* (pp. 3-41). Baltimore, USA: University Park Press.

Clarys, J. P. (1985). Hydrodynamics and electromyography: ergonomics aspects in aquatics. *Applied Ergonomics, 16*(1), 11-24.

Clarys, J. P. (1986). Human body dimensions and applied hydrodynamics: Selection criteria for top swimmers. *Snipes Journal, 9*(2), 32-41.

Clarys, J. P., & Jiskoot, J. (1975). Total resistance of selected body positions in the front crawl. In L. Lewillie & J. P. Clarys (Eds.), *International Series on Sport Sciences, Volume 2; Swimming II* (pp. 110-117). Baltimore, USA: University Park Press.

Clarys, J. P., Jiskoot, J., Rijken, H., & Brouwer, P. J. (1974). Total resistance in water and its relation to body form. In R. C. Nelson & C. A. Morehouse (Eds.), *Biomechanics IV* (pp. 187-196). Baltimore, USA: University Park Press.

Counsilman, J. E. (1955). Forces in swimming two types of crawl stroke. *Research Quarterly, 26*, 127-139.

Craig, A. B. & Pendergast, D.R. (1979). Relationships of stroke rate, distance per stroke, and velocity in competitive swimming. *Medicine and Science in Sports. 11*(3), 278-83.

Cureton, T. K. (1940). Review of a decade of research in aquatics at Springfield College. *Research Quarterly, 9*, 68-79.

D'Acquisto, L. J., Costill, D. L., Gehlsen, G. M., Young, W. T., & Lee G (1988) Breaststroke economy skill and performance: study of breaststroke mechanics using a computer based "velocity video". *Journal of Swimming Research. 4*, 9–14

Du Bois, D., & Du Bois, E. F. (1916). Clinical calorimetry. A formula to estimate the approximate surface area if height and weight be known. Arch Intern Med *17*, 863–871

Feldkamp, S. D. (1987). Swimming in the California sea lion: morphometrics, drag and energetics. *Journal of Experimental Biology. 131*, 117-135

Fish, F. E. & Hui, C. A. (1991). Dolphin swimming – a review. *Mammal Review. B 21*, 181–195.

Fish, F. E., & Rohr, J. J. (1999). *Review of dolphin hydrodynamics and swimming performance* (Technical Report 1801). San Diego, CA: US Navy.

Fox, W.R. & McDonald, A.T. (1992). *Introduction to Fluid Mechanics*. 4th edition, John Wiley and Sons, New York.

Hairabedian, A. (1964). *Kinetic Resistance Factors Related to Body Position in Swimming*. Unpublished Ph.D. thesis, Stanford University, Stanford,

Halliday, D., Resnick, R., & Walker, J. (1996). *Fundamentals of Physics.* John Wiley & Sons, New York

Hay, J. G., Guimares, A. C. S. (1983). A quantitative look at the swimming biomechanics. *Swimming Technique*, Aug-Oct 1983, 11-17.

Hay, J. G. (1987). The development of deterministic models for qualitative analysis. In Shapiro, R. and Marett, J. R. (Eds.) *Proceedings of the Second National Symposium on Teaching Kinesiology and Biomechanics in Sports.*

Hay, J. G. (1992). *The Biomechanics of Sports Techniques* (4th ed.). Englewood Cliffs, USA: Prentice Hall International Inc.

Hertel, H. (1966). *Structure-Form-Movement*. New York: Reinhold Publishing Corporation.

Hoerner, S. F. (1965). *Fluid-Dynamic Drag.* Published by the author, Bricktown, NJ.

Howe, M.S., Lauchle, G. C. & Wang, J. (2001). Aerodynamic lift and drag fluctuations of a sphere. *Journal of Fluid Mechanics 436*, 41–57.

Jensen, R. K. (1978): Estimation of the biomechanical properties of three body types using a photogrammetric method. *Journal of Biomechanics*, *11*,349-358.

Jiskoot, J., & Clarys, J. P. (1975). Body resistance on and under the water surface. In L. Lewillie & J. P. Clarys (Eds.), *International Series of Sport Sciences, Volume 2; Swimming II (*pp. 105-109). Baltimore, USA: University Park Press.

Karpovich, P. V. (1933). Water resistance in swimming. *Research Quarterly, 4*, 21- 8.

Karpovich, P.V., & Pestrikov (1939). Mechanical work and efficiency in swimming crawl and backstroke. *Arbeitphysiol. 10*, 504-514.

Katch, F. I. (1969). Practice curves and errors of measurement in estimating underwater weight by hydrostatic weighing. *Medicine and Science in Sports, 1*, 212-216.

Kent, M. R., & Atha, J. (1971). Selected critical transient body positions in breast stroke and their influence upon water resistance. In L. Lewillie & J. P. Clarys (Eds.), *Proceedings of the First International Symposium on Biomechanics in Swimming, Waterpolo and Diving* (pp. 119-125). Brussels, Belgium: Universite libre de Bruxelles.

Klauck, J. & Daniel, K.(1976) Determination of man's drag coefficient and effective propelling forces in swimming by means of chronocyclography. In Komi.P.V. ed. *Biomechanics VB, Intentional Ser. on Biomechanics*. Vol. 1 B, PP.250-257

Klauck, J. (1998). Man's water resistance in accelerated motion: An experimental evaluation of the added mass concept. In K. L. Keskinen, P. V. Komi & P. Pitkanen (Eds.), *Prodeedings of the VIII International Symposium on Biomechanics and Medicine in Swimming; Biomechanics and Medicine in Swimming VIII* (pp. 83-88). Saarijavi, Finland: University of Jyvaskyla.

Landweber, L. (1961). Motion of immersed and floating bodies. In *Handbook of Fluid Dynamics* (ed. V. L. Streeter), pp. 13.1-13.50. New York: McGraw-Hill Book Co.

Lang, T. G. & Daybell, D. A. (1963). *Porpoise performance tests in a sea-water tank.* U.S. Naval Ordinance Test Station, Technical Report, China Lake, California

Larsen, O. W., Yancher, R. P., & Baer, C. L. H. (1981). Boat design and swimming performance. *Swimming Technique, 18*(2), 38, 40, 42-44

Lyttle, A. D. (1999). *Hydrodynamics of the Human Body during the Freestyle Tumble Turn*. Unpublished Doctoral dissertation, The University of Western Australia, Nedlands, Australia.

Lyttle, A. D., Blanksby, B. A., Elliott, B. C., & Lloyd, D. G. (1998). The effect of depth and velocity on drag during the streamlined glide. *Journal of Swimming Research, 13*, 15-22.

Lyttle, A. D., Blanksby, B. A., Elliott, B. C., & Lloyd, D. G. (2000). Net forces during tethered simulation of underwater streamlined gliding and kicking techniques of the freestyle turn. *Journal of Sport Sciences, 18*, 801-807.

Lyttle, A. D., Elliott, B. C., Blanksby, B. A., & Lloyd, D. G. (1999). An instrument for quantifying the hydrodynamic drag of swimmers - a technical note. *Journal of Human Movement Studies, 37*(5), 261-270.

Maiello, D., Sabatini, A., Demarie, S., Sardella, F., & Dal Monte, A. (1998). Passive drag on and under the water surface. *Journal of Sports Sciences, 16*(5), 420-421.

Massey, B. S. (1998). *Mechanics of fluids.* 7th ed. Cheltenham: Stanley Thornes, xii,722p

Matlab Manual, (2002). Matlab Student Version, 6.5.0 Releases 13, Matworks Inc.

Mazza, J. C., Ackland, T. R., Bach, T. M., & Cosolito, P. (1994). Absolute body size. In J. E. L. Carter & T. R. Ackland (Eds.), *Kinanthropometry in Aquatic Sports: A Study of World Class Athletes* (pp. 15-54). Champaign, USA: Human Kinetics Publishers.

McLean, S. P. & Hinrichs, R. N. (1998). Sex differences in the centre of buoyancy location of competitive swimmers. *Journal of Sports Sciences, 16*(4), 373-383.

McLean, S. P. & Hinrichs, R. N. (2000). Influence of arm position and lung volume on the center of buoyancy of competitive swimmers. *Research Quarterly for Exercise and Sport, 71*(2), 182-189.

McNeill, A. R. (1968). *Animal Mechanics.* Sandwich and Jackson, London.

Miyashita, M., & Tsunoda, R. (1978). Water resistance in relation to body size. In B. Eriksson & B. Furberg (Eds.), *International Series of Sport Sciences, Volume 6; Swimming Medicine IV* (pp. 395-401). Baltimore, USA: University Park Press.

Mollendorf, J.C., Termin II, A.C., Oppenheim, E., & Pendergast, D.R. (2004). Effect of swim suit design on passive drag. *Medicine and science in sports and exercise, 36*(6), 1029-1035

Mordvinov, Y. E. (1972). Some hydrodynamic parameters of body shape in pinnipeds. *Hydrobiologia, 8*, 81-84.

Naemi, R. & Sanders, R.H., (2004). A Comparison of Two Functions Representing Velocity of a Human Body Subject to Passive Drag. *In Proceedings of XXII International Symposium on Biomechanics in Sports*, Ed. Lamontagne, M; Gordon, D., Roberstson, E. and Sveistrup, H., pp. 430-433, University of Ottawa, Canada.

Newman, J. N. (1977). *Marine hydrodynamics.* Cambridge, Mass.: MIT Press. xiii, 402 p.

Oppenheim, E. (1997). *Model Parameter and Drag Coefficient Estimation from Swimmer Velocity Measurements.* Unpublished MSc dissertation, University of Buffalo, Buffalo.

Ramsay, R. (2004). *Drag Reduction through Flow Modelling of Competitive Swimmers.* Unpublished MSc dissertation, The University of Edinburgh, Edinburgh.

Roberts, B. S., Kamel, K. S., Hedrick, C. E., McLean, S. P., & Sharp, R. L. (2003). Effect of a FastSkin suit on sub maximal freestyle swimming. *Medicine and Science in Sports and Exercise, 35*(3), 519-524.

Rushall, B. S., Holt, L. E., Sprigings E. J. & Cappaert. J. M. (1994). A re-evaluation of forces in swimming. *Journal of Swimming Research, 10*, 6-30.

Sanders, R.H., & Byatt-Smith, J. (2001). Improving feedback on swimming turns and starts exponentially. In J. Blackwell and R.H. Sanders (Eds.) *Proceedings of Swim Sessions XIX International Symposium on Biomechanics in Sports* (pp. 91-94). San Francisco, California, June 26, 2001.

Sanders, R. H. (2002). New analysis procedure for giving feedback to swimming coaches and swimmers. *In applied Proceeding - Swimming- XXth International Symposium of Biomechanics in Sports Proceeding.* In Jianikelis, K. E, Mason, B. R., Toussaint, H. M., Arellano, R., and Sanders, R. H., (Eds).

Schlichting, H. (2000). *Boundary-Layer Theory.* Springer 8th rev. and enl. ed Berlin; London : Springer, c2000, xxiii, 799 p. Herrmann[sic] Schlichting, Klaus Gersten, with contributions from Egon Krause and Herbert Oertel Jr. ; translated by Katherine Mayes

Sharp, R. L., & Costill, D. L. (1989). Influence of body hair removal on physiological responses during breaststroke swimming. *Medicine and Science in Sports an Exercise, 21*(5), 576-580.

Sheehan, D. P., & Laughrin, D. M. (1992). Device for qualitative measurements of hydrodynamic drag on swimmers. *Journal of Swimming Research, 8*, 30-34.

SPSS Statistical Analysis Package. (2004). Version 13.0.1. SPSS Inc. United States of America.

Starling, R.D., Costill, D. L., Trappe T. A., Jozsi, A. C. , Trappe S.W. , Goodpaster B. H. (1995). Effect of swimming suit design on the energy demands of swimming. *Medicine Science in Sports Exercise*, *27*(7):1086-9.

Stelle, L. L., Blake, R. W. & Trites, A. W (2000). Hydrodynamic drag in Steller sea lions (*Eumetopias jubatus*). Journal of Experimental Biology, *203*, 1915-1923.

Thayer, A. L., & Hay, J. G. (1984). Motivating start and turn improvement. *Swimming Technique, 20*(4), 17-20.

Van Manen, J. D., & Rijken, H. (1975). Dynamic measurement techniques on swimming bodies at the Netherlands ship model basin. In L. Lewillie & J. P. Clarys (Eds.), *International Series on Sport Sciences, Volume 2; Swimming II* (pp. 70-79). Baltimore, USA: University Park Press.

Vennell, R., Pease, D., & Wilson, B. (2005). Wave drag on human swimmers, *Journal of Biomechanics*, *39*(4), 664-671

Videler, J., & Kamermans, P. (1985). Difference between upstroke and downstroke in swimming dolphins. *Journal of Experimental Biology, 119*, 265-274.

Vorontsov, A. R., & Rumyantsev, V. A. (2000). Resistive Forces in Swimming. In V. Zatsiorsky (Ed.), *Biomechanics in Sport* (1 ed., Vol. 1, pp. 184-204). Oxford: Blackwell Science Ltd.

Vogel S. (1994). *Life in Moving Fluids*; *The physical biology of flow*, 2nd ed. Princeton, N.J.: Princeton University Press.

Wang, J., Lauchle, G. C., & Howe, M. S. (2003). Flow-induced force fluctuations on a sphere at high Strouhal number. *Journal of fluid and structure. 17*, 365-380

Walton, J. S. (1981). Close-range Cine-photogrammetry: A Generalized Techniques for Quantifying Gross Human Motion. Unpublished dissertation at Pennsylvania State University.

Waring J. (1999). *Reduction of Drag of a Submerged Swimmer using Vortex Generators.* Unpublished MSc dissertation, Carleton University, Ottawa.

Wicke, J. & Lopers, B. (2003).Validation of the Volume Function within Jensen's (1978) Elliptical Cylinder Model. *Journal of Applied Biomechanics*, *19*(1). 3-12

Williams, T. M. (1987). Approaches for the study of exercise physiology and hydrodynamics in marine mammals. *In Approaches to Marine Mammal Energetics*. Pp. 127-145, A. A. Huntley, D. P. Costa, G. A. J. Worthy, and M. A. Castellini Eds. Specl. Pub. Soc. Marr. Mamm. No 1

Williams, T. M., & Kooyman, G. L. (1985). Swimming performance and hydrodynamic characteristics of harbour seals. *Physiological Zoology, 58*, 576-589.

Appendix A

In each setup a definite number of points were considered as a glide interval. For each setup the glide factors were quantified for different velocities and the following errors were calculated. As there was a slight change between the even and odd frames (due to interlacing) that might have resulted in slight changes in the shape of the detected marker, for each setup one frame (two fields) were added to eliminate the possible effect of this problem on the fitted curve values. As each point represented the raw position of the whole body at each field, errors at each setup with increments of two points were calculated.

A.1. Calculating the Error Associated with the Curve Fitting Procedure

The certainty level for calculating the glide factors was 95 % that indicates that the real glide factor falls within a range of the calculated glide factor plus or minus two times the standard error of calculation. Thus the confidence bound width for a glide interval is four times the standard error of calculation.

The relative confidence bound width for each glide factor (that is the ratio of the confidence bound width to the value of glide factor) was used to find the relative standard error of calculation according to the following formulae.

$$SEC\% = \frac{CBW\%}{4} \qquad \text{(Equation A.1)}$$

Where the CBW% represents the relative confidence bound width at certainty level of 95% and SEC% represents the relative standard error of measurement.

The relative standard error of calculation (SEC %) was calculated, for each interval of different length that represented in Figure (A.1).

A.2. Calculating the Error Associated with the Glide Factor Consistency Assumption

The quantified glide factor for a glide interval is attributed to the average velocity of a glide interval. Since the glide factor changes with velocity, and the velocity in each glide interval is not constant, the glide factor is expected to change over a glide interval.

The error associated with the assumption of the consistency of the glide factor over a glide interval can be calculated as the difference between the true glide factor and the quantified glide factor at each point. The true glide factor at each velocity can be approximated by the regression line that represents the variations of glide factor over the velocity ranges. The quantified glide factor refers to the one that was determined by the curve parameters for a glide interval.

As the difference between the instantaneous velocity and the average velocity is at its highest at the beginning and the end of a glide interval the maximum error as a result of difference between the true glide factor and the quantified glide factor is expected to happen at these points. This error was calculated at by the following formulae.

$$ERR\% = \frac{C_{GV_0} - C_G}{C_G} \qquad \text{(Equation A.2)}$$

Where C_G represents the glide factor determined by the curve fitting technique for each glide interval and C_{GV_0} represents the glide factor for the initial velocity that was approximated by the regression line that represented the variations of glide factors over the average velocities.

A.3. Finding the Optimum Number of Points

The standard error of measurement and the error associated with the assumption consistency of glide factor were calculated for a subject in the pilot work for the glide intervals of different length.

These values were plotted against the number of points in each glide interval in Figure (A.1). As it can be seen the decrease in the relative standard error of calculation (SEC%) was 0.74 % when the number of points increased from 18 to 20, while the increase in the relative error (ERR %) was 0.33 %. By increasing the number of points from 20 to 22 the decrease in the SEC% was 0.35 % while the increase in the ERR% was 0.36 %. By further increase in the number of points for example increasing the number of points from 22 to 24, SEC% decreased by just 0.12% while ERR% increased by 0.20 %. Thus 20 points in each glide interval was chosen as the best compromise.

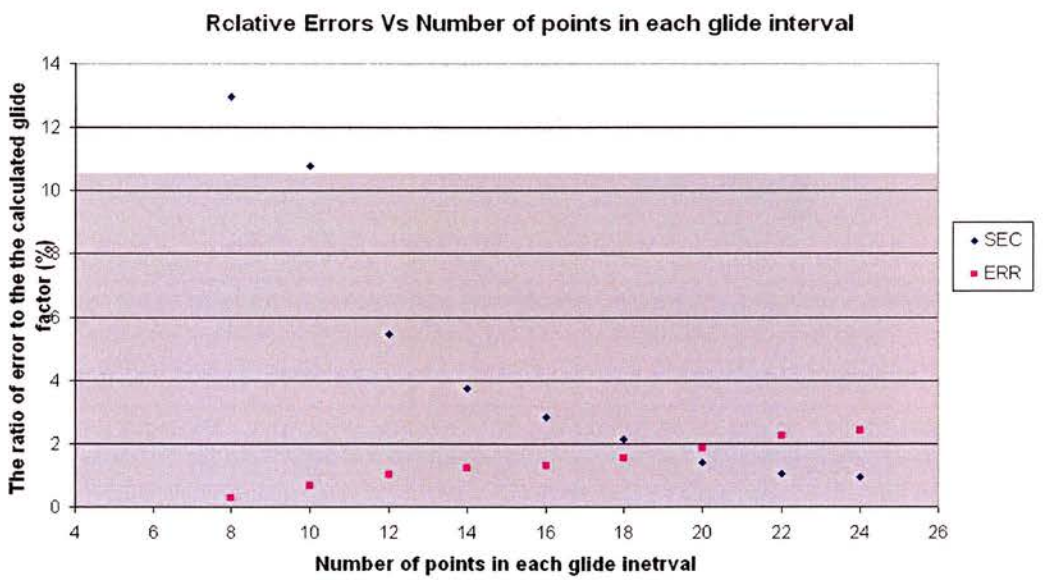

Figure A. 1. The Relative Standard Error of Calculation and the relative Error associated with the consistency of the glide factor over a glide interval Vs numbers of points in each glide interval

Appendix B

B.1. Underwater Glide Study

Dear Swimmer,

This study measures the glide efficiency and the resistive and inertial parameters contributing to the glide efficiency.

Prior to the data collection swimmers will be fully briefed as to the nature of the research, the task to be undertaken, the layout of the pool and the safety concerns regarding the pool and weighting tank equipment. Informed consent will also be required before subjects can participate in the study. Prior to the pool sessions the swimmers height and weight will be measured. Two digital pictures from side and front view will be captured from the swimmer in standing streamlined posture on land. The hydrostatic weight will be measured in the weighting tank to get the net buoyancy force in the maximum inhalation. The familiarization trials will be started prior to the real data collection to familiarize the subject with the glide procedure, which is suitable for the purpose of this study. The familiarization process will be continued until the subject will be able to do glide according to the requirements. The data collection process will be started after the subject has been completely familiar with the process. These will be repeated in two sets of 15 horizontal and inclined glides. The study is conducted over consequent lab and pool sessions. The lab session consists of marking the subject in joint centres and get the photos in an upright streamlined position. Then measuring the height, and weight and taking two digital photos from subject in streamlined upright standing position. After that the subject will be weighted in the hydrostatic tank. The lab session would take around 45 minutes. The pool session starts with warm ups and familiarization process. First the subject will be instructed to do the horizontal glides according to the instructions. Each trial will be filmed to give visual feedback to the swimmer at poolside. After being sure that the subject is able to do the horizontal glides in accordance with the requirements, the data of horizontal rectilinear glides trials would be collected. After finishing the first session, the subject will be instructed to do the inclined glide according to the instructions. Each trial will be filmed to give visual feedback to the swimmer at poolside. After being sure that the subject is able to do the inclined glides in accordance to the instructions, the data would be collected similar to the horizontal glides. Depending on the swimmer's skill to do the glides in accordance to the requirements, each of the pool sessions takes about 75 minutes.

Appendix C

C.1. Informed Consent

Dear Swimmer,

We are seeking your participation in a research study, which will examine the glide performance in swimming. This study will assess resistive and inertial characteristics during an underwater glide task. Your participation in this study will be on a voluntary basis. If you agree to participate you will be asked to do underwater passive glide following push-off from the wall. Prior to pool sessions your height, head girth and weight will be measured. Two digital photographs from side and front view will be captured from you in streamlined standing position on land. The hydrostatic weight will be measured in the weighting tank in lab to get the buoyancy force. In pool after warm-up the familiarization trials will be started prior to the real data collection to familiarize you with the glide procedure. The familiarization process will be continued until you will be able to do glide according to the requirements. The actual data collection process will be started after you have been completely familiar with the glide procedure according to the requirement. This procedure will be repeated for two sets of horizontal and inclined glides as 15 acceptable trials each consequently. Potential benefits from this analysis include a better understanding of your glide efficiency, and its contributing factors like resistive and inertial parameters. If you have read and understood the requirements of your participation in the research study and do not have any further questions regarding the study, please read the following and print and sign the form to indicate your informed consent.

I, _____ (clearly print YOUR name), agree to participate in an analysis of swimming biomechanics. I understand that to participate, I will be photographed and videotaped during a scheduled session. The research team will apply oil based black ink to anatomical landmarks for purposes of digitizing. I am aware that the research team will keep the video data. It has been explained to me that this data will be assigned a number and kept separate from the consent forms, thus ensuring that all data will be anonymous and confidential. Furthermore it has been explained that, once the data is processed, it will be electronically stored and protected by the research team. The results will be aggregated, and if the study is publicly disseminated through publication, it will not be possible to identify myself or anyone else who participated in the study. I am aware that I have the right to not participate and that I may discontinue at any time. Furthermore, I understand that my participation in the analysis is not in response to financial or other inducements. I have had the instructions to use the hydrostatic weighting tank explained to me and I am aware of the additional risks associated with using the weighting tank. I have had the unique features of this swimming pool explained to me and I am aware of the additional risks associated with swimming in a swimming pool.

I DO / DO NOT grant permission to be recorded by video cameras

I DO / DO NOT grant permission for the video recordings to be shown to others for educational purposes, for example, on the World Wide Web.

Signature Date